
Wayne State University Dissertations

January 2018

Design, Synthesis And Biological Evaluation Of Pyrido[2,3-D]pyrimidines As Inhibitors Of N5-Cair Synthetase

Qian Lin

Wayne State University, qianlin.kilo@gmail.com

Follow this and additional works at: https://digitalcommons.wayne.edu/oa_dissertations

 Part of the [Medicinal Chemistry and Pharmaceutics Commons](#)

Recommended Citation

Lin, Qian, "Design, Synthesis And Biological Evaluation Of Pyrido[2,3-D]pyrimidines As Inhibitors Of N5-Cair Synthetase" (2018). *Wayne State University Dissertations*. 2112.
https://digitalcommons.wayne.edu/oa_dissertations/2112

This Open Access Dissertation is brought to you for free and open access by DigitalCommons@WayneState. It has been accepted for inclusion in Wayne State University Dissertations by an authorized administrator of DigitalCommons@WayneState.

DESIGN, SYNTHESIS AND BIOLOGICAL EVALUATION OF PYRIDO[2,3-D]PYRIMIDINES AS INHIBITORS OF N^5 -CAIR SYNTHETASE

by

QIAN LIN

DISSERTATION

Submitted to the Graduate School

of Wayne State University,

Detroit, Michigan

in partial fulfillment of the requirements

for the degree of

DOCTOR OF PHILOSOPHY

2018

MAJOR: PHARMACEUTICAL SCIENCES

Approved By:

Advisor

Date

ACKNOWLEDGMENTS

My doctoral study was completed under the guidance of my advisor, Dr. Steven M. Firestine, toward whom I owe great gratitude from many aspects. First, the resources and opportunity that he provided enabled me to emerge myself in gaining knowledge and exploring science without distractions. Second, his intelligent and critical way of scientific thinking gave me the most powerful tool used in future research and life beyond. Third, his patience and wisdom toward life often calmed my anxiety and doubt and helped me sail through difficulties. Without his advice, guidance, and support, this work would not be possible.

I would like to thank my committee members, Dr. Tamara Hendrickson, Dr. Timothy Stemmler, and Dr. Zihui Qin. They gave me great insights toward pushing this project forward. They also provided great comments and helped me improve my public speaking and boost my self-esteem.

I was fortunate to work with many great lab members and enjoy their friendship. I would like to thank Dr. Shiv Sharma for sharing his experiences in theoretical and experimental synthesis. I enjoyed the broad discussions over a variety of topics with Dr. Cale Streeter and wished the best for the rest of his medical studies. I would also like to thank Marcella Sharma, seeing her reminded me of where I started and the sometimes forgotten passion for research. I wish her good luck with her projects.

TABLE OF CONTENTS

ACKNOWLEDGMENTS	ii
TABLE OF CONTENTS	iii
LIST OF TABLES	vi
LIST OF FIGURES.....	vii
LIST OF SCHEMES	x
CHAPTER 1 INTRODUCTION	1
1.1 Antimicrobial resistance	1
1.2 Purine nucleotide biosynthesis.....	6
1.2.1 Salvage pathway	6
1.2.2 De novo pathway.....	7
1.3 Divergences in the <i>de novo</i> pathway.....	11
1.4 Target verification of PurK.....	15
1.5 Previous attempts at PurK inhibitor development	16
1.6 ATP-grasp Family	17
1.6.1 General introduction	17
1.6.2 ATP-site inhibitors of ATP-grasp family	19
CHAPTER 2 RESULTS AND DISCUSSIONS	22
2.1 Preliminary testing of potent BC inhibitors against PurK.....	22
2.1.1 Synthesis.....	22
2.1.2 BC inhibitor pyrido[2,3-d]pyrimidine weakly inhibited PurK _{Asp}	23

2.2 Computation studies suggested optimization positions	25
2.3 Ribose-binding position (R ₁) modifications	33
2.3.1 Synthesis.....	33
2.3.2 Biological evaluations	34
2.4 Phosphate-binding position (R ₂) modifications	37
2.4.1 Synthesis.....	37
2.4.2 Biological evaluations.....	39
2.5 Double modifications.....	42
2.5.1 Synthesis.....	42
2.5.2 Biological evaluations.....	44
2.6 1,6-naphthyridines and 1,8-naphthyridines.....	47
2.6.1 Synthesis.....	47
2.6.2 Functions of the aza atoms in pyridopyrimidine	49
2.7 Development of binding models to PurK _{Asp} for pyrido[2,3- <i>d</i>]pyrimidine inhibitors....	50
2.7.1 Binding model based on structural alignment	51
2.7.2 Binding model based on docking studies.....	54
CHAPTER 3 CONCLUSIONS	62
CHAPTER 4 FUTURE DIRECTIONS	63
4.1 General future directions.....	63
4.2 Apply covalent inhibitor strategy to increase target specificity and selectivity	63
4.2.1 Using the cysteine modifier to probe cysteine functions in PurK _{Asp}	65

4.2.2 Probe the cysteine function using N-methyl maleimide	65
4.2.3 N-FITC maleimide binds PurK _{Asp} and PurK _{E. coli} covalently	66
4.2.4 ATP protected PurK _{Asp} from the time-dependent inhibition of N-methyl maleimide	67
4.2.5 The time-dependent inhibition of N-methyl maleimide against PurK _{Asp} is not due to the modification of Cys266, but Cys216.....	68
CHAPTER 5 METHODS AND MATERIALS	72
5.1 Chemistry.....	72
5.2 Biology.....	93
5.2.1 Phosphate Assay (Malachite green assay).....	93
5.2.2 PK/LDH coupled PurK assay.....	94
5.2.3 Thermal shift assay	95
5.2.4 Construction, expression and purification of PurK mutant proteins.	96
5.2.5 PK/LDH coupled PurK assay used in the study of cysteines functions.....	96
REFERENCES.....	97
ABSTRACT	124
AUTOBIOGRAPHICAL STATEMENT	125

LIST OF TABLES

Table 1. Drug-resistant threat to the United States.	5
Table 2. List of abbreviations of intermediates in <i>de novo</i> purine biosynthetic pathway... ..	10
Table 3. List of abbreviations of enzymes in <i>de novo</i> purine biosynthetic pathway.	11
Table 4. Activity of BC inhibitors against PurK.	24
Table 5. Ribose position (R_1) modifications.	35
Table 6. Phosphate position (R_2) modifications.	39
Table 7. Double modifications.	45
Table 8. 1,6-naphthyridines (left), 1,8-naphthyridines (middle) and the parent pyridopyrimidines (right).	50
Table 9. The docking scores and RMSD values of the 5 output poses of ADP. The ranking was determined by the scoring function.....	55
Table 10. The docking scores and RMSD values of the 5 output poses of inhibitor 11. The ranking was determined by the scoring function.	57
Table 11. Primers used for the creation of mutant PurK _{Asp}	96

LIST OF FIGURES

Figure 1. Precursors of inosine monophosphate used in <i>de novo</i> purine biosynthesis.....	7
Figure 2. <i>De novo</i> purine biosynthetic pathway.	9
Figure 3. Divergence between microbial and human <i>de novo</i> purine pathway.....	14
Figure 4. General representation of the ATP-grasp enzymes based on the 3-D structure of the <i>A. clavatus</i> PurK enzyme.....	17
Figure 5. Similarities between PurK and BC. a. Reaction similarity. b. Crystal structural superimposition of PurK (pdb: 3K5I, green) and BC (pdb: 2J9G, cyan) with ADP in the binding sites of both enzymes.	19
Figure 6. ATP-binding site inhibitors of BC developed by Pfizer.	20
Figure 7. ATP-binding site inhibitors of BC developed by Schering-Plough.	21
Figure 8. Compounds tested in the preliminary study.	22
Figure 9. Lineweaver-Burke plot of 1 against PurK _{<i>E. coli</i>} using the malachite green assay.	25
Figure 10. Alignment of BC (PDB: 3G8C, green) and PurK _{<i>Asp</i>} (PDB: 3K5I, cyan).	26
Figure 11. Alignment and key fingerprint residues in the BC and PurK _{<i>Asp</i>} ATP-grasp site.	26
Figure 12. 2-D illustration of the ATP binding interactions in BC (left) and PurK _{<i>Asp</i>} (right).	27
Figure 13. 2-D illustration of the pyrido[2,3- <i>d</i>]pyrimidine inhibitor 11 binding interactions with the ATP-binding site of PurK _{<i>Asp</i>} (PDB: 3K5I). Left: direct structure superimposition of BC and PurK _{<i>Asp</i>} . Right: Energy minimization of inhibitor 11 and PurK _{<i>Asp</i>}	27
Figure 14. 2-D illustration of the proposed binding orientation of pyrido[2,3- <i>d</i>]pyrimidine overlapping with ADP in the ATP-site of PurK _{<i>Asp</i>}	29
Figure 15. 2-D illustration of the pyrido[2,3- <i>d</i>]pyrimidine inhibitor 11 binding interactions with the ATP-binding site of BC (PDB: 2V58).....	30

Figure 16. Crystal structural superimposition of PurK (pdb: 3K5I, green) and BC (pdb: 2V58, yellow) with pyridopyrimidine 11 in the binding site.....	30
Figure 17. Surfaces of the ATP-site for PurK _{E. coli} (left) and PurK _{Asp} (right).	31
Figure 18. Crystal structural superimposition of PurK _{Asp} (pdb: 3K5I, green) and PurK _{E. coli} (pdb: 3ETJ, cyan) with pyridopyrimidine (purple) aligned in the ATP-site.....	32
Figure 19. Modification strategy.....	33
Figure 20. Lineweaver-Burke plot of 14 against PurK _{Asp} using the PK/LDH coupled PurK assay.....	37
Figure 21. Binding affinity of compound 1 and 56 against PurK _{Asp} as measured by the thermal shift assay.	47
Figure 22. Structures of pyrido[2,3- <i>d</i>]pyrimidine, 1,6-naphthyridine and 1,8-naphthyridine.	48
Figure 23. The hypothetical binding model generated by structural superimposition of PurK _{Asp} (pdb: 3K5I) and BC (pdb: 2V58).....	51
Figure 24. Correlation of calculated affinity (kcal/mol) vs. experimental %RA.	53
Figure 25. 2-D illustration of the 5 docked ADP poses interacting with the ATP-binding site of PurK _{Asp} (PDB: 3K5I).. ..	56
Figure 26. 2-D illustration of the 5 docked 11 poses interacting with the ATP-binding site of PurK _{Asp} (PDB: 3K5I).	58
Figure 27. Population display of the PLIF generated by all the docking poses of the C-6 and N-7 non-urea derivatives.	59
Figure 28. 2-D illustration of the docking pose 5 of pyrido[2,3- <i>d</i>]pyrimidine overlapping with ADP in the ATP-site of PurK _{Asp}	60
Figure 29. 2-D illustration of the docking pose 5 of 54 in PurK _{Asp}	61

Figure 31. Examples of covalent inhibitors. The Rhinovirus 3C protease inhibitor (a) and the epidermal growth factor receptors (EGFR) protein kinase inhibitor (b).....	64
Figure 32. Interaction of Cys266 with ADP in PurK _{Asp} (pdb: 3K5I).....	65
Figure 33. PK/LDH coupled PurK reaction was initiated with PurK at time 0 and the conversion of NADH to NAD ⁺ was measured at 340 nm.....	66
Figure 34. FITC-maleimide covalently labeled both PurK _{Asp} (45 kDa) and PurK _{E. Coli} (40 kDa).	67
Figure 35. PK/LDH coupled PurK reaction was initiated with PurK at time 0, and the conversion of NADH to NAD ⁺ was measured at 340 nm. A fixed concentration of 100 μM N-methylmaleimide was presented in all reactions with increased concentrations of ATP as shown in the left. The progression curves were fitted to equation 1 to generate k_{obs} . The secondary plot of k_{obs} vs. $[ATP]/K_m$ ($K_{m[ATP]} = 60 \mu M^{142}$) was shown to the right and demonstrates a clear decrease in rate as the ATP concentration increases.	68
Figure 36. PK/LDH coupled PurK reaction was initiated with PurK (WT or mutants) at time 0 and the conversion of NADH to NAD ⁺ was measured at 340 nm. A fixed concentration of 100 μM N-methylmaleimide was presented in all runs.	70
Figure 37. PurK _{Asp} (pdb: 3K5I). 5 cys, ADP, and AIR are shown in sticks.	71
Figure 38. The relative position of Cys216 compared to the enzymatic substrates. (This is a preliminary figure just to show the position).	71

LIST OF SCHEMES

Scheme 1. Synthesis of pyrido[2,3- <i>d</i>]pyrimidines.	23
Scheme 2. Synthesis of methyloxazole-carboxamide.	23
Scheme 3. Synthesis of pyrido[2,3- <i>d</i>]pyrimidines with various substitutions at the 6-phenyl position.	34
Scheme 4. Synthesis of pyrido[2,3- <i>d</i>]pyrimidines with various N/O-alkylations at the 7-NH ₂ position.	38
Scheme 5. Synthesis of pyrido[2,3- <i>d</i>]pyrimidines with various ureas at the 7-NH ₂ position.	38
Scheme 6. The failed synthesis for the key intermediate of the double modified compounds.	42
Scheme 7. Synthesis of pyrido[2,3- <i>d</i>]pyrimidines with double modifications.	44
Scheme 8. Synthesis of 1,6-naphthyridines.	49
Scheme 9. Synthesis of 1,8-naphthyridines.	49
Scheme 10. Synthesis of 7.	72
Scheme 11. Synthesis of 6.	73
Scheme 12. Synthesis of 14.	75
Scheme 13. Synthesis of 23.	76
Scheme 14. Synthesis of pyrido[2,3- <i>d</i>]pyrimidines with various substitutions at the 7-NH ₂ position.	76
Scheme 15. Synthesis of 24 and 25.	79
Scheme 16. Synthesis of 26.	81
Scheme 17. Synthesis of 30.	81
Scheme 18. Synthesis of 36.	83

Scheme 19. Synthesis of 56.....	89
Scheme 20. Synthesis of 57.....	90

CHAPTER 1 INTRODUCTION

1.1 Antimicrobial resistance

Microorganisms not only have a much longer history than human beings, they exist in greater quantities as well. Life on earth has a history of 3.7 billion years, 3 billion years of which microorganisms have been the single dominant form.¹⁻² They are found from the highest mountains to the deepest trenches; their biochemical reactions shaped the biosphere that we now live in today.³⁻⁴ If we were to summarize the earth's history into one calendar year with the earth born on Jan 1st, the first two months would be barren, but from sometime in March, tiny microbes would start swimming in the warm coastal waters and around thermal vents. From March to October, two thirds of a year, microbes were the only life form; humans arrived on the last hour of the last day (Dec 31st) and have existed for no more than 30 minutes. The sheer quantity of microbes is almost beyond imagination. If we gather all the microbes on earth, not only would they outnumber all the humans, trees, pets, birds – all the visible world combined, they would outweigh them as well!⁵ As a late comer who falls short in number, it is no wonder that humans have developed mechanisms to coexist with microbes.

Microbes do not just live with us, they also live on us. The exact number of microbes living on each person is still under debate. The most well-known ratio is 1:10,⁶⁻⁷ with microbes outnumbering human cells. A closer look suggests this famous ratio is perhaps only a back-of-the-envelope calculation⁸ with a more accurate estimate being that each human contains about 30 trillion human cells and 39 trillion microbial cells⁸ – nearly a tie. By any standard however, we are walking ecosystems and “we contain multitudes” as the science journalist Ed Yong puts it.⁹ We live in harmony with most of these microbes; some are even beneficial, they help us digest food, build immune systems, and may even

contribute to our mental health.¹⁰⁻¹¹ Occasionally however, some microbe-human relationships go rogue, with devastating consequences.

Before 1940, infections were a leading cause of death.¹² The standard treatment for tuberculosis used to be fresh air; any chance of infection, even a paper cut could be fatal. The advent of antibiotics, considered by many to be one of the greatest achievements in modern medicine, has greatly reduced the mortality of bacterial infections in the United States and around the globe.¹³⁻¹⁴ Antibiotics, together with vaccination, sanitation and better hygiene practices to control infectious diseases¹⁵ contribute to an increase in successful child birth, a sharp drop in infant and child mortality¹⁶ and doubling of the average lifespan.¹⁷ Unfortunately, resistance has accompanied antibiotics from nearly the first day of their use¹⁸⁻¹⁹ and the influences of resistance have grown constantly over time.²⁰⁻²¹

Contrary to popular belief, resistance is not a new phenomenon. The first reports of a pathogen developing resistance to penicillin appeared in 1944,²²⁻²⁴ a mere year after the drug began to be mass produced in 1943. Even Alexander Fleming, the discoverer of penicillin, warned of the development of resistance in his 1945 Nobel Prize acceptance speech.²⁵ He described a hypothetical scenario where Patient X, who:

buys some penicillin and gives himself, not enough to kill the streptococci but enough to educate them to resist penicillin. He then infects his wife. Mrs. X gets pneumonia and is treated with penicillin. As the streptococci are now resistant to penicillin the treatment fails. Mrs. X dies.

Indeed, resistance has been found for every antibiotic ever discovered.²⁶⁻²⁷

The origin of antibiotic resistance can be dated long before antibiotics being used by humans²⁸⁻³⁰ as studies have shown that antibiotic biosynthetic pathways and antibiotic resistant mechanisms began to co-evolve at least 30,000 years ago.³¹⁻³² Consistent with this notion is the finding that antibiotic resistance occurs in microbes isolated from extreme natural habitats including the deep ocean³³ and deep terrestrial subsurface³⁴, places

presumably that have little human influence.³⁵⁻³⁶ These reports suggest the unpleasant conclusion that resistance cannot be eradicated and thus humans must continue to develop new agents to treat otherwise intractable bacterial infections.³⁷⁻⁴⁰

Historically, resistance was not a big concern because new antibiotics kept being launched into the market. From the discovery of the antimicrobial effects of sulfonamides in 1932 by the German bacteriologist and pathologist Gerhard Domagk, penicillin and streptomycin were discovered in 1943, tetracycline in 1945, cephalosporin in 1948, erythromycin in 1949, and vancomycin in the 1950s. New classes of antibiotics were constantly emerging, not to mention upgrades of existing ones were also occurring.

Since the end of the so-called “golden era” of antibacterial drug discovery in the 1970s, however, only two new classes of antibiotics have been launched to the market, linezolid⁴¹⁻⁴² and daptomycin.⁴³⁻⁴⁵ Not unexpectedly, resistance to both have been detected⁴⁶⁻⁵¹. Unfortunately, the rate of antibacterial discovery has slowed dramatically, and many big pharmaceutical companies have stopped developing new antibiotics.⁵²⁻⁵⁴ Based on a review article published in 2016,⁵⁵ there are only 40 products in the antibiotic pipeline, compared to more than 120 compounds for treatment of non-small cell lung cancer and melanoma alone, for example.

Antimicrobial resistance has enormous health and economic implications. It is estimated that antimicrobial resistance is directly responsible for 23,000 deaths annually in the United States⁵⁶ and more than 25,000 in the European Union.⁵⁷⁻⁵⁸ A conservative estimate of the economic cost of bacterial resistance in the United States is \$20 billion in healthcare costs and \$35 billion in societal costs annually.⁵⁹ Moreover, since antibiotics are often used as prophylaxis, resistance has the potential to lead us back to a pre-antibiotic world.⁶⁰⁻⁶¹ For example, surgeries would become more dangerous. Economists have used hip

replacements as an example and estimated that the infectious rate would rise from 0.5-2% currently (with antibiotics) to 40-50% without effective antibiotics and 30% of patients would die.⁶² The most authoritative prediction of the impact of antimicrobial resistance was published in the *Review on Antimicrobial Resistance* by a team lead by the world-renowned macroeconomist Lord Jim O'Neill,⁶³ former chairman of Goldman Sachs Asset Management, and former British government minister. He estimated that by 2050, based on the current rate of resistance and if no interventions take place, deaths from antimicrobial resistance could skyrocket to 10 million each year and cost \$100 trillion globally. No other diseases except pandemic influenza can make such a claim. In fact, if the current trend is not altered, antimicrobial resistance could become the world's single greatest killer, surpassing heart disease or cancer.⁶⁴

In 2013, the Centers for Disease Control and Prevention (CDC) published a list of 18 drug-resistance threats to the United States.⁶⁵ The list was further grouped into three different urgent categories: urgent, serious and concerning threats (Table 1). Three bacteria were listed in the urgent threat category: *C. difficile*, carbapenem-resistant *Enterobacteriaceae* and *N. gonorrhoeae*.⁶⁵ The first two usually affect patients in medical facilities and/or those being treated with other antibiotics; however *N. gonorrhoeae* is a sexually transmitted disease that can infect healthy people.⁶⁶⁻⁶⁷ In early 2018, a man in the United Kingdom was diagnosed with a strain of *N. gonorrhoeae* that is resistant to all existing classes of antibiotics, perhaps the first occurrence of such an infection.⁶⁸ The sexual transmission of these strains means that antibiotic resistance could spread much more rapidly. Twelve additional bacterial strains were grouped in the serious threat category.⁶⁵ Among them are notorious bacteria such as multidrug-resistant *Pseudomonas aeruginosa*, methicillin-resistant *S. aureus* (MRSA), and drug-resistant *M. tuberculosis*. A

fungal infection, fluconazole-resistant *Candida*, was also included in the list. *Candida* is ranked 4th in a list of the most common hospital-acquired bloodstream infections,⁶⁹ and it is estimated to cause more than 400,000 cases annually, mostly in developed countries.⁷⁰ Vancomycin-resistant *S. aureus* (VRSA) was in the concerning threat group.⁶⁵

Table 1. Drug-resistant threat to the United States.

Threat level	Microbes
Urgent	<i>C. difficile</i>
Serious	Carbapenem-resistant Enterobacteriaceae
	Drug-resistant <i>N. gonorrhoeae</i>
	Multidrug-resistant <i>Acinetobacter</i>
	Drug-resistant <i>Campylobacter</i>
	Fluconazole-resistant <i>Candida</i>
	Extended spectrum β -lactamase producing Enterobacteriaceae (ESBLs)
	Vancomycin-resistant <i>Enterococcus</i> (VRE)
	Multidrug-resistant <i>Pseudomonas aeruginosa</i>
	Drug-resistant non-typhoidal Salmonella
	Drug-resistant <i>Salmonella</i> Typhi
	Drug-resistant <i>Shigella</i>
	Methicillin-resistant <i>Staphylococcus aureus</i> (MRSA)
	Drug-resistant <i>Streptococcus pneumoniae</i>
Drug-resistant tuberculosis	
Concerning	Vancomycin-resistant <i>Staphylococcus aureus</i> (VRSA)
	Erythromycin-resistant Group A <i>Streptococcus</i>
	Clidamycin-resistant Group B <i>Streptococcus</i>

Clearly, the threat of infections from resistant microbes is real. There is an urgent and growing need for new antibiotics, particularly ones with novel mechanisms of action. One potential target for new therapeutics lies in the *de novo* purine biosynthetic pathway.

1.2 Purine nucleotide biosynthesis

Nucleotides play a variety of essential roles in cellular function. Most notably, they are the building blocks of DNA and RNA and act as carriers of chemical energy (ATP and to some extent GTP). Nucleotides are also components of cofactors such as NAD, FAD and coenzyme A and they can act as chemical messengers, such as cAMP and cGMP.⁷¹ The concentration of nucleotides in cells varies by its function and tissue type. The concentration of ATP concentration is quite high, while the cellular pools of other nucleotides are usually limited to less than that needed to synthesize 1% of the genome.⁷¹ Therefore, cells must constantly make nucleotides during rapid proliferation, suggesting that relevant biosynthetic enzymes may be logical targets against rapid dividing cells in diseases such as cancer and infections.⁷² Inhibitors against nucleotides biosynthesis, such as fluorouracil, methotrexate and mercaptopurine are valid and important chemotherapeutic and anti-viral agents.

1.2.1 Salvage pathway⁷¹

Given the critical nature of purine nucleotides to life, it is not surprising that there are two pathways for their synthesis: the *de novo* and the salvage pathways. *De novo* synthesis assembles nucleotides from basic metabolic precursors, including amino acids, ribose 5-phosphate, CO₂, and NH₃ (Figure 1). The salvage pathways recycles free bases released from nucleic acid breakdown. Free adenine is salvaged by adenosine phosphoribosyltransferase which catalyzes the reaction of adenine with phosphoribosyl pyrophosphate (PRPP) to yield adenosine nucleotide. Free guanine and hypoxanthine are recycled in the same way by hypoxanthine-guanine phosphoribosyltransferase. These

salvage pathways play an important role in recycling nucleotides from the environment/tissue, and are usually considered necessary for maintaining cellular functions, while the *de novo* pathway is required for cell division.

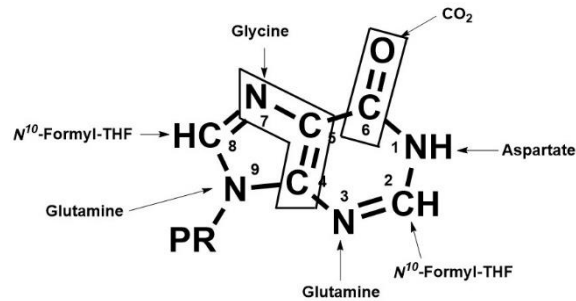


Figure 1. Precursors of inosine monophosphate used in *de novo* purine biosynthesis. PR is ribose phosphate.

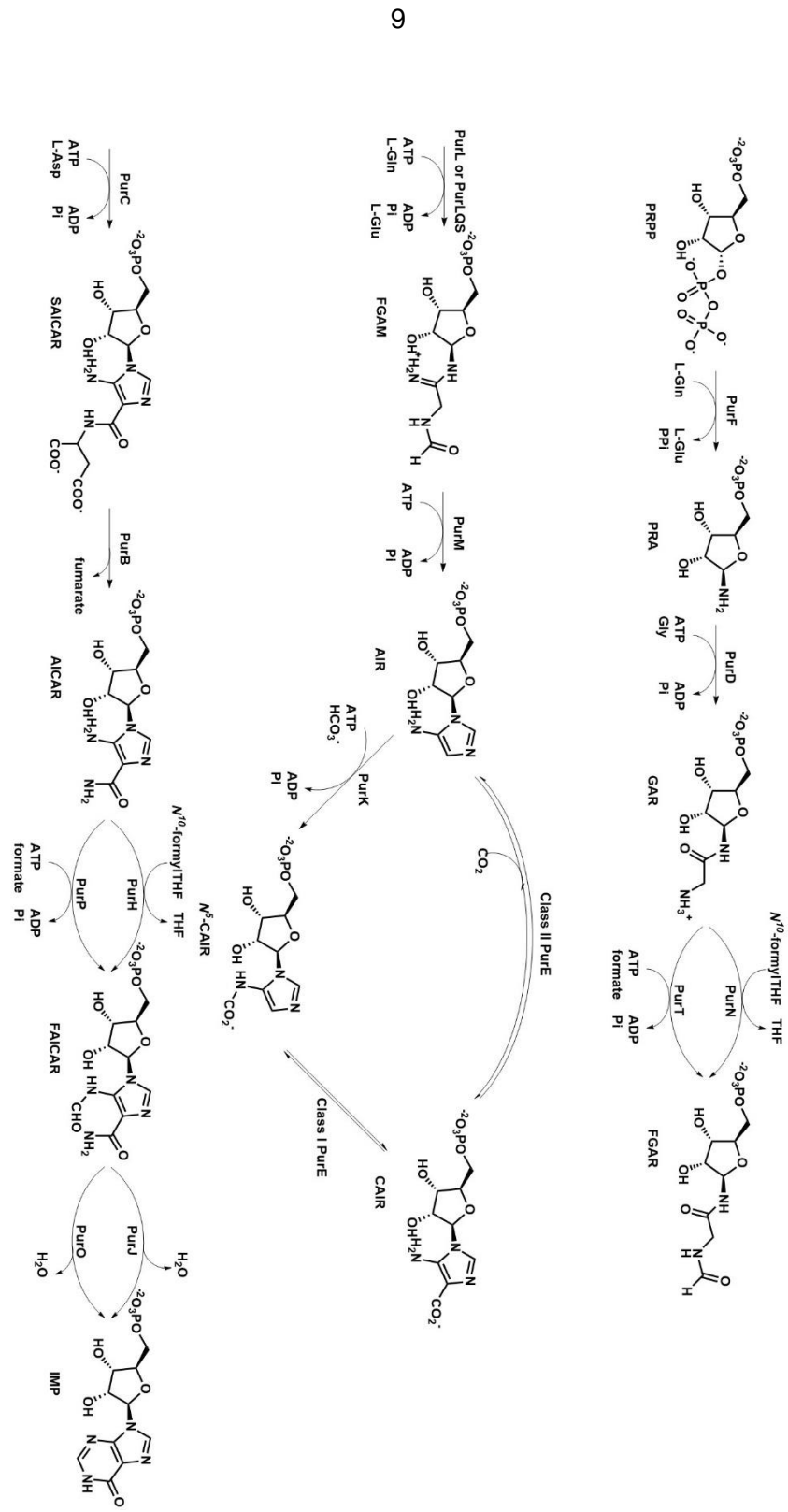
1.2.2 De novo pathway

In mammalian cells, the *de novo* synthesis of purines (Figure 2) starts from PRPP and takes 10 steps, while consuming 4 molecules of ATP. Microbes undergo a similar process except one additional energy-consuming step is necessary.⁷³⁻⁷⁵ Thus, in microbes, 11 steps are needed along with 5 molecules of ATP. The detailed pathway of purine biosynthesis was worked out primarily by John Buchanan and G. Robert Greenberg in the 1950s from isotopic tracing experiments.⁷¹ Atoms from basic precursors are connected to ribose phosphate creating the purine ring in a step-wise manner.

In the first committed step, N-9 is connected to the sugar. An amino group, donated by glutamine, is attached to the C-1 position of PRPP yielding 5-phosphoribosylamine (PRA), a short-lived intermediate with a half-life of only 38 seconds at pH 7.5.⁷⁶ In the second step, C-4, C-5 and N-7 are added onto the amino group of PRA from glycine, resulting in glycinamide ribonucleotide (GAR). ATP is used in this step to activate the glycine carbonyl group for condensation with the amine. Formylation of the amino group of GAR occurs in the third step to give *N*¹⁰-formyl glycinamide ribonucleotide (FGAR); this reaction adds C-8.

The fourth step converts the amide from the second reaction into an imine and adds N-3 by the addition of ammonia (from glutamine), while also consuming a molecule of ATP. The fifth step is a dehydration and ring closure reaction, yielding the five-membered ring, aminoimidazole ribonucleotide (AIR). This step requires ATP to activate the formyl group. At this point, the five-membered ring and three atoms of the six-membered ring (N-3, C-4, and C-5; C-4 and C-5 are shared between the two rings) are in place, requiring the addition of another two carbons and one nitrogen atom. C-6 is added in the sixth step, which represents a major difference between mammalian and microbial *de novo* purine synthesis.⁷³⁻⁷⁵ In mammals, carbon dioxide is added directly to the C-5 of AIR to generate carboxyaminoimidazole ribonucleotide (CAIR). In microbes, bicarbonate and ATP are used to add CO₂ to the exocyclic amine of AIR (N-3) to generate N⁵-carboxyaminoimidazole ribonucleotide (N⁵-CAIR). Rearrangement of the CO₂ group from N-3 to C-5 later generates CAIR. A detailed description of this clade-specific divergence is provided in the following section. The seventh and eighth steps add the last nitrogen (N-1) to the skeleton via an energy-consuming amide bond forming reaction between C-6 and aspartate amino group followed by the elimination of fumarate to give aminoimidazole-4-carboxamide ribonucleotide (AICAR). The final carbon, C-2, is contributed by N¹⁰-formyltetrahydrofolate. The last step is a second ring closure event, yielding the purine nucleus inosine monophosphate (IMP). IMP is then converted to GMP and AMP by subsequent enzymes.

For clearness and simplicity, enzymes involved in *de novo* synthesis are not described in the text above. Abbreviations of the enzyme names are used in Figure 2 and throughout the following text. Full names of the enzymes are listed in Table 3.



9

Figure 2. De novo purine biosynthetic pathway.

Table 2. List of abbreviations of intermediates in *de novo* purine biosynthetic pathway.

Abbreviations	Full names
PRPP	5-Phosphoribosylpyrophosphate
PRA	5-Phospho-D-ribosylamine
GAR	Glycinamide ribonucleotide
FGAR	N-Formylglycinamide ribonucleotide
FGAM	N-Formylglycinamide ribonucleotide
AIR	Aminoimidazole ribonucleotide
N^5 -CAIR	N^5 -Carboxyaminoimidazole ribonucleotide
CAIR	Carboxyaminoimidazole ribonucleotide
SAICAR	Succino 5-aminoimidazole-4-carboxamide ribonucleotide
AICAR	Aminoimidazole-4-carboxamide ribonucleotide
FAICAR	5-Formamido-4-imidazolecarboxamide ribonucleotide
IMP	Inosine monophosphate

Table 3. List of abbreviations of enzymes in *de novo* purine biosynthetic pathway.

Gene name	Enzyme Abbreviations	Enzyme Full names
<i>purF</i>	PurF	Aminophosphoribosyltransferase
<i>purD</i>	PurD	GAR synthetase
<i>purN</i>	PurN	GAR transformylase
<i>purT</i>	PurT	FGAR synthetase
<i>purL</i>	PurL	FGAR synthetase
<i>purM</i>	PurM	AIR synthetase
<i>purE</i> (Class II)	PurE Class II	AIR carboxylase
<i>purK</i>	PurK	N^5 -CAIR synthetase
<i>purE</i> (Class I)	PurE Class I	N^5 -CAIR mutase
<i>purC</i>	PurC	SAICAR synthetase
<i>purB</i>	PurB	SAICAR lyase
<i>purH</i>	PurH	AICAR transformylase
<i>purP</i>	PurP	AICAR synthetase
<i>purJ</i>	PurJ	IMP cyclohydrolase
<i>purO</i>	PurO	IMP cyclohydrolase

1.3 Divergences in the *de novo* pathway

Several differences exist between prokaryotes and eukaryotes in the enzymes catalyzing the *de novo* pathway. These represent potential novel antimicrobial targets and are outlined and discussed in detail here.

PurF: PurF catalyzes the first step in *de novo* purine synthesis, which is the conversion from PRPP to PRA. Structurally, two types of PurF have been found. The first is found in

higher vertebrates, plants, cyanobacteria, and Gram-positive bacteria, while the second is from yeast and Gram-negative bacteria.⁷⁷⁻⁸⁰ The main difference is that the first type contains a structural Fe₄S₄ cluster⁸¹ and a cleavable N-terminal propeptide, while the second does not. PurFs from *B. subtilis*⁸²⁻⁸³ and *E. coli*⁸⁴⁻⁸⁵ have been studied extensively. The two enzymes share 40% sequence identity and are structurally homologous.

PurD: Only one known enzyme PurD catalyzes the second step, from PRA to GAR. In *E. coli*, it is a single enzyme, in higher organisms, however, PurD is fused with PurM and PurN forming a trifunctional enzyme.

PurN/PurT: Two different enzymes catalyze the third, formylation step. PurN is found in most organisms and formylates the amino group using N¹⁰-formyltetrahydrofolate. In higher organisms, PurN is the C-terminal domain of the trifunctional enzyme PurD-PurM-PurN. Researchers have investigated human PurN as an anticancer target.⁸⁶⁻⁹² *E. coli* can use an alternative enzyme PurT to catalyze this transition, and some archeobacteria have been found to rely solely on PurT. PurT is an ATP-grasp enzyme⁹³⁻⁹⁴ and catalyzes the ATP-assisted ligation directly using formate as the carbon source.⁹⁵⁻⁹⁶ Being a redundant metabolic enzyme, PurT is generally not considered a therapeutic target. A recent study from Denmark however demonstrated that single-gene deletion of either *purT* or *purN* resulted in attenuation in *Salmonella enterica* serovar Typhimurium.⁹⁷ This result suggests a revisit of the redundancy relationship of PurT and PurN is merited.

PurL: Two different types of PurL have been found, termed large and small based on their respective sizes. Large PurL is found in eukaryotes and Gram-negative bacteria, while small PurL is found in Gram-positive bacteria and archaea.^{72, 98-99} Large PurL has three domains: the glutaminase, the FGAM synthetase, and the N-terminal domains. The glutaminase domain produces ammonia, which is then channeled to the FGAM synthetase

domain.¹⁰⁰ The N-terminal domain helps to form the ammonia channel that links the other two catalytic domains.⁹⁸ Small PurL only contains the FGAM synthetase domain and requires assistance from PurQ and PurS to complete its function.^{98, 101} PurQ is homologous to the glutaminase domain in large PurL,¹⁰² while PurS is similar to the N-terminal domain.¹⁰³ Recently, researchers have reconstructed the PurLSQ complex from *B. subtilis* and small molecules such as MgADP and glutamine have proved necessary for complex formation.⁹⁹

PurK, class I and II PurE (Figure 3): The largest divergence in the *de novo* purine synthesis pathway lies in the steps used to convert AIR to CAIR. Mammalian cells and microbes utilize different enzymes and different intermediates to complete this process.^{73-75, 104} In vertebrates, it is a one-step conversion;⁷⁴ however, two individual steps are needed in bacteria,^{73, 75, 104} yeast, and fungi.¹⁰⁵ In human cells, AIR is carboxylated by class II PurE to CAIR directly utilizing CO₂ as the carbon source.^{74, 105-107} No energy is needed in this transition. Mechanistically, direct carboxylation without co-factors such as biotin is unusual, and this step has attracted investigation from many researchers.¹⁰⁸ In bacteria, yeast, and fungi, this conversion is broken down into two sequential steps. AIR is first converted by PurK to N⁵-CAIR using HCO₃⁻ as the one carbon source and consuming one molecule of ATP.^{75, 104} N⁵-CAIR then undergoes direct CO₂ transfer from N5 to C4 to generate CAIR.¹⁰⁹⁻¹¹⁰ This second reaction is catalyzed by class I PurE. One type of bacteria however, the spirochete dental pathogen *Treponema denticola*, was found to contain a class II PurE with no PurK, and this is the first and only example of a prokaryotic class II PurE.¹¹¹

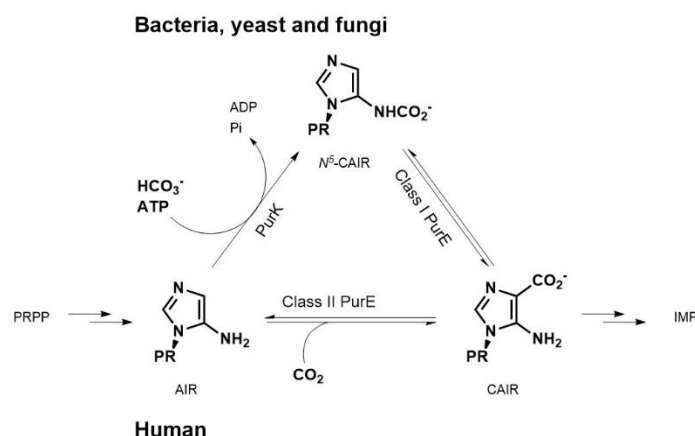


Figure 3. Divergence between microbial and human *de novo* purine pathway. PR is ribose phosphate.

Class I and II PurEs both form octamers in the native state,^{106, 110, 112-113} and their structures can be largely superimposed. They also share considerable sequence similarities. It is intriguing how these two almost identical enzymes catalyze distinct reactions. In human cells, class II PurE is fused with PurC to form a bifunctional enzyme.¹¹⁰ A third type of PurE is found in archaea. Some methanobacteria have a *purE-purE'* gene that encodes a 37 kDa polypeptide,¹¹⁴ twice the length of both Class I and II PurE. The C-terminus half of the polypeptide can be aligned with its N-terminus half with 36% identity. Only the N-terminal half contains the universally conserved active site residues that exist in both class I and class II PurE, and its sequence can be characterized as a class I PurE by class-specific residues.¹¹⁵ Although sequence alignment suggests methanogens contain a class I PurE, the whole protein encoded by the *M. thermoautotrophicum purE-purE'* gene has been purified and characterized to be a pure class II PurE utilizing AIR and CO₂ as substrates without ATP.¹¹⁶ Complementary assays have been conducted on the *M. smithii* whole *purE-purE'* gene and several truncated versions. Only the complete sequence can complement both PurK and PurE deficient *E. coli* strains; deletions of peptides of the length of 9 kDa, 25 kDa, 28 kDa and 30 kDa from the C-terminus, or even 7 amino acids at the

beginning of the C-terminus half abolished its ability to complement either PurK or PurE deficient strains.¹¹⁷⁻¹¹⁸ The methanogen PurE-PurE' is the only identified PurE which may have an N-terminal PurE fused with other proteins. In other fused PurE system, such as the human bi-functional PurCE,^{74, 106} yeast bi-functional PurKE,¹⁰⁵ the PurEs are all at the C-terminus. No PurK homolog has been found in these organisms.

In contrast with the three different types of PurEs, PurK is found only in microbes and does not have any human homologs. It is a separate enzyme in bacteria but fused with class I PurE as a bifunctional enzyme in fungi.¹⁰⁵ PurK is a member of the ATP-grasp enzyme superfamily¹¹⁹⁻¹²⁰ and it forms a dimer in its native state.¹²¹

PurH, PurJ/PurP, PurO: Archaea use different enzymes in the last two steps compared to bacteria and eukaryotes. PurH and PurJ are found in bacteria and eukarya,¹²² while PurP and PurO occur in archaea.¹²³ PurH catalyzes formylation of AICAR in a manner similar to PurN, using *N*¹⁰-formyltetrahydrofolate as a cofactor.¹²⁴ In contrast, PurP is like PurT, catalyzing an ATP-assisted ligation of AICAR with formate.¹²³ PurHJ is a bi-functional enzyme^{122, 125} and has been explored as an anticancer target.¹²⁶⁻¹²⁷

1.4 Target verification of PurK

Since the differences in the step from AIR to CAIR is divided strictly from mammalian cells to microbes, it is logical to explore PurK and microbial class I PurE as potential antimicrobial targets. There have been published studies on the development of inhibitors of both PurE¹²⁸⁻¹²⁹ and PurK.¹³⁰ The development of PurE inhibitors is challenging because Class I and Class II PurEs are evolutionarily related. They each form an octamer in the native state, and their structures can be largely superimposed. They also share considerable sequence similarities complicating the discovery of class-specific inhibitors.

Indeed, the only known selective inhibitor of PurE shows selectivity for Class I over Class II PurE.^{108, 129}

PurK, on the other hand, does not have any human homologs. Therefore, it is more likely that selective antimicrobial agents targeting PurK could be identified. Genetic studies on PurK support the role of the enzyme in microbial growth and disease progression. In the 1950s, Bacon described the loss of virulence of *Bacterium typhosum* mutants with purine synthesis deficiencies in a murine intraperitoneal infection model.¹³¹⁻¹³³ Studies with different microorganisms, such as *S. aureus*,¹³⁴ *Bacillus anthracis*,¹³⁵ *Candida albicans*,¹³⁶ and *Cryptococcus neoformans*¹³⁷ both in vivo and in vitro have given similar results. These results have also shown that the salvage pathway alone is not sufficient to produce enough purines for growth, validating the *de novo* purine pathway as an antimicrobial target. Taken together, both biochemical and genetical evidence support that PurK is an attractive antimicrobial target.

1.5 Previous attempts at PurK inhibitor development

Despite intensive biochemical and structural investigations of PurK, no one has developed selective inhibitors of this enzyme. To fill in this gap, our lab previously conducted a high-throughput screening study.¹³⁰ Using a UV-based discontinuous assay measuring the free phosphate concentration in the system, we screened a 48,000 drug-like commercially available library. The screen identified 14 hits; however, additional studies revealed that none of these agents actually bound to PurK. Instead, 12 out of 14 agents covalently reacted with AIR.¹³⁸ One compound was riboflavin, a vitamin, and several analogs of the last agent failed to give improved activity against the enzyme. Thus, a new approach towards identifying inhibitors against PurK was needed. This previous work forms the basis for this thesis.

1.6 ATP-grasp Family

1.6.1 General introduction

One approach towards finding inhibitors is to examine inhibitors of biochemically related enzymes. PurK belongs to the ATP-grasp enzyme superfamily.^{112, 121, 139-141} The ATP-grasp enzymes catalyze the ligation between an amino group and an activated carboxylate.¹¹⁹⁻¹²⁰ Activation requires one molecule of ATP to generate a proposed acylphosphate intermediate,¹⁴²⁻¹⁴³ though this intermediate has not been captured by crystallization. Enzymes within this family share a large degree of structural similarity among their ATP-binding domains. In fact, the name of this group, ATP-grasp, is derived from the unique binding orientation of ATP in its ATP-binding site.

Structurally, the ATP-grasp family is characterized by a three-domain architecture with A, B and C domains⁹³ (Figure 4). The A and C domains form a central cleft where substrates reside.^{94, 144} The B domain holds ATP and is flexible upon nucleotide binding.^{123, 145} The polyphosphate group of the ATP is firmly bound to a conserved P-loop in the B domain and interacts with one to three Mg^{2+} ions.⁹⁴ The high degree of topological similarity of the ATP-binding domain is the signature of the ATP-grasp enzymes.

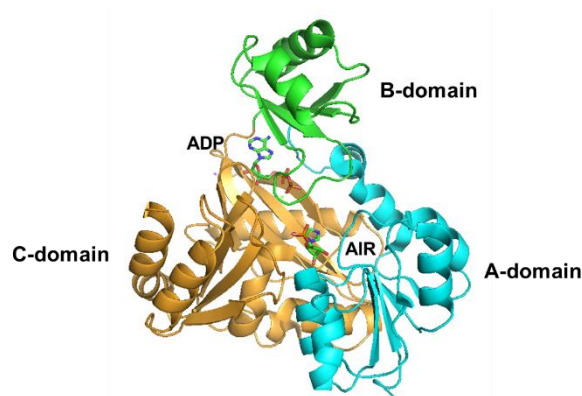
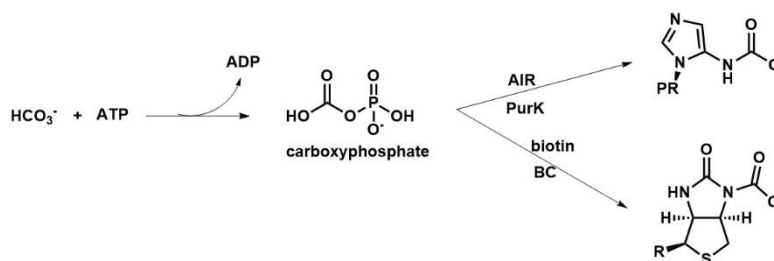


Figure 4. General representation of the ATP-grasp enzymes based on the 3-D structure of the *A. clavatus* PurK enzyme (PDB ID: 3K5I).

Mechanistically, the ATP-grasp enzymes catalyze their reactions in a two-step fashion.¹⁴⁶⁻¹⁴⁸ First, the carboxylate is activated by ATP to generate an acylphosphate intermediate. Second, nucleophilic attack on the activated carbonyl group by the amino group occurs, eliminating free phosphate and resulting in the final ligation amide product.

About 20 enzymes have been found to belong to this family. Four enzymes in the *de novo* purine biosynthetic pathway, PurD, PurT, PurK and PurP belong to this group, implying evolutionary significance.¹⁴⁹ Other ATP-grasp enzymes play important roles in various critical metabolic pathways, such as fatty acid synthesis, gluconeogenesis and cell metabolism.¹¹⁹ Another member of this superfamily is biotin carboxylase (BC). BC catalyzes the first committed step in fatty acid synthesis, which is the ATP-dependent carboxylation of biotin using HCO_3^- as the one carbon source.¹⁵⁰ Mechanistically, the first half reactions of BC and PurK are identical, namely the activation of bicarbonate by ATP to generate the putative common intermediate, carboxyphosphate¹⁵¹⁻¹⁵² (Figure 5a). The second reaction is the carboxylation of the substrate to generate the desired product and phosphate. Structural comparisons of both enzymes indicate that the ATP-grasp domains of PurK^{139-140, 153} and BC^{148, 154} can be largely superimposed (Figure 5b). Root mean square deviation (RMSD) in the aligned ATP-grasp regions is 1.609 Å, and the distances between the 6-NH₂ and 2'-OH of the two aligned ADPs are 1.1 Å and 1.5 Å, respectively.

a. Reaction



b. Structure

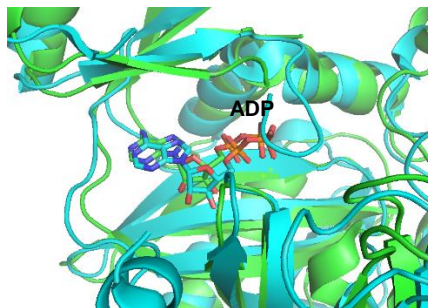


Figure 5. Similarities between PurK and BC. a. Reaction similarity. b. Crystal structural superimposition of PurK (pdb: 3K5I, green) and BC (pdb: 2J9G, cyan) with ADP in the binding sites of both enzymes.

1.6.2 ATP-site inhibitors of ATP-grasp family

It has been estimated that about 9-10% of all enzymes bind ATP, and cells contain ATP in the millimolar range.¹⁵⁵ It is no doubt challenging to develop selective inhibitors against a particular ATP-binding enzyme while also being able to compete against the high cellular concentration of ATP. However, kinase and phosphatase inhibitors are mainstream drugs for important diseases and demonstrate that these challenges can be overcome.¹⁵⁶⁻¹⁵⁸ In contrast, relatively few studies on inhibitors of ATP-grasp enzymes have been reported. However, one critical study came from Pfizer's work on BC.¹⁵⁹⁻¹⁶⁰

In a phenotypic HTS campaign,¹⁶⁰ researchers from Pfizer focused on finding compounds that inhibited bacteria growth using a library of protein kinase inhibitors. A group of pyridopyrimidine compounds were found to possess potent antibacterial activity. The mechanism of action of these compounds was via inhibition of fatty acid synthesis specifically by targeting the ATP-grasp domain of BC. Investigations of additional analogs revealed a pyridopyrimidine (compound **1** Figure 6) with a K_d of 0.8 nM against purified *E. coli* BC with an IC_{50} of less than 5 nM in *in vitro* activity testing. X-ray crystallography studies

confirmed that these pyridopyrimidines bound to the ATP-site of the ATP-grasp domain of BC. Researchers also confirmed the selectivity of these agents against other ATP-utilizing enzymes, demonstrating that the ATP-grasp domain was divergent enough for selective targeting over protein kinases. Encouraged by these results, follow-up studies¹⁵⁹ were carried out using virtual and fragment-based methods, and additional ATP-site inhibitors with diverse scaffolds (Figure 6. The rest than compound 1) were identified. These pioneering proof-of-concept studies demonstrated that bacterial ATP-grasp enzymes could be selectively targeted over other ATP-utilizing enzymes and that these agents could be promising antimicrobial compounds. Inspired by the encouraging BC inhibitors published by Pfizer, a group of researchers from Slovenia and the UK tested the pyridopyrimidines against D-ala-D-ala ligase and demonstrated moderate inhibition activity.¹⁶¹

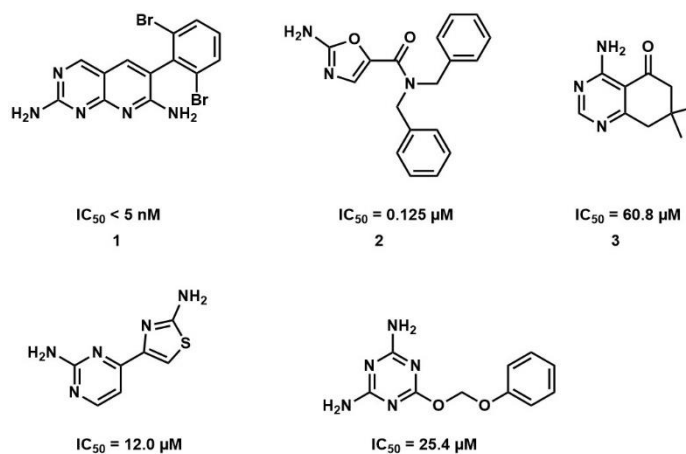


Figure 6. ATP-binding site inhibitors of BC developed by Pfizer.

At approximately the same time, a similar study from Schering-Plough was independently reported.¹⁶²⁻¹⁶⁴ Using an affinity-based assay coupled with mass spectroscopy, researchers identified a group of benzimidazole (Figure 7) compounds with low micromolar affinity against BC. Rapid hit-to-lead research resulted in the best compound possessing an IC_{50} of 20 nM with confirmed antibacterial activity. The authors

demonstrated that these compounds inhibit fatty acid synthesis but spare DNA, RNA, and protein synthesis. They also validated the target by using an *E. coli* strain sensitized to BC inhibitors by overexpression of apo-BCCP. These independent reports of distinct chemical classes of BC inhibitors demonstrate that the selective targeting of the ATP-grasp domain can be done and that these agents have the potential to be antimicrobial agents.

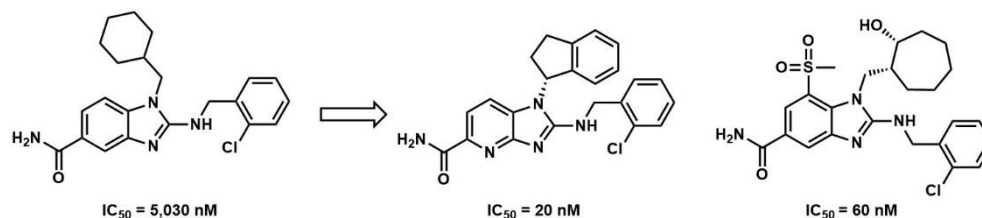


Figure 7. ATP-binding site inhibitors of BC developed by Schering-Plough.

Inspired by the reported high potency of ATP-site inhibitors of BC and the similarity between PurK and BC, we decided to test BC inhibitors to see if they provide a starting point to further develop selective PurK inhibitors. The results outlined below indicate that these agents can indeed be inhibitors of PurK, although with modest affinity when compared to BC. Our results have also provided information on the binding of these agents to PurK.

CHAPTER 2 RESULTS AND DISCUSSIONS

2.1 Preliminary testing of potent BC inhibitors against PurK

2.1.1 Synthesis

Three potent BC inhibitors (**1**, **2**, and **3** in Figure 6) were selected to test as potential inhibitors of PurK. These compounds were selected because they are the most potent BC inhibitors in the Pfizer study and are either synthetically accessible (**1** and **2**) or commercially available (**3**). A fourth compound **4**, 6-methylpyrido[2,3-d]pyrimidine-2,4-diamine, was selected because it is commercially available and structurally similar to compound **3** and **1**. To reduce the influences of the side chains only keeping the core scaffold, we deleted the dibromo substituents on the 6-pheny ring of compound **1**. The dibromo compound was later tested as a derivative in section 2.3.2 as compound **11**. Compounds and their numbers used in this preliminary test are listed in Figure 8.

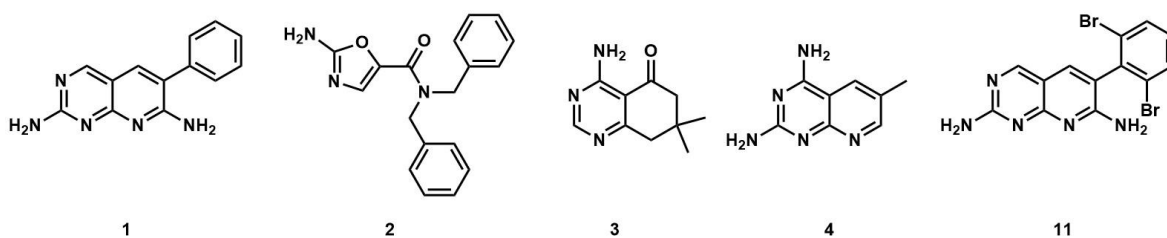
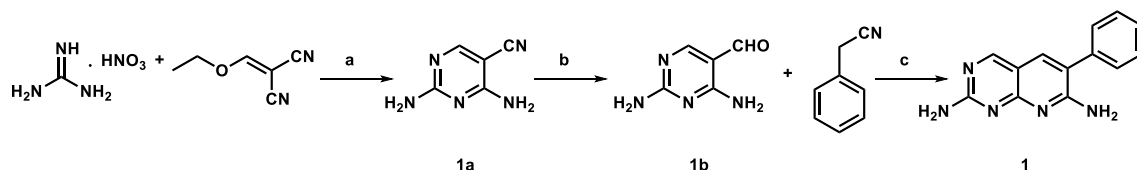


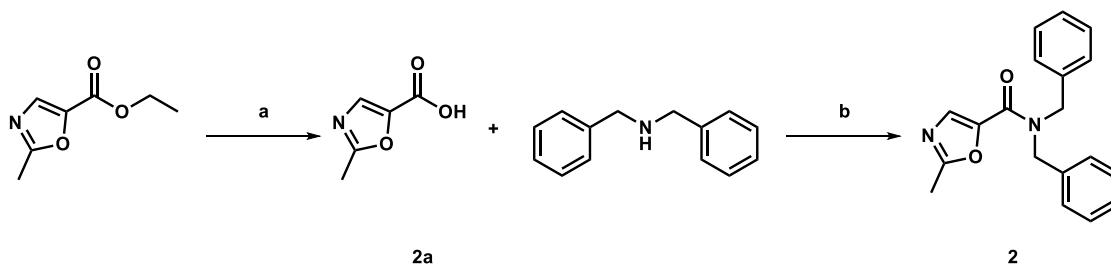
Figure 8. Compounds tested in the preliminary study.

Compound **1** and **2** were made following literature methods¹⁵⁹⁻¹⁶¹ from commercially available starting materials (Schemes 1 and 2). The approach outlined in scheme 1 gave the desired heterocyclic pyridopyrimidine starting from the pyrimidine ring. The pyrimidine was made by a ring formation reaction using commercially available starting materials guanidine nitrate and (ethoxymethylene)malononitrile. The nitrile group of **1a** was readily reduced to aldehyde (**1b**) by Raney nickel in formic acid. The final pyrido[2,3-*d*]pyrimidine scaffold was prepared through a condensation reaction with benzyl nitrile. The approach

described in scheme 2 gave the second scaffold to be tested, methyloxazole carboxamide. This compound was made from the commercially available ethyl 2-methyloxazole-4-carboxylate. Base hydrolysis revealed the carboxylic acid group, which was subsequently activated with HBTU and condensed with dibenzylamine to give the desired amide **2**.



Scheme 1. Synthesis of pyrido[2,3-*d*]pyrimidines. Reagents and conditions: (a) NaH, EtOH, -5 °C to r.t., 18 h, 83%; (b) Ra-Ni, 98-100% HCOOH, reflux, 18 h, 89%; (c) NaH, EtO(CH₂)₂OH, reflux, 4 h, 84%.



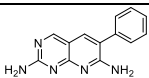
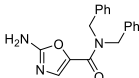
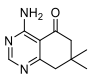
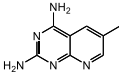
Scheme 2. Synthesis of methyloxazole-carboxamide. Reagents and conditions: (a) 2 M NaOH, 60 °C, 45 min, 82%; (b) HBTU, NMM, DMF, r.t., 18 h, 20%.

2.1.2 BC inhibitor pyrido[2,3-*d*]pyrimidine weakly inhibited PurK_{Asp}

We collected three potent BC inhibitors, **1**, **2**, **3**, and another structurally related compound **4** and tested them against PurK from *E. coli* and *A. clavatus* (Table 4). Residual activities (RA%) were collected at a single inhibitory concentration, either 100 or 200 μM (depending upon solubility), using the malachite green assay we previously developed to monitor PurK activity.¹³⁰ This assay is a discontinuous assay and measures the free phosphate concentration in a system. To compare inhibitory activity with the enzyme substrate ATP, adenine and adenosine were used as positive controls. Compounds **1** and

4 weakly inhibited PurK from *A. clavatus* whereas **2** and **3** were completely inactive at the concentrations tested. Compound **1** also exhibited weak inhibitory effect against PurK from *E. coli*. The enzymatic reaction time was optimized for different ATP concentrations to ensure the reaction stays in the linear range, and the assay was used for PurK kinetics with varied ATP concentration, while holding the concentration of AIR fixed. Steady state kinetics of **1** against PurK from *E. coli* confirmed that it is competitive with ATP and has a K_i of 255 μM (Figure 9). These results validate that **1** binds to the ATP site of PurK as expected.

Table 4. Activity of BC inhibitors against PurK.

#	Structure	Conc. (μM)	RA%	
			PurK _{Asp}	PurK _{E.coli}
1		200	43	83
2		100	101	102
3		200	97	101
4		200	82	--
	Adenine	200	91	91
	Adenosine	200	53	53

-- Not tested.

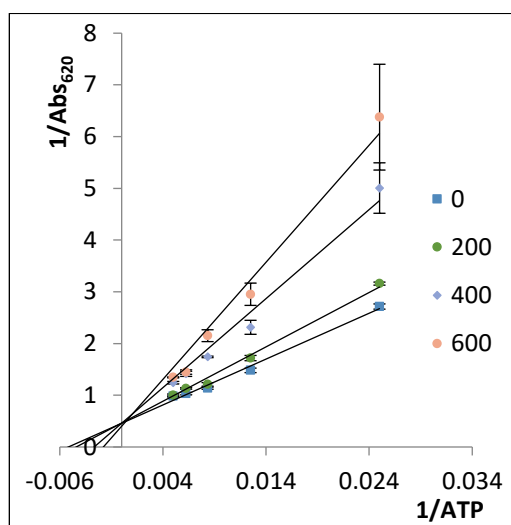


Figure 9. Lineweaver-Burke plot of **1** against PurK_{*E. coli*} using the malachite green assay. The concentration of **1** (μM) is listed to the right of the graph.

2.2 Computation studies suggested optimization positions

While we expected that the BC inhibitors would not be as potent against PurK, we were puzzled by the $\sim 250,000$ -fold weaker inhibitory activity of these inhibitors against PurK. Using a computational binding model generated by superimposition of the ATP-grasp regions of BC and PurK, we could propose theories explaining the decreased activity and potential positions for structural modifications to attempt to improve activity. We also examined the structures to identify the potential reasons why pyridopyrimidine **1** inhibited PurK from *A. clavatus* better than that from *E. coli*. Four X-ray structures were used in model generation: BC in complex with biotin, bicarbonate, ADP and Mg (PDB: 3G8C), BC in complex with pyrido[2,3-*d*]pyrimidine inhibitor **11** (PDB: 2V58), PurK_{*Asp*} in complex with AIR, ADP and Mg (PDB: 3K5I), and PurK_{*E. coli*} in complex with ADP and Mg (PDB: 1B6S).

First, BC and PurK_{*Asp*} in complex with ADPs were aligned to check for topological similarities. Chain A from each structure was used in the study. The sequences of ATP-grasp domains for BC and PurK were selected based on previous literature¹¹⁹ and selected

sequences are shown in Figure 11. The structural alignment (selection to selection) was carried out using PyMOL. Root mean square deviation (RMSD) in the aligned regions was 1.609 Å (Figure 10). The distances between the 6-NH₂ and 2'-OH of the two aligned ADPs are 1.1 Å and 1.5 Å, respectively. The key fingerprint residues in the ATP-binding sites are also aligned (Figure 10) and the ADP binding interactions are highly similar (Figure 12).

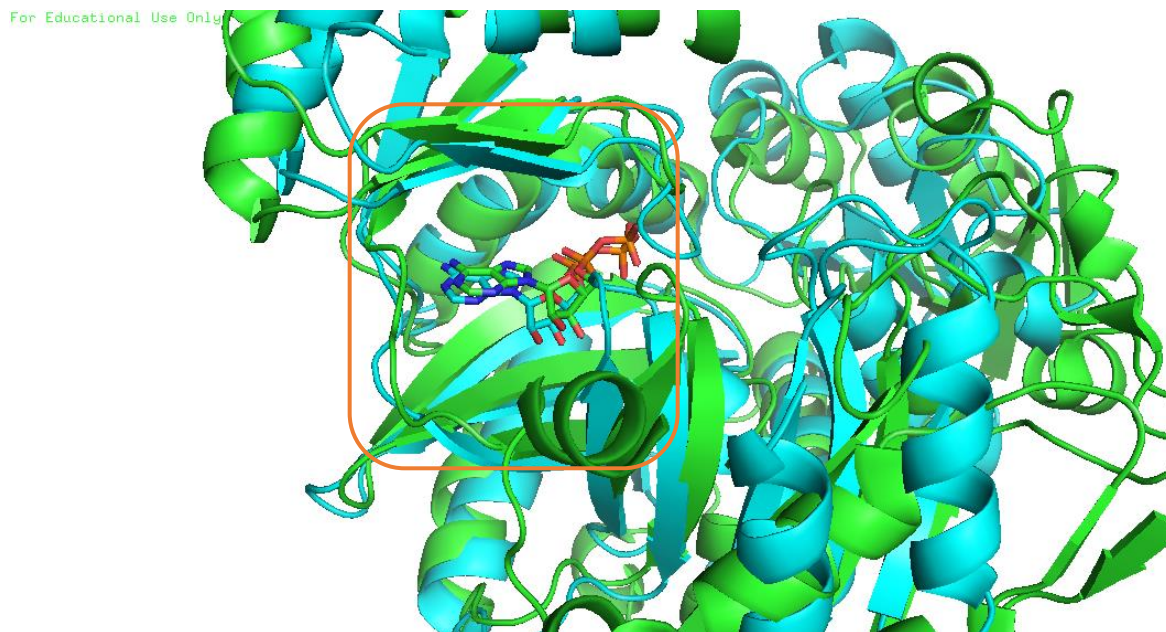


Figure 10. Alignment of BC (PDB: 3G8C, green) and PurK_{Asp} (PDB: 3K5I, cyan). The square highlights the ATP-grasp domain. Figure generated using PyMOL.

```

BC      113 MGDKVS  34  I GTPVI KASGGG- GGRGMRVV  26  VYMEK- - YLENPRHVEI
Purk_asp 101 I QNKFN  33  LGYPLMLKSKT MAYDGRGNFRV  18  LYAEKWAYFK- - - - MEL
      59 GAGTFE- - - FLF  4  FYFI EMNTRIQVEHP  298
      57 GKGVFGVEMFLL  4  IMLCEI ASRIHNSGH  277

```

Figure 11. Alignment and key fingerprint residues in the BC and PurK_{Asp} ATP-grasp site. Residues in bold are conserved or similar residues involved in ATP binding.

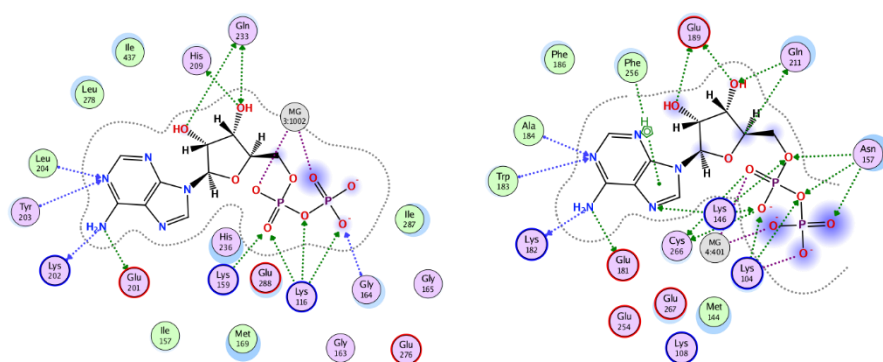


Figure 12. 2-D illustration of the ATP binding interactions in BC (left) and PurK_{Asp} (right). This diagram was generated using the ligand interaction plot as generated MOE.

After confirmation of the structural similarities between the ATP-grasp domains of BC and PurK_{Asp}, the X-ray structures of BC in complex with a pyrido[2,3-*d*]pyrimidine inhibitor **11** (PDB: 2V58) was aligned to PurK_{Asp} (PDB: 3K5I). RMSD in the aligned ATP-grasp regions was 2.01 Å. This direct structural superimposition resulted in the 6-phenyl and 2-NH₂ of the pyrido[2,3-*d*]pyrimidine clashing with the C-domain of PurK_{Asp} (Figure 13, left). Energy minimization of the system resulted in a slight shift of the inhibitor (RMSD = 0.3 Å) to avoid the clashes and generate additional interactions with the protein (Figure 13, right).

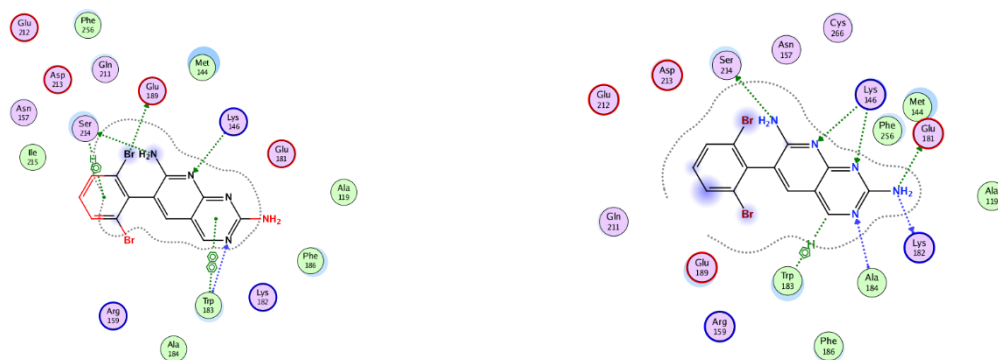


Figure 13. 2-D illustration of the pyrido[2,3-*d*]pyrimidine inhibitor **11** binding interactions with the ATP-binding site of PurK_{Asp} (PDB: 3K5I). Left: direct structure superimposition of BC and PurK_{Asp}. Right: Energy minimization of inhibitor **11** and PurK_{Asp}.

This ligand interaction diagram (Figure 13 right) thus forms the hypothetical binding model for pyrido[2,3-*d*]pyrimidines binding to PurK. A couple of assumptions are made with this model and its use. First, the weaker inhibitory activity of **1** against PurK compared to **11** against BC was not due to the dibromo substitutions on the 6-phenyl ring. Thus, the binding model of **11** in the ATP-site of PurK represents **1** in the same place. (This assumption was later proved correct in section 2.3.2.) Second, the pyrido[2,3-*d*]pyrimidine compound binds in the same location and orientation in the ATP-site of PurK_{Asp} as in the ATP-site of BC. Without direct structure evidence, it is difficult to evaluate the accuracy of this assumption.

Despite the hypothetical nature of the model, it reveals some information regarding how the pyrido[2,3-*d*]pyrimidine compounds interact within the ATP-site of PurK_{Asp}. First, the key residues that contribute to the adenine-binding in the ATP-site also play important roles in binding with pyrido[2,3-*d*]pyrimidines (Figure 14). This makes sense considering pyrido[2,3-*d*]pyrimidine is a nitrogen-containing heterocycle similar to adenine. Ala184 contributes a H-bond donor to both the N-1 in adenine and the N-3 in pyrido[2,3-*d*]pyrimidine. Glu181 and Lys182 provide H-bond acceptors to the 6-NH₂ and 2-NH₂ in adenine and pyrido[2,3-*d*]pyrimidine, respectively. Lys146 donates H-bonds to the N-7 in adenine and N-1 and N-8 in pyrido[2,3-*d*]pyrimidine. Among these four residues, Lys146 and Glu181 are conserved fingerprint residues among all ATP-grasp enzymes. Although Lys182 is not conserved among the enzymes of the ATP-grasp family in general, BC happens to possess a lysine residue at the corresponding position, Lys202.

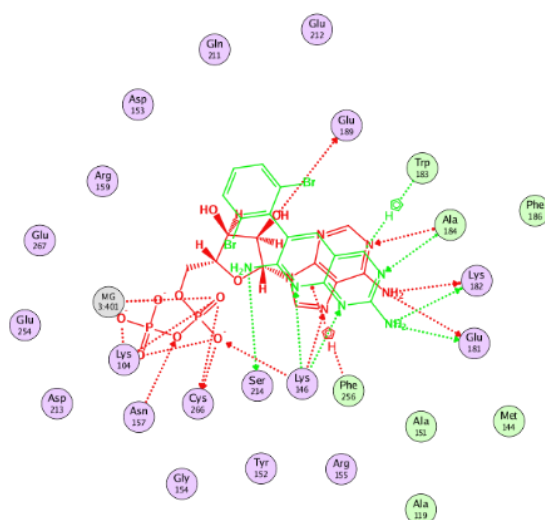


Figure 14. 2-D illustration of the proposed binding orientation of pyrido[2,3-*d*]pyrimidine overlapping with ADP in the ATP-site of PurK_{Asp}. Interactions with inhibitors were shown in green, while interactions with ADP were shown in red.

Second, despite the proposed six H-bond interactions between pyrido[2,3-*d*]pyrimidine with the adenine-binding regions in the ATP-site of PurK_{Asp}, few interactions were found between either the ribose or the phosphate binding domains and the pyrido[2,3-*d*]pyrimidine. In fact, we believe the limited interactions between these domains and the compound could explain the large difference in activity of the pyrido[2,3-*d*]pyrimidines between BC and PurK_{Asp}. In BC, stacking interactions are found between His236 and His438 with the substituted phenyl ring of the compound, and key hydrophobic interactions are also found between this ring and Ile437 (Figure 15). In the Pfizer study of pyrido[2,3-*d*]pyrimidines inhibiting BC¹⁶⁰, a I437T mutant renders **11** more than 112-fold less active compared to the wild-type enzyme (IC₅₀ of 560 nM vs 5 nM) while a H438P mutant results in a more than 32-fold decrease in activity (IC₅₀ 160 nM vs 5 nM). In PurK_{Asp}, the residue corresponding to His236 is Ser214, and other than an analogous H-bond acceptor toward 7-NH₂, no corresponding stacking or hydrophobic interaction with the 6-phenyl ring was identified.

PurK_{Asp} is also shorter in its C-terminus compared to BC (Figure 16) and thus there is a loss of the analogous hydrophobic contacts between the enzyme and the substituted phenyl ring. The decreased length of the C-terminus, in turn, makes the ATP-binding site more spacious in PurK_{Asp} resulting in a decrease in shape complementarity between the inhibitor and the binding pocket.

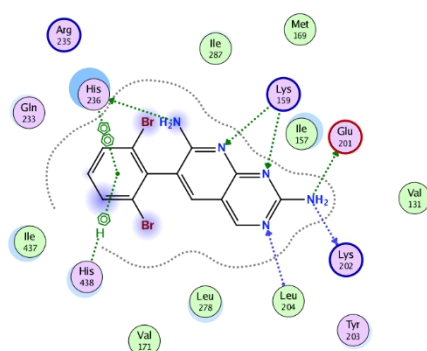


Figure 15. 2-D illustration of the pyrido[2,3-*d*]pyrimidine inhibitor **11** binding interactions with the ATP-binding site of BC (PDB: 2V58).

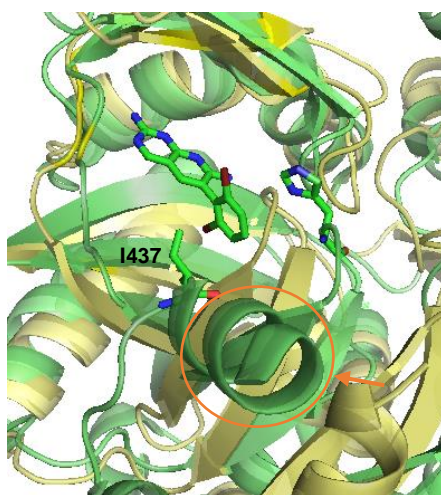


Figure 16. Crystal structural superimposition of PurK (pdb: 3K5I, green) and BC (pdb: 2V58, yellow) with pyridopyrimidine **11** in the binding site. The orange circle highlights the additional C-terminus of BC, and the arrow points to the PurK C-terminus end.

A similar method was applied to search for the potential explanations of the relatively poor inhibitions of pyrido[2,3-*d*]pyrimidine against PurK_{*E. coli*} compared to PurK_{*Asp*}. A structural alignment was conducted between BC and PurK_{*E. coli*} (RMSD 7.10 Å) and PurK_{*Asp*} with PurK_{*E. coli*} (RMSD 5.46 Å). There were a few features that were noted in this comparison. First, the ATP-site of PurK_{*E. coli*} is more open than PurK_{*Asp*} (Figure 17) resulting in a greater loss of shape complementarity. Second, Trp183 in PurK_{*Asp*} could contribute to a stacking interaction with the heterocycle core in pyrido[2,3-*d*]pyrimidine. The corresponding residue in PurK_{*E. coli*} is Gly155 which lacks the ability for π -stacking (Figure 18). Finally, despite the poor predictive outcome of the calculated binding energy, forcefield calculations indicated that the calculated affinity for the system was -5.5 kcal/mol, worse than that of **11** and PurK_{*Asp*}. Due to the poor inhibition against PurK_{*E. coli*}, pyrido[2,3-*d*]pyrimidines are less ideal hits for antibacterial than antifungal drug development. All further activities were measured against PurK_{*Asp*} only.

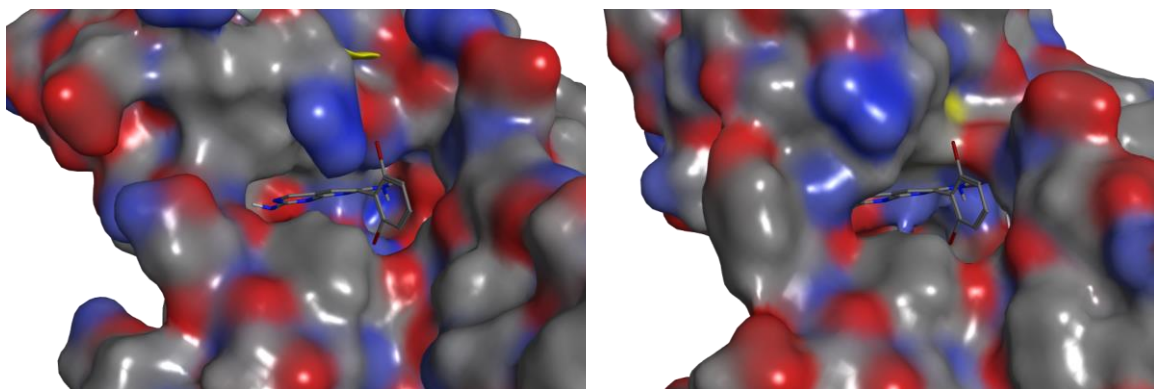


Figure 17. Surfaces of the ATP-site for PurK_{*E. coli*} (left) and PurK_{*Asp*} (right). Molecular surfaces are colored by atom color with blue for nitrogen, red for oxygen, yellow for sulfur and grey for the carbon backbone.

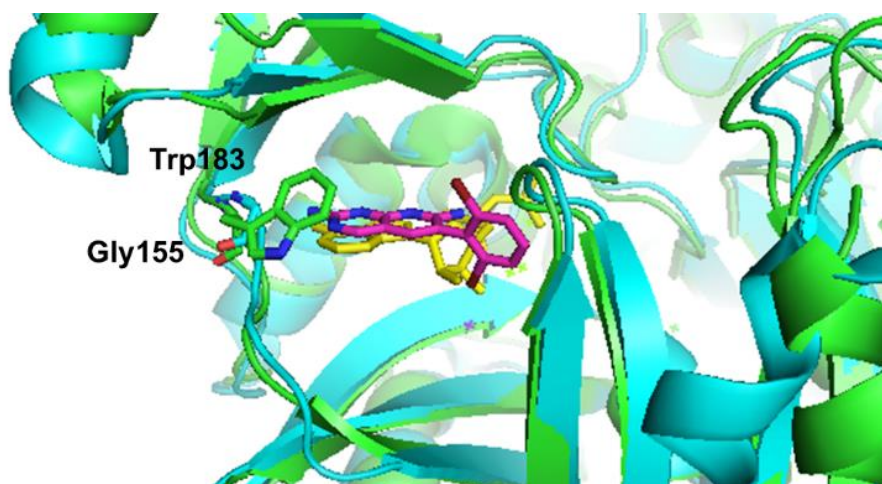


Figure 18. Crystal structural superimposition of PurK_{Asp} (pdb: 3K5I, green) and PurK_{E. coli} (pdb: 3ETJ, cyan) with pyridopyrimidine (purple) aligned in the ATP-site. The PurK_{Asp} residue W183 could form stacking interaction with the heterocycle, while correspondingly G155 resides in PurK_{E. coli}.

The hypothetical binding model suggests further regions on the pyrido[2,3-*d*]pyrimidine that could be modified to improve the activity. The model shows that there are extensive hydrogen bonding interactions of the pyrido[2,3-*d*]pyrimidine heterocycle with residues in the adenine position of the ATP-site; however, there are no obvious interactions between the molecule and the protein within the ribose and triphosphate binding sites. This suggested that modifications of the pyrido[2,3-*d*]pyrimidine at the 6-phenyl and 7-amine positions might generate interactions with amino acids in the ribose and triphosphate sites leading to pyrido[2,3-*d*]pyrimidine analogs with higher potency (Figure 19).

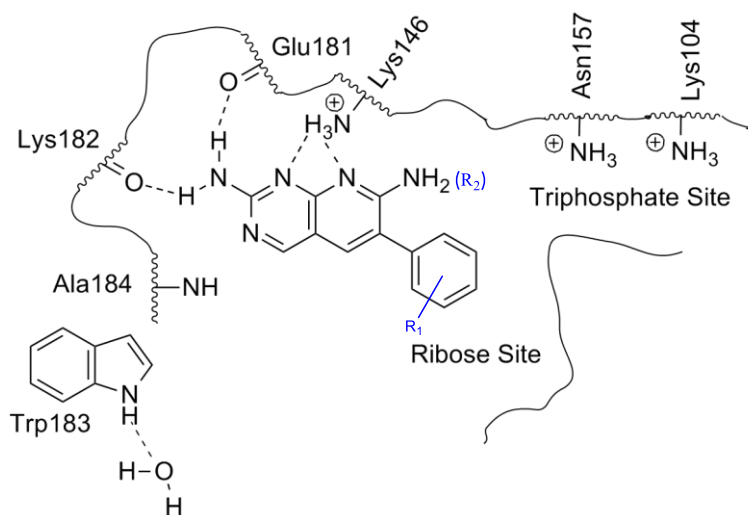
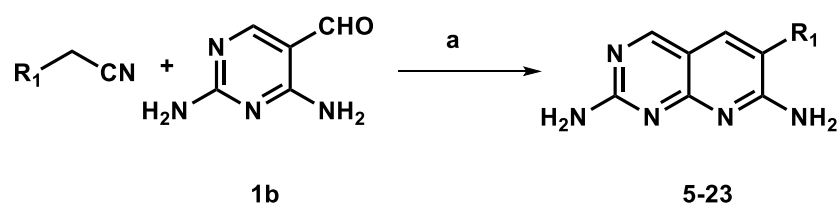


Figure 19. Modification strategy.

2.3 Ribose-binding position (R_1) modifications

2.3.1 Synthesis

Based on the model from the structural alignment with BC, the 6-phenyl group sits in the ribose binding site. Thus, we prepared a series of compounds in which various substitutions on the 6-position (R_1 in Scheme 3) were generated. Synthesis of these agents (**5-23**) was conducted by condensation of aldehyde **1b** and nitriles to make pyrido[2,3-*d*]pyrimidine derivatives with various groups at the 6-phenyl position (Scheme 3). Nitriles with an aliphatic R_1 were used for compounds **5** to **8** whereas substituted benzyl nitriles were used for compounds **9** to **20**, and nitriles in which R_1 contained of heterocycles were used for compounds **21** to **23**.



Scheme 3. Synthesis of pyrido[2,3-*d*]pyrimidines with various substitutions at the 6-phenyl position. Reagents and conditions: (a) NaH, EtO(CH₂)₂OH, reflux, 4 h, 11-84%.

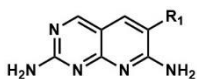
2.3.2 Biological evaluations

We examined a series of substituted 6-phenyl analogs at a single concentration (200 μM) using the malachite green PurK assay. For analogs displaying better inhibition than **1**, IC₅₀ values were determined using the malachite green assay as well as a secondary PK/LDH coupled PurK assay. This assay couples PurK to pyruvate kinase (PK) and lactate dehydrogenase (LDH) and use changes in the absorption of NADH as a measure of ATP consumption.

Three groups of variances were explored at the R₁ position. The 6-phenyl was first replaced by smaller substitutions (compound **5-8**), due to a lack of obvious interactions between the phenyl and PurK_{Asp}. Each compound displayed weaker activity than the parent agent. This implies that the 6-phenyl group may have unrecognized hydrophobic or aromatic interactions or that it may help to orient the pyrido[2,3-*d*]pyrimidine heterocycle into the adenine site. Indeed, minimization of molecular models of **5** indicate that there is a substantial loss of interaction of the pyridopyrimidine with the adenine site due to movement of **5** into the ribose binding pocket. We subsequently explored different substitutions on the phenyl ring. Small substitutions at the 2 and 6 positions improved activity whereas large groups decreased activity. Notably, the most active BC inhibitor, compound **11**, only exhibited 23% inhibition at 200 uM against PurK_{Asp} and was worse than the parent compound **1**. This is interesting since **11** is a potent inhibitor of BC and this reemphasizes

the difference among the ATP-grasp domains of enzymes within the same superfamily. Substitutions at the 3 and 5 positions decreased activity significantly, except for the diol substitutions, **14**. This compound nearly inactivated PurK_{Asp} at 200 μ M, and subsequent studies indicated an IC₅₀ of 14 μ M, a nearly 12-fold improvement from **1**. The PK/LDH coupled PurK assay was used to investigate the inhibition kinetics of **14**. This study indicated that **14** is competitive with ATP and has a K_i of $7.9 \pm 1.6 \mu\text{M}$ against PurK_{Asp} (Figure 20). This activity increase offered by polar substitutions fit well with the hypothetical binding model in which 6-phenyl sits in the ribose-binding site. Finally, we tested several heterocycles and found that the phenyl ring appears to be the optimal option.

Table 5. Ribose position (R₁) modifications.



#	R ₁	RA%	IC ₅₀	IC ₅₀
		200 μ M	Malachite green assay	PK-LDH assay
1		43	167 \pm 16	97 \pm 16
5	H	73	-	-
6	COOH	98	-	-
7		64	-	-
8		58	-	-
9		21 \pm 2	41 \pm 7	38 \pm 9

Table 5. Cont.

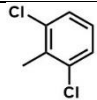
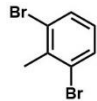
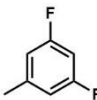
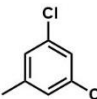
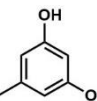
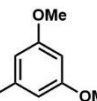
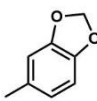
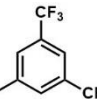
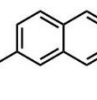
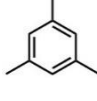
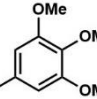
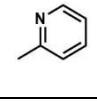
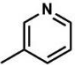
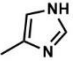
10		24±1	40±11	58±9
11		77	-	-
12		71	-	-
13		117 (100 µM)	-	-
14		3	14±2	15±1
15		75	-	-
16		47	-	-
17		88 (100 µM)	-	-
18		NA	-	-
19		58±7	-	-
20		78±4	-	-
21		65±8	-	-

Table 5. Cont.				
22		51±5	-	-
23		75±4	-	-

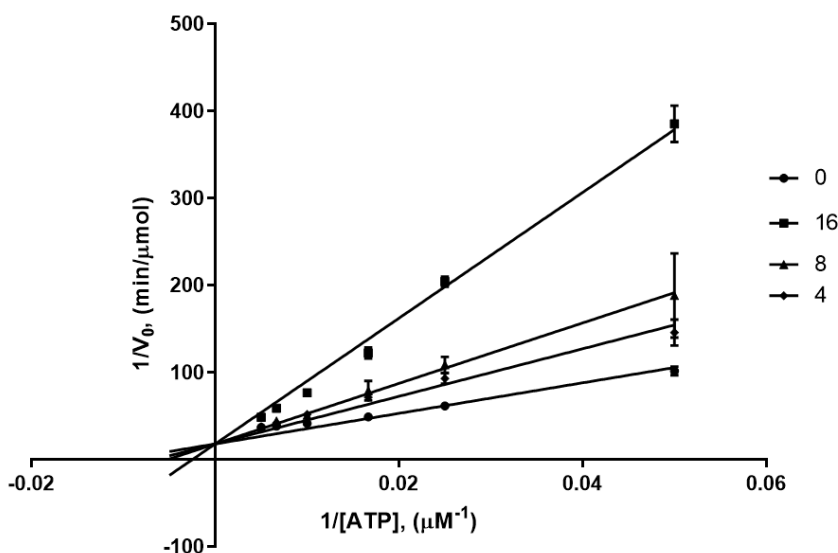


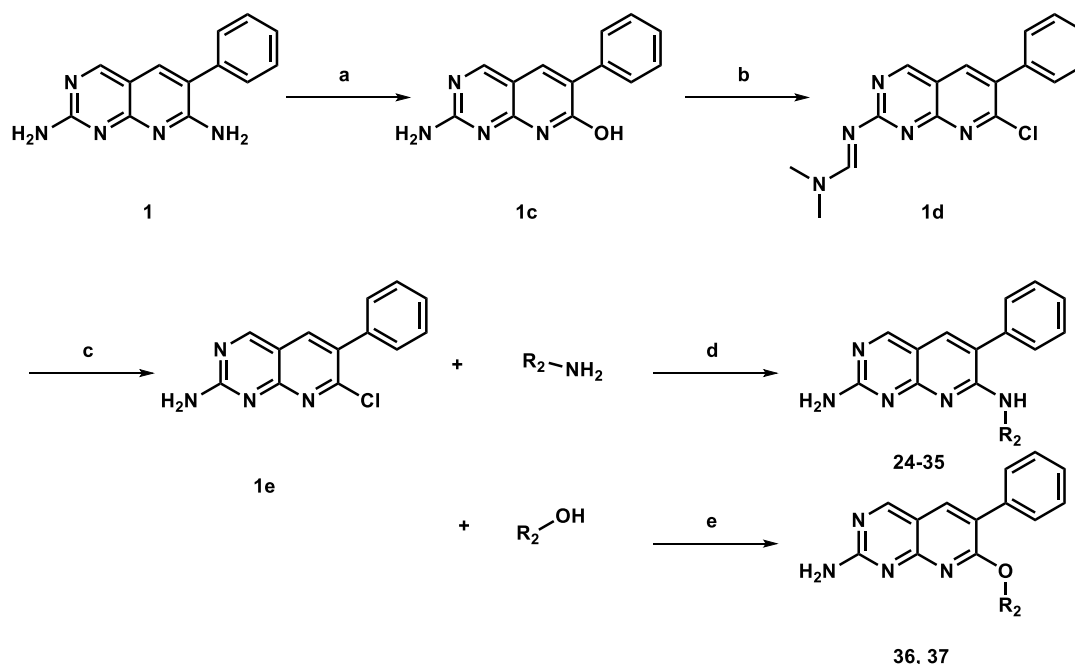
Figure 20. Lineweaver-Burke plot of **14** against PurK_{Asp} using the PK/LDH coupled PurK assay. The concentration of **14** (in μM) is listed to the right of the graph. The experiment was done at an AIR concentration of 25 μM .

2.4 Phosphate-binding position (R₂) modifications

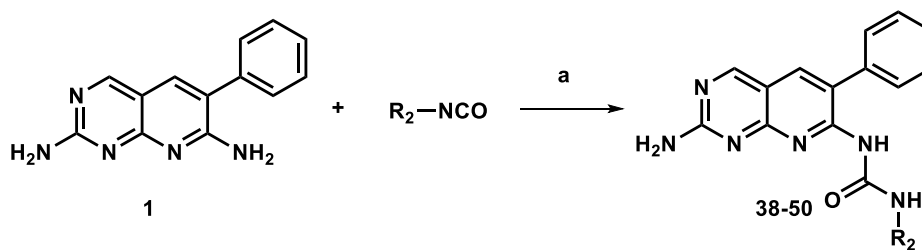
2.4.1 Synthesis

Two types of derivatives were explored at the phosphate (R₂) position, N-alkylation (or O-alkylation) and urea substitutions. These two groups were selected based on two reasons: synthetic feasibility and improved activity in other ATP-utilization enzymes, such as kinases¹⁶⁵⁻¹⁷¹. N-alkylation (**24-35**) and O-alkylation (**36, 37**) were achieved through the critical intermediate **1e**, 7-chloro-6-phenylpyrido[2,3-*d*]pyrimidin-2-amine. To achieve this intermediate, the amine group of compound **1** was first hydrolyzed to the alcohol (**1c**) under

acidic condition followed by chlorination using thionyl chloride. Once the chloropyridopyrimidine (**1e**) was obtained, the chlorine atom was readily displaced by either amines (**24-35**) or alcohols (**36, 37**) (Scheme 4). Urea substitutions (**38-50**) were introduced by direct reaction of the amines with isocyanate under basic conditions (Scheme 5).



Scheme 4. Synthesis of pyrido[2,3-*d*]pyrimidines with various N/O-alkylations at the 7-NH₂ position. Reagent and conditions: (a) 8 M HCl, reflux, 24 h, 62%; (b) SOCl₂, DMF, CH₂Cl₂, mw, 45 °C, 1 h, 78%; (c) 95 % EtOH, reflux, 8 h, 57%; (d) DIPEA, DMF, 100 °C, 45%; (e) MeOH, reflux, 95%.



Scheme 5. Synthesis of pyrido[2,3-*d*]pyrimidines with various ureas at the 7-NH₂ position. Reagent and conditions: (a) NaH, DMF, r.t., 12h, 15-42%.

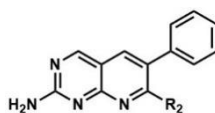
2.4.2 Biological evaluations.

Based on the hypothetical model, the 7-NH₂ points to the triphosphate binding site. Two types of derivatives were explored at this position, N-alkylation (or O-alkylation) and urea substitutions. These two groups were selected based upon synthetic feasibility and their abilities to improve inhibition in other ATP-utilizing enzymes. Activities were measured as described in the previous section.

For alkylation derivatives, cyclic (**24-29**), chain (**30-35**) and two O-alkylates (**36, 37**) were explored. In the cyclic group, decreasing ring size improved activity indicating that there is a small hydrophobic pocket at this location. Moderate activity increases were achieved by the pyrrolidine (**27**) and cyclopropane (**29**) substitutions. Significant improvement in activities were reached in the chain group (**30-35**). Simply decreasing the polarity by one or two small alkyl substitutions (**30-33**) improved the activity 2-4-fold which indicated the existence of a small hydrophobic pocket. A polar group at the end of this alkyl chain also improved activity with a 3-carbon length (**34**) showing better activity than a 2-carbon one (**35**). No significant change in activity was achieved by the O-alkylated compounds, **36** and **37**.

All the urea substitutions decreased activity and led to significant solubility issues. This was surprising given their wide utilization in kinases inhibitors. Again, these differences suggest the fundamental uniqueness in the ATP-binding sites of the ATP-grasp proteins versus the protein kinases.

Table 6. Phosphate position (R₂) modifications.



R ₂	RA%	IC ₅₀	IC ₅₀
----------------	-----	------------------	------------------

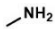
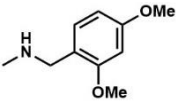
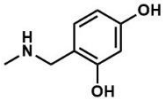
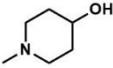
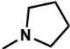
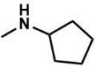
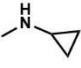
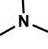
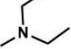
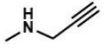
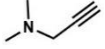
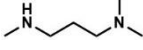
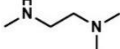
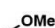
		200 μ M	phosphate assay	PK-LDH assay
1		43	167 \pm 16	97 \pm 16
24		42 \pm 2 (100 μ M)	75 \pm 15	81 \pm 3
25		36	-	-
26		43 \pm 3	116 \pm 12	-
27		31 \pm 2	90 \pm 5	68 \pm 3
28		48 \pm 5	-	-
29		25 \pm 1	-	-
30		18 \pm 1	39 \pm 2	33 \pm 5
31		21 \pm 1	-	-
32		38 \pm 3	69 \pm 7	71 \pm 9
33		21 \pm 1	42 \pm 4	-
34		19 \pm 1	24 \pm 5	37 \pm 2
35		35 \pm 1	91 \pm 10	-
36		46	-	-

Table 6. Cont.

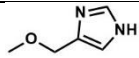
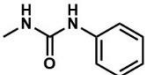
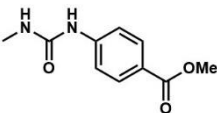
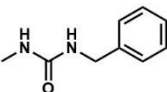
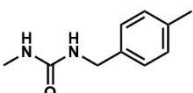
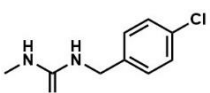
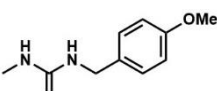
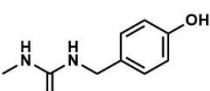
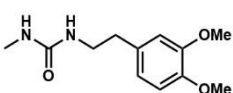
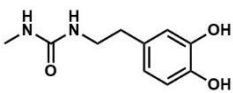
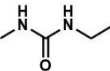
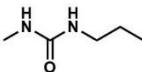
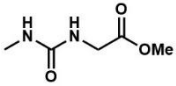
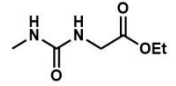
37		69±5 (100 μM)	-	-
38		--	-	-
39		65 (50 μM)	-	-
40		76 (50 μM)	-	-
41		83	-	-
42		88 (26 μM)	-	-
43		90 (50 μM)	-	-
44		69 (100 μM)	-	-
45		--	-	-
46		86 (26 μM)	-	-
47		69	-	-
48		70	-	-

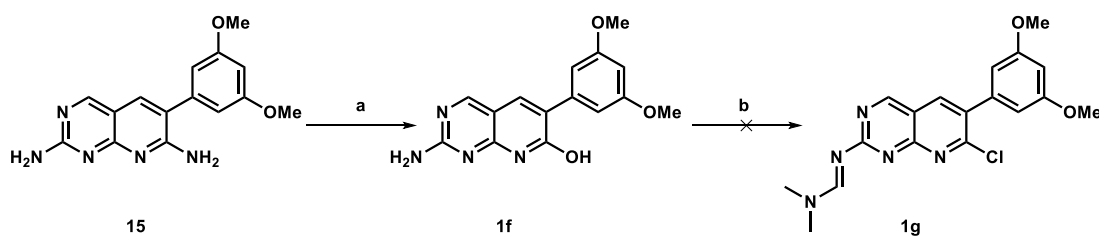
Table 6. Cont.

49		88	-	-
50		86	-	-

2.5 Double modifications

2.5.1 Synthesis

When we decided to combine both the R₁ and R₂ modifications to make the double modified pyrido[2,3-*d*]pyrimidines, we first tried reactions similar to those listed in Scheme 4. The analogous critical intermediate to **1e** was 7-chloro-6-(3,5-dimethoxyphenyl)pyrido[2,3-*d*]pyrimidin-2-amine. Unfortunately, this initial approach failed to give this intermediate presumably due to the instability of methoxy groups under acidic conditions (Scheme 6). In fact, even the first hydrolysis reaction of converting the amine to the alcohol group gave a majority of mono-demethylated product.



Scheme 6. The failed synthesis for the key intermediate of the double modified compounds.

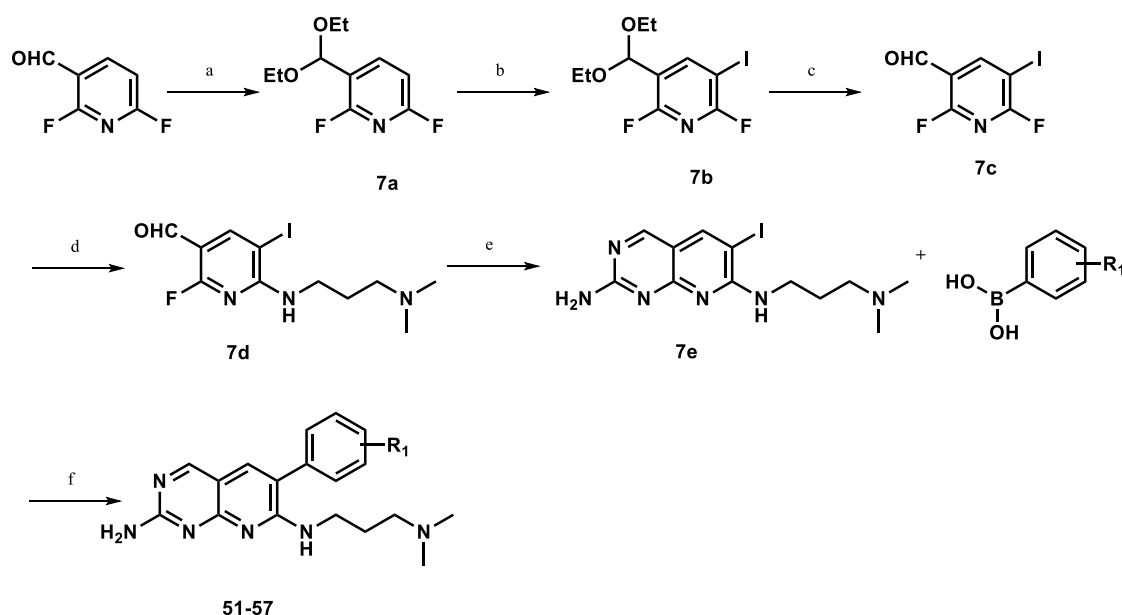
Reagent and conditions: (a) 8 M HCl, reflux, 3 h, 21%.

After retrosynthetic analysis, we decided to investigate a different route. Instead of assembling the pyrido[2,3-*d*]pyrimidines from the pyrimidine ring as in the previous schemes, we set out to make the pyridine ring first (Scheme 7).

The critical intermediate in this new synthetic route is 2,6-difluoro-5-iodonicotinaldehyde, **7c**. This intermediate contains three handles needed for the synthesis of the final product. Compound **7c** contained a 2-fluorine and 3-aldehyde which enables cyclization with guanidine to yield the pyrimidine, a 5-iodine which is necessary for aryl-aryl coupling via a Suzuki reaction, and a 6-fluorine which enables N-substitutions. The only published protocol for the synthesis of **7c** was a patent method which produced the compound from commercially available 2,6-difluoro-3-pyridinecarboxaldehyde¹⁷². Unfortunately, details in the patent were limited which led to difficulty with the iodination reaction (step b in Scheme 7). Ultimately, we found that after generating the anion by LDA deprotonation, the iodine solution needed to be added slowly during a span of at least 2 hours to ensure a consistent and optimum yield.

After obtaining the critical intermediate **7c**, we tried the subsequent three reactions toward the final products: cyclization, Suzuki reaction and N-substitution reaction. Compound **7c** failed to undergo direct Suzuki coupling presumably due to the interference of the aldehyde. The cyclization reaction on **7c** also failed likely because of competition reactions at the two fluorines in the molecule.

Gaining inspiration from the chemoselective reactions of 3-substituted-2,6-difluoropyridines with benzylamine¹⁷³, we tried to react **7c** with 3-(dimethylamino)propylamine directly and obtained **7d** in a reasonable yield. No reaction at the 2-position or Schiff base were observed. This intermediate **7d** readily underwent cyclization followed by Suzuki coupling to give a series of double-modified compounds (**51-57**).



Scheme 7. Synthesis of pyrido[2,3-*d*]pyrimidines with double modifications. Reagents and conditions: (a) triethyl orthoformate, PTSA, EtOH, reflux, 18 h, 83%; (b) I₂, LDA, THF, -78 °C, 2 h, 96%; (c) HCl, THF/H₂O, r.t., 4 d, 96%; (d) 3-(dimethylamino)propylamine, K₂CO₃, DMSO, r.t., 2 h, 78%; (e) guanidine nitrate, TEA, MeCN, mw, 150 °C, 1 h, 33%; (f) Pd(PPh₃)₄, Na₂CO₃, MeCN/DMF/H₂O, 90 °C, 6 h, 45-68%.

2.5.2 Biological evaluations.

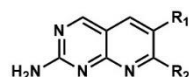
Examination of compounds with modifications in the ribose (R₁) or triphosphate (R₂) binding sites resulted in compounds (**14** and **34**) with improved activity. Thus, it was logical to explore agents in which both sites were substituted with the best substituent. Together with the exact combination of **14** and **34**, we also explored a few other substituents on the phenyl ring. Due to synthetic limitations, only one N-alkylation substituent was explored at the R₂ position.

Double-modified compounds indeed combined the activity gain of each modification. Interestingly, cyclohexene substituted **55** has similar activity with phenyl **34**, while cyclohexane **57** decreased activity. Both indoles, **53** and **54**, improved activity with **53** better

than **54**. The most active compound **56** – directly merging **14** and **34** – has an IC_{50} of 1.7 μ M. This is 100-fold improvement from the parent hit **1**, and the most active ATP-site PurK_{Asp} inhibitor to date.

To confirm binding affinity, we developed a thermal shift assay^{128, 174-175} for PurK. To develop the condition of thermal shift assay for PurK, 1 mM ADP was used as the positive control to optimize the buffer type, concentration, pH and salt additives. The condition in which ADP achieved the largest shift of the protein melting point was selected as the optimized condition. We examined a range of buffers including 50 mM Tris (pH 8.0), 50 mM HEPES (pH 8.0), 50 mM sodium phosphate (pH 8.0), 50 mM MOPS (pH 8.0) and 50 mM MES (pH 6.5). MES was selected and further tested for optimal pH from 5.5 to 8.0 in 0.5 pH interval. A pH 6.0 was selected followed by the optimization of the MES concentration. Three different concentrations were tested, 20 mM, 50 mM and 100 mM, and 20 mM achieved the maximum thermal shift for ADP. Finally, NaCl was tested as an additive (0, 50 mM and 250 mM) and it was found that no salt achieved the best melting curve. The optimized condition was 20 mM MES buffer, pH 6.0. Under this condition, 1 mM ADP achieved a 7.2 ± 0.5 °C shift of the PurK melting point. Using the optimized condition, we validated the binding of **1** and **56** (Figure 21) giving a K_d of 117.2 ± 53.9 μ M and 9.0 ± 1.7 μ M. The low accuracy for the K_d of **1** is likely because of the inability to measure melting at higher concentrations due to solubility issues. This prevents the reaching of a plateau reducing the accuracy of the curve fit.

Table 7. Double modifications.



#	R ₁	R ₂	RA%	IC ₅₀
---	----------------	----------------	-----	------------------

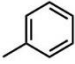
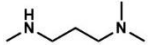
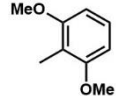
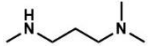
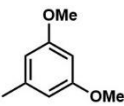
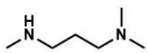
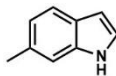
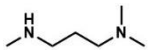
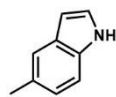
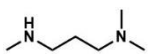
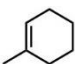
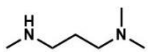
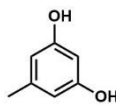
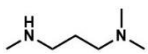
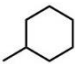
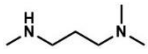
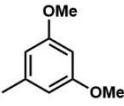
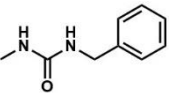
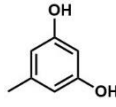
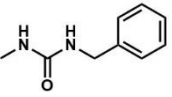
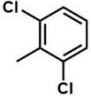
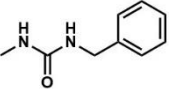
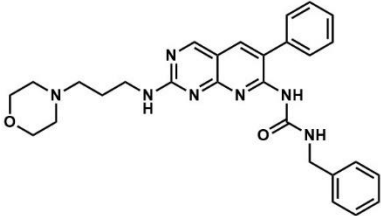
			200 μ M	phosphate assay
34			19 \pm 1	24 \pm 5
51			72 \pm 4	-
52			38 \pm 2	-
53			6 \pm 0.4	6.1 \pm 0.6
54			12 \pm 1	-
55			20 \pm 1	-
56			3.1 \pm 0.2	1.7 \pm 0.2
57			32 \pm 2	-
58			86 (26 μ M)	-
59			28 (100 μ M)	-
60			60 (26 μ M)	-

Table 7. Cont.

61		63 (100 μM)	-
----	---	----------------	---

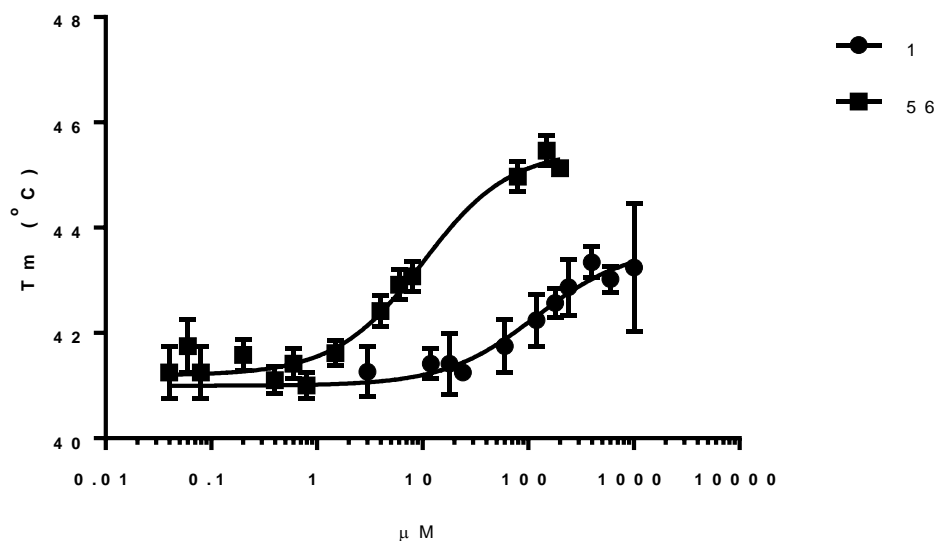


Figure 21. Binding affinity of compound **1** and **56** against PurK_{Asp} as measured by the thermal shift assay.

2.6 1,6-naphthyridines and 1,8-naphthyridines

2.6.1 Synthesis

Previously, we have discovered that pyrido[2,3-*d*]pyrimidine weakly inhibited PurK_{Asp}, and through modifications of the 6-phenyl and 7-NH₂ positions we were able to obtain compounds with better inhibitory activity. To study the functions of the aza atoms of the pyridopyrimidine moiety in interacting with PurK_{Asp}, we synthesized two small groups of compounds containing 1,6-naphthyridine and 1,8-naphthyridine, respectively (Figure 22).

The knowledge of the heteroatoms' contributions in affinity not only extends the SAR of the pyridopyrimidine core, but also helps to evaluate the computational binding model between $PurK_{Asp}$ and the pyridopyrimidine compounds.

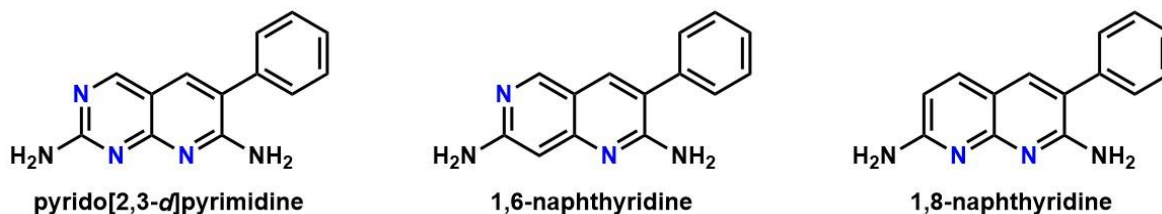
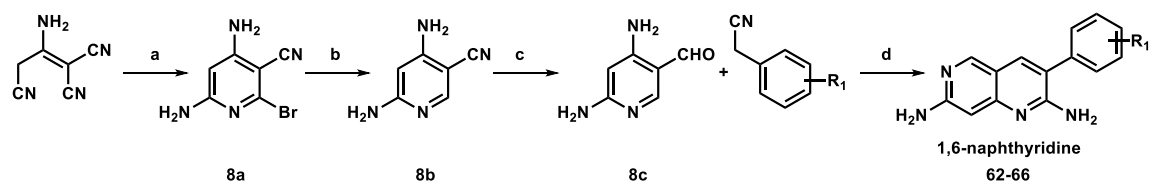


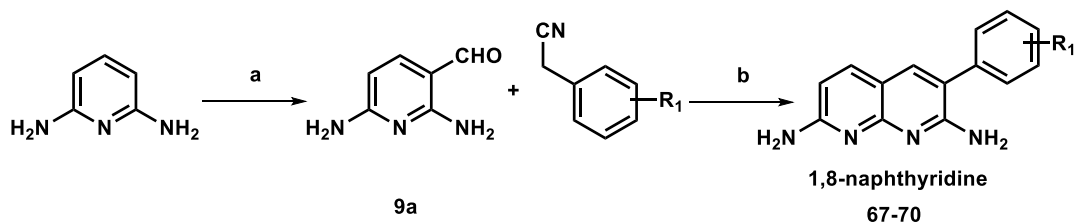
Figure 22. Structures of pyrido[2,3-*d*]pyrimidine, 1,6-naphthyridine and 1,8-naphthyridine.

Both 1,6-naphthyridines and 1,8-naphthyridines were made using similar approaches as that for pyrido[2,3-*d*]pyrimidines in Scheme 1. In short, the heterocycle was obtained by a condensation reaction between a molecule possessing both an amine and an aldehyde group ortho to the amine and different acetonitriles (Scheme 8 and 9).

The precursor for 1,6-naphthyridines, 4,6-diaminonicotinaldehyde (**8c**), was made from the commercially available 2-amino-1,1,3-propanetricarbonitrile using a three-step published method¹⁷⁶⁻¹⁷⁸. Condensation reactions between 4,6-diaminonicotinaldehyde and different acetonitriles resulted in the corresponding 1,6-naphthyridines (Scheme 8). The precursor for 1,8-naphthyridines, 2,6-diaminonicotinaldehyde (**9a**), was made from pyridine-2,6-diamine using a published method¹⁷⁹, and similar condensations with acetonitriles gave the desired 1,8-naphthyridines (Scheme 9). In both cases, we chose R_1 groups based upon the activity of the parent pyridopyrimidine compounds outlined in previous tables.



Scheme 8. Synthesis of 1,6-naphthyridines. Reagents and conditions: (a) HBr/HOAc, r.t., 18 h, 79%; (b) H₂, 10% Pd/C, NaHCO₃, MeOH, 15 psi, 6 h, 42%; (c) Ra-Ni, 98-100% HCOOH, reflux, 24 h, 34%; (d) NaH, EtO(CH₂)₂OH, reflux, 2-24 h, 13-96%.

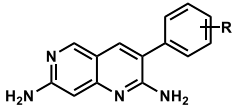
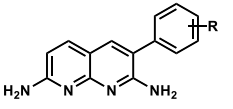
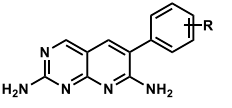
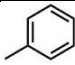
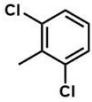
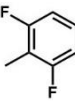
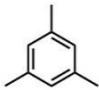
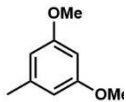


Scheme 9. Synthesis of 1,8-naphthyridines. Reagents and conditions: (a) NaOH, CHCl₃, ethanol, reflux, 18 h, 29%; (b) NaH, EtO(CH₂)₂OH, reflux, 3-7 h, 19-87%.

2.6.2 Functions of the aza atoms in pyridopyrimidine

The activity of the 1,6-naphthyridines and 1,8-naphthyridines against PurK_{Asp} were evaluated at a single concentration of 200 μM using the malachite green phosphate assays (Table 8). Compared with the parent pyridopyrimidines, all 1,8-naphthyridines completely lost activity indicating that the N-3 forms crucial interaction within the PurK_{Asp} active site. The 1,6-naphthyridines generally possessed small to modest reductions in activity compared to the parent compounds. Compounds bearing the 2,6-F and 3,5-OCH₃ substituents were essentially as active as the pyridopyrimidines while other substitutions generally lost about 20% of their potency. This data suggests that unlike N-3, N-1 is not critical for binding to the enzyme.

Table 8. 1,6-naphthyridines (left), 1,8-naphthyridines (middle) and the parent pyridopyrimidines (right).

#	RA%		#		#	
		1,6-naphthyridine		1,8-naphthyridine		pyridopyrimidine
62		68±2	67	98±7	1	43±2
63		57±2	68	92±6	10	24±1
64		14±1	-	-	9	21±2
65		77±5	69	84±4	19	58±7
66		77±4	70	94±3	15	75±4

2.7 Development of binding models to PurK_{Asp} for pyrido[2,3-*d*]pyrimidine inhibitors

In this thesis, we have identified a group of pyrido[2,3-*d*]pyrimidine containing compounds as PurK_{Asp} ATP-competitive inhibitors. Modifications were made at the N-1, N-3, C-6, and C-7 positions and the resulting compounds were utilized to determine a structure-activity relationship (SAR). To understand the structural basis for their potency and selectivity and to rationalize the observed SAR to benefit future structural-based optimization efforts, we were interested in developing a computational binding model of these compounds against PurK. Two different approaches were taken to generate models. The first took advantage of the structural similarities among the ATP-grasp domain proteins

and the extensive ligand: enzyme crystal structures for some of these enzymes, while the second utilized docking to generate hypothetical binding models.

2.7.1 Binding model based on structural alignment

The construct of this model was described in section 2.2 (Figure 23). This model was built from structural superimposition of the crystal structures of PurK and BC. Based on the interactions found in this model, we decided to explore structural modifications of the 6-phenyl and 7-NH₂ positions. Each position gave a full range of SAR with both improved and decreased activity ranging at least two magnitudes in the differences in IC₅₀. This change in SAR verified the suitability of these two positions for medicinal chemistry optimization. In this section, we evaluate whether this model could explain the SAR obtained from our studies.

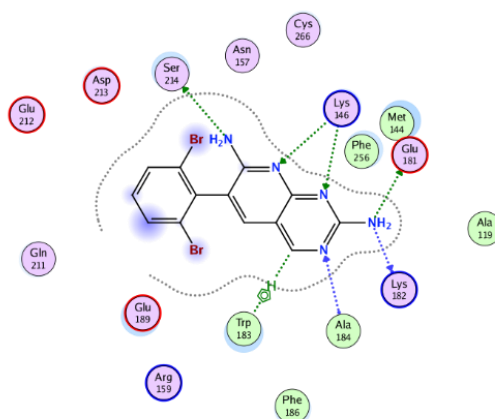


Figure 23. The hypothetical binding model generated by structural superimposition of PurK_{Asp} (pdb: 3K51) and BC (pdb: 2V58).

First, we examined whether the proposed H-bond interactions in the model are supported by the SAR observed by the two groups of naphthyridine compounds. Based on the model, N-3 forms a critical interaction with Ala184, while N-1 and N-8 share an interaction with Lys146. Due to synthetic limitations, we did not convert the N-8 in

pyrido[2,3-*d*]pyrimidine to C to make a group of quinazolines; however, we expected the quinazolines would have similar activity to 1,6-naphthyridines. These results indicate that N-3 forms a critical binding interaction while the bifurcated nature of the H-bond to Lys146 indicates that removal of the N-1 was not detrimental to the activity. This suggests that the H-bond interaction to Lys146 is not critical for binding to the enzyme.

We next wished to test the validity of the binding model based on the SAR of the 6-phenyl and 7-NH₂ modified compounds. The calculated binding affinity of the compounds were plotted against the percent residual activity to determine whether the calculated binding affinity based upon the model could accurately predict the potency of the inhibitors.

PurK_{Asp} was prepared using the QuickPrep function in MOE which checks the structure for completeness and protonation state. Non- active-site water molecules, defined as waters farther than 4.5 Å away from ligand, were deleted. Residues that are 8 Å away from ligand were fixed during minimization. Forcefield energy minimization was terminated when the RMS gradient fell below 0.1 kcal/mol/Å. Each compound was placed into the model using the same orientation and location as **11**, and energy minimization was performed to calculate potential affinity¹⁸⁰.

Figure 24 summarized the calculated affinity (kcal/mol) vs. experimental %RA of all compounds that were tested at 200 µM. Linear regression was performed resulting in an R² of 0.22, suggesting that the predictive ability of the binding model is poor. The binding model also failed to predict that compound **14** and **34** were the most active derivatives at the C-6 and N-7 positions respectively. However, when the data was separated by the modification position and indicated in different colors, the calculated affinity was generally the largest for C-6 modifications (orange) and smallest for the double modifications (blue) with the N-7 modifications (grey) in between. This general trend agrees with their relative activity shown

in the experimental test. With a few exceptions (**9**, **10**, and **14**), the C-6 modifications did not improve activity, while most N-7 non-urea modifications gave more active compounds, and the double modified compounds were able to combine the activity gain of each position. Most N-7 urea modifications had solubility limitations at 200 μM , and therefore were not included in the graphic analysis. However, an examination of the calculated binding affinity of the urea substituted compounds indicated that these compounds were poor binders due to clashes with PurK_{Asp}, a result supported by experimental evidence.

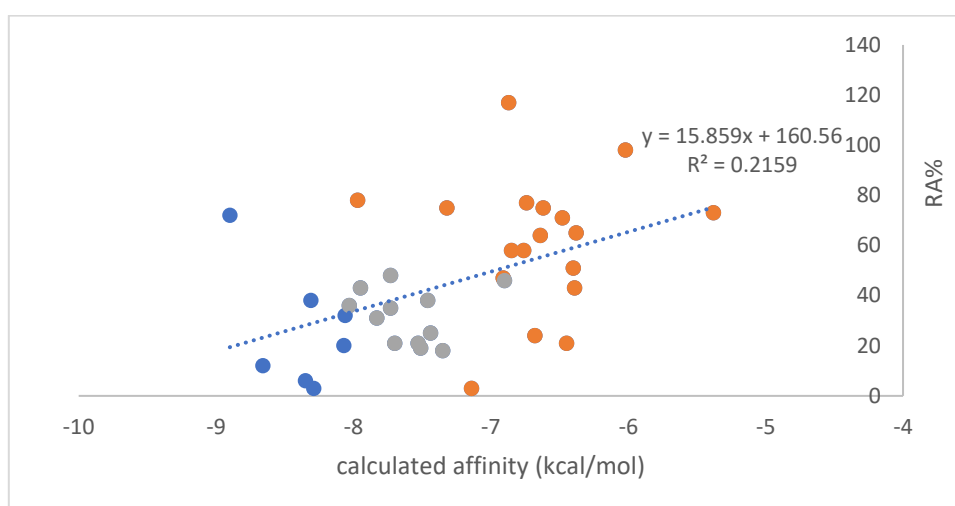


Figure 24. Correlation of calculated affinity (kcal/mol) vs. experimental %RA. Different modifications are represented by different colors: orange for C-6 modifications, grey for N-7 modifications, and blue represents the double modifications

There are several potential reasons why the calculated affinity is in poor correlation with experiment %RA. First, the original assumptions made in the model (pyrido[2,3-*d*]pyrimidine binds the active site of PurK the same as in BC, and all pyrido[2,3-*d*]pyrimidines bind in the ATP-site in the same orientation as the parent compound **11**) are inaccurate. Second, the binding energy calculations do not consider the issue of desolvation energy upon binding to the enzyme. Third, the protein structure is rigid in the forcefield calculation and fails to

represent the real protein structure. Fourth, there could be structural water molecules that are necessary for binding and these are not included in the model or the energy calculations.

2.7.2 Binding model based on docking studies

While the binding model generated by structural alignments could provide some information on the interactions between the ligand and the enzyme, the model gave a poor correlation between the calculated binding energy and the observed potency. While other factors explained in the previous section could provide an explanation for the poor performance, we felt that the initial assumptions of the model could be incorrect. Namely, we were concerned that the pyrido[2,3-*d*]pyrimidine might not bind to the ATP-site of PurK in the same orientation as in BC and consequently, we were also worried that different derivatives of the compounds may adopt different binding orientations within the more open ATP-binding site of PurK. Studies on the ATP-site inhibitors of kinases suggested that derivatives of the same scaffolds could indeed bind the active site in different orientations¹⁸¹. To eliminate the bias of the orientation provided by the alignment to the structure of the ligand:BC complex, we conducted docking studies to explore other binding models.

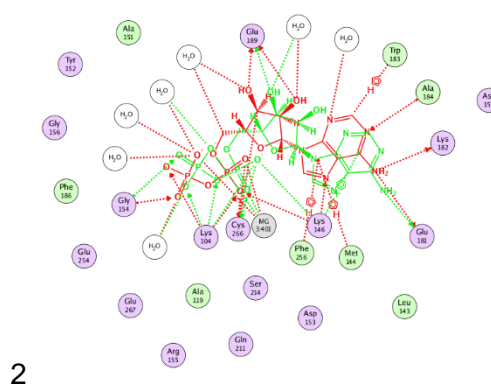
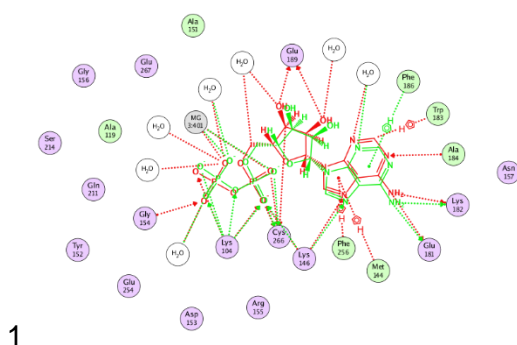
Docking studies were done using chain A of PurK_{Asp} in complex with AIR, ADP and Mg (PDB: 3K5I). The crystal structure was corrected and prepared using the MOE Structure Preparation application, the hydrogen bond network was optimized through Protonate 3D, and charges were calculated via Partial Charges. Since pyrido[2,3-*d*]pyrimidine was confirmed as an ATP-competitive inhibitor in our kinetics analysis, the binding site was specified as the ATP-binding site.

Before docking of the inhibitors was conducted, studies using the natural substrate ADP was done to refine the docking parameters. A Triangle Matcher placement method¹⁸⁰ with London dG scoring function was applied with a maximum of 30 poses returned. The

structures generated by the placement method was further refined by either rigid receptor or induced fit with GBVI/WSA dG as the final scoring function, and the final output was 5 poses. Both the rigid receptor and the induced fit refinement methods gave similar final poses, and for simplicity considerations, rigid receptor was used in the remaining docking studies. The final docking scores for the 5 output poses ranged between -11.72 to -11.31, and RMSD between the docked poses from the original ligand ranged between 1.07 to 2.12 Å (Table 9). All five docked poses process similar interactions with the enzyme as observed in the crystal structure with ADP (Figure 25). Thus, these docking parameters were utilized in the exploration of binding models of the pyrido[2,3-*d*]pyrimidines.

Table 9. The docking scores and RMSD values of the 5 output poses of ADP. The ranking was determined by the scoring function.

#	S	RMSD (Å)
1	-11.7250	1.0668
2	-11.6590	1.9729
3	-11.5331	1.7365
4	-11.4915	1.0982
5	-11.3173	2.1226



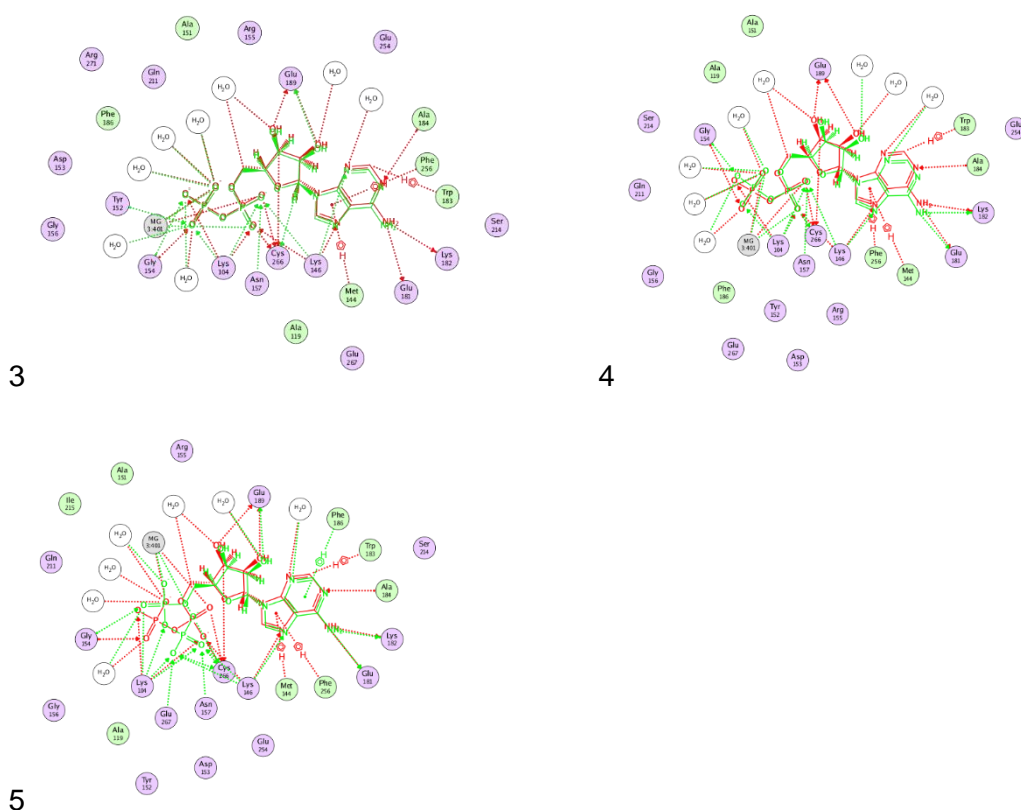
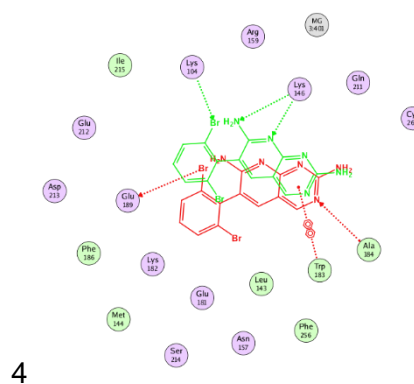
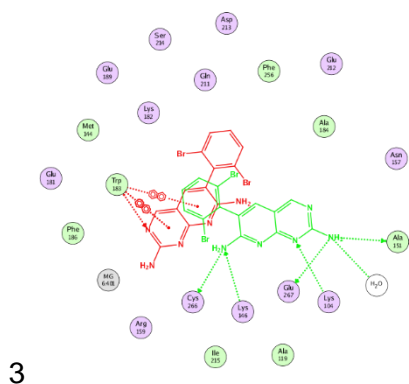
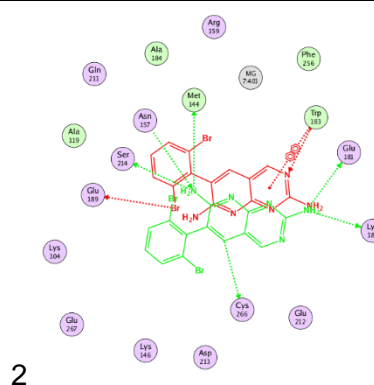
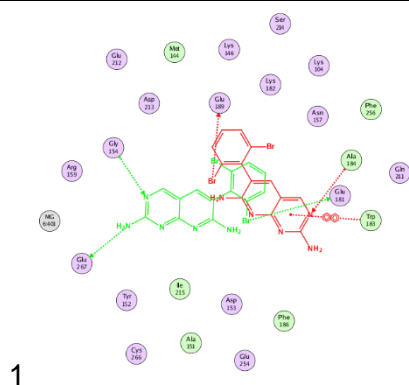


Figure 25. 2-D illustration of the 5 docked ADP poses interacting with the ATP-binding site of PurK_{Asp} (PDB: 3K5I). Red: original ADP from X-ray structure. Green: docked ADP.

To examine the binding of ligands, the parent inhibitor **11** was docked into the ATP-site of PurK_{Asp} according to the method described above. The crystal structure of **11** came from it complexed with BC (PDB: 2V58). The 3D conformation of the ligand went through the conformation-check in MOE with no changes. The final scores for the 5 output poses ranged between -3.86 to -2.08, and RMSD between the docked **11** from the original ligand ranged between 0.92 to 2.07 Å (Table 10). All five docked poses differ from each other with the fourth pose (ranked by score) most resembling the binding model built from the structural alignment (Figure 26).

Table 10. The docking scores and RMSD values of the 5 output poses of inhibitor **11**. The ranking was determined by the scoring function.

#	S	RMSD (Å)
1	-3.8590	1.6131
2	-3.5136	1.6142
3	-3.3461	2.0675
4	-2.7844	0.9206
5	-2.0818	1.3119



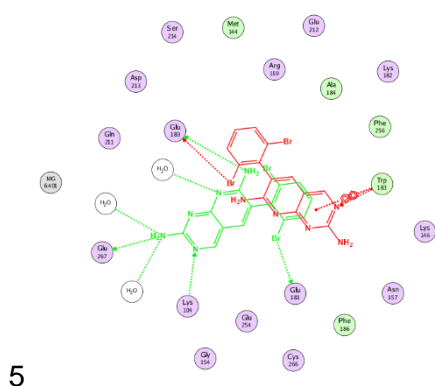


Figure 26. 2-D illustration of the 5 docked **11** poses interacting with the ATP-binding site of PurK_{Asp} (PDB: 3K5I). Red: binding orientation from structural alignment. Green: docked pose. The enzyme was positioned to catch maximum interactions with the docked poses instead of the one from structural alignment.

The SAR generated by 1,6-naphthyridine and 1,8-naphthyridine was used to evaluate the likelihood of the docked poses. The SAR of these two groups of compounds was weighed more heavily than the C-6 and N-7 derivatives because they are direct changes of the pyrido[2,3-*d*]pyrimidine core scaffolds while others are changes on side chains. Based on the SAR of 1,6-naphthyridine and 1,8-naphthyridine, N-1 and N-3 should form critical interactions with PurK_{Asp} with the N-3 interaction being indispensable. Among the five docked poses, poses 3, 4, and 5 displayed the importance of N-1; and pose 1 and 5 indicated that N-3 is significant. Given the fact that pose 4 is similar to the orientation generated by the structural alignment, we believe that docking pose 4 and 5 explains the SAR the best and should be given more consideration in future studies.

Finally, all the C-6 and N-7 non-urea derivatives were docked into the ATP-site of PurK_{Asp} using the same parameters. The crystal structure of **11** from it complexed with BC (PDB: 2V58) formed the basis of all the derivative conformation, and changes in the side chains were manually built into **11**. The 3D conformations and charges of the ligands

manual input were then calculated and corrected by MOE's Conformation Import. This function returns the lowest energy conformation of each derivative by decomposing each ligand into constituent overlapping fragments, performing stochastic conformational search on each fragment, and then assembling the fragments into unique conformers. Five docked poses were returned for each derivative. All the poses were further analyzed by the Protein Ligand Interaction Fingerprints (PLIF) tool in MOE. The PLIF is a method for summarizing the interactions between ligands and proteins using a fingerprint scheme¹⁸⁰.

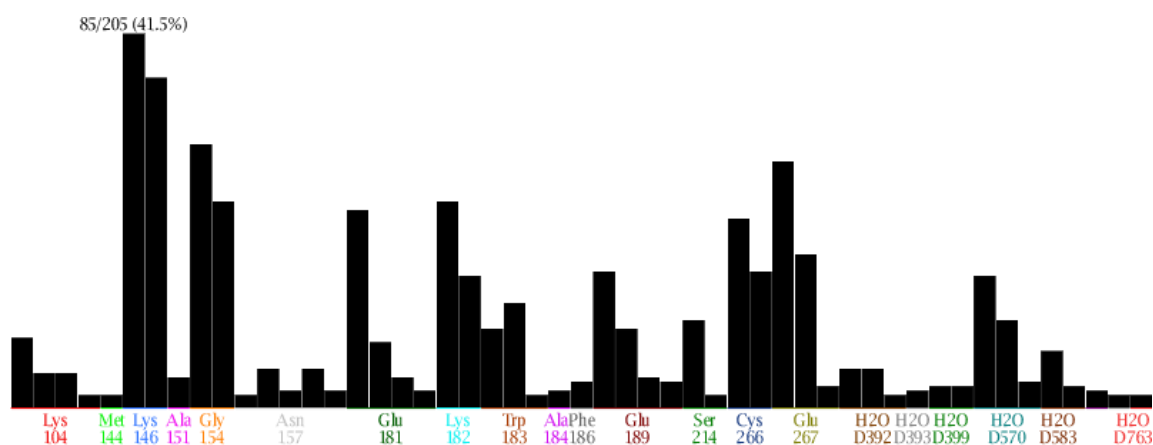


Figure 27. Population display of the PLIF generated by all the docking poses of the C-6 and N-7 non-urea derivatives.

Figure 27 is a population display of the generated fingerprint. The columns for each residue represents the number of potential modes of interaction between this residue and the ligands. If there is more than one column for a residue, there is more than one pose that interacts with that residue. When we examine the residues interacting with the pyrido[2,3-*d*]pyrimidine core scaffold, the four residues in the adenine binding pocket are Lys146, Glu181, Lys182, and Ala184. Among these four residues, each possess at least two poses, suggesting there are two dominant poses for the pyrido[2,3-*d*]pyrimidine core in all derivatives. A close examination revealed that these two dominant poses were represented

by the pose 4 and 5 in Figure 26, suggesting that the binding orientations generated by unbiased docking studies matched with that derived by SAR analysis.

Since pose 4 is the same as that generated by the structural alignment to BC, detailed examination of this model was given in were given in section 2.7.1. Pose 5 was examined in the original PurK_{Asp} structure. Rather than binding in the adenine-site, the pyrido[2,3-*d*]pyrimidine core sat in the ribose-phosphate site of the ATP-binding site in pose 5, and the 6-phenyl occupied the adenine binding site (Figure 28). Compared with the orientation generated by structural alignment, pose 5 was able to predict that the 3', 5'-OH substituted 6-phenyl and 3-(dimethylamino) propyl substituted 7-amino could form more interactions with PurK_{Asp} (Figure 29), hence increasing activity. Pose 5 has its limitations as well. For example, this pose fails to predict the activity gain by small hydrophobic groups at 7-N.

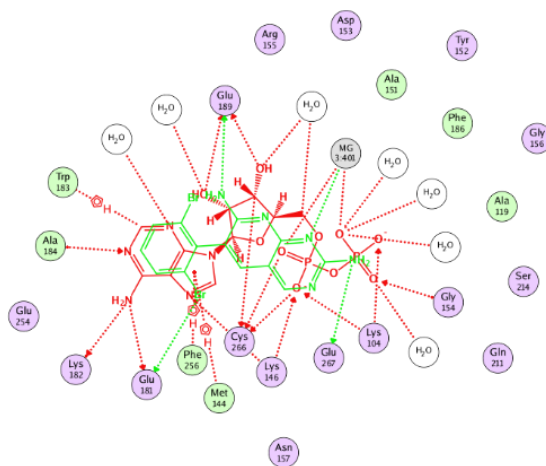


Figure 28. 2-D illustration of the docking pose 5 of pyrido[2,3-*d*]pyrimidine overlapping with ADP in the ATP-site of PurK_{Asp}. Interactions with inhibitors were shown in green, while interactions with ADP were shown in red.

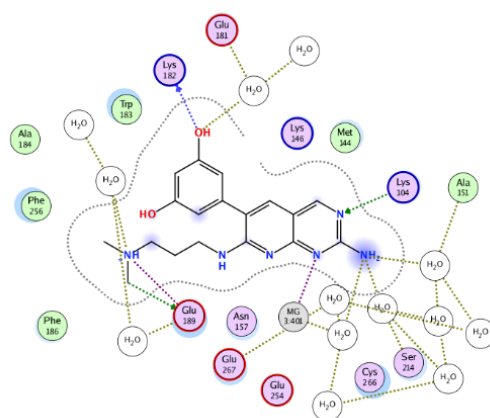


Figure 29. 2-D illustration of the docking pose 5 of **54** in PurK_{Asp}.

The docking studies remove the assumption that pyrido[2,3-*d*]pyrimidine binds the ATP-site of PurK_{Asp} in the same orientation as it binds BC. However, with no direct structural information, the possibilities for different derivatives possessing various orientations still hold. We should keep this in mind when using computational models to design future modifications.

In summary, structural alignments and docking were used to generate potential binding orientations of pyrido[2,3-*d*]pyrimidine in the ATP-site of PurK_{Asp}. The two most likely poses were identified with the heterocycle core sitting in the adenine site and ribose phosphate site, respectively. Both poses provide valid explanations for the SAR of changes on the heterocycle core. The second pose in which the pyrido[2,3-*d*]pyrimidine occupies the ribose-phosphate site is partially explained by the observed side chain SAR. Both poses should be given equal considerations when designing new pyridopyrimidine analogs.

CHAPTER 3 CONCLUSIONS

Taking inspiration from the nanomolar inhibitors described against BC, we tested four different known scaffolds against PurK from two different microbial species. Only one compound, **1**, containing a pyrido[2,3-*d*]pyrimidine core, weakly inhibits PurK_{Asp} with an IC₅₀ of 167 μ M, however this compound is inactive against PurK_{E. coli}. Kinetic assays confirmed that **1** is an ATP-competitive inhibitor. With the guidance of computational modeling, we examined analogs of this lead agent with substituents in the ribose and triphosphate binding sites within the ATP-site. The ribose position modification, compound **14**, has an IC₅₀ of 14 μ M, a 12-fold increase in activity. Additional studies revealed a compound (**34**), with modification in the phosphate binding site with an IC₅₀ of 24 μ M. Combining these two substitutions gave compound **56** with an IC₅₀ of 1.7 μ M, a 100-fold improvement in potency from the lead agent. This compound is the most potent ATP-binding site inhibitor against PurK_{Asp} described to date. The compounds reported here will serve as starting point to develop anti-fungal agents targeting the *de novo* purine biosynthesis pathway.

CHAPTER 4 FUTURE DIRECTIONS

4.1 General future directions

No antimicrobial studies were conducted for these compounds in our study. Considering pyrido[2,3-*d*]pyrimidines inhibited PurK from *A. Clavatus* better than that from *E. coli*, an antifungal study is warranted. However, the compounds described here still resemble inhibitors of BC and thus, further studies are needed to determine the BC activity of these agents. Even if BC activity is limited, any potential antifungal activity must still be validated as the result of inhibiting PurK instead of BC. This could be accomplished by the use of CO₂ rescue studies¹⁸² which has been shown to be a selective rescue for PurK inactivity. For the long-term goal of antimicrobial drug development, a dual target inhibitor against both PurK and BC could be an interesting approach since this could reduce the chance of resistance development.

To improve specificity and potency, continued structural modifications to obtain more potent compounds is a necessary. In the current study, computational models were used to suggest structural modifications. Although improved compounds were obtained, our models are hypothetical at best and are not based upon experimental evidence. To obtain direct binding information, X-ray analysis of protein:ligand complexes are needed. Fortunately, PurK has been crystallized^{121, 139}, although no structure of an inhibitor:PurK complex has been described in the literature.

4.2 Apply covalent inhibitor strategy to increase target specificity and selectivity

Other approaches to increase activity could also be explored, including the use of covalent strategies. Traditionally, covalent inhibitors were often associated with a lack of target specificity and increased off-target and side effects¹⁸³. However, the recent

successes with quiescent affinity labels used in protease¹⁸⁴ and kinase inhibitors¹⁸⁵ have reinvigorated interest in covalent inhibitors among many drug discovery researchers¹⁸⁶⁻¹⁸⁷.

Affinity labels are molecules that have a chemically reactive functional group and will undergo chemical reaction to form a covalent bond with another molecule that possesses a complementary group¹⁸⁸. A popular example of an affinity label used as drugs is omeprazole. Omeprazole is converted to a more reactive sulphenamide under the acidic environment in the stomach. The sulphenamide reacts with a cysteine residue of the gastric H⁺/K⁺ ATPase to inhibit the enzyme activity and therefore is used to treat acid reflux disease¹⁸⁸. Other examples of quiescent affinity labels in medical uses include aspirin and penicillin, and they both label a serine residue in their target proteins.

More recent successes for covalent inhibitors as drugs are the applications in the protease¹⁸⁹⁻¹⁹⁰ and kinase¹⁹¹ inhibitors. Added Michael acceptors onto the original non-covalent inhibitors have led to agents that target cysteine residues in their target proteins rendering the protein inactive. Examples of these inhibitors are shown in Figure 30.

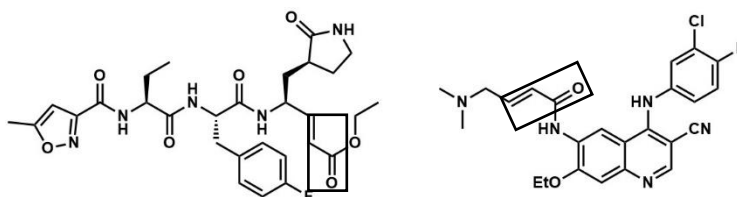


Figure 30. Examples of covalent inhibitors. The Rhinovirus 3C protease inhibitor¹⁸⁹⁻¹⁹⁰ (a) and the epidermal growth factor receptors (EGFR) protein kinase inhibitor¹⁹¹ (b). The boxes indicate the Michael acceptor.

Inspired by these results, we were interested to see if we could apply the covalent inhibitor strategy by adding a covalent warhead to our reversible PurK inhibitor pyrido[2,3-*d*]pyrimidines. We will discuss our preliminary results in the following sections.

4.2.1 Using the cysteine modifier to probe cysteine functions in PurK_{Asp}

A close examination of the ATP-binding site of PurK_{Asp} revealed that Cys266 has the potential to be targeted by quiescent affinity labels. Cys266 is in a β -sheet of the C1-domain of PurK_{Asp}, and it is involved in the binding of the ribose phosphate part of the ATP (Figure 31). Cys266 is about 40% conserved and involved in the binding of ATP in the ATP-grasp enzymes. Other than cysteine, a more common residue at this location is asparagine. Among the PurKs from different species, cysteine is conserved within all species of *Aspergillus*, *Histoplasma capsulatum*, *Paracoccidioides brasiliensis*, and *Pseudogymnoascus*. Asparagine is found from *E. coli*, *S. aureus*, *Candida*, and *Cryptococcus*. This divergence would increase the selectivity of the potential covalent inhibitors targeting PurK.

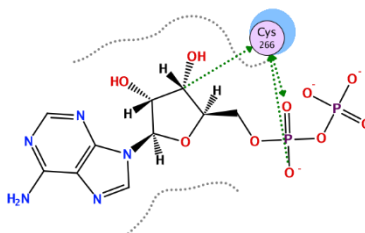


Figure 31. Interaction of Cys266 with ADP in PurK_{Asp} (pdb: 3K5I).

A key question is whether Cys266 is reactive and thus could be targeted by covalent inhibitors. Given this question, we conducted studies aimed at examining whether N-methyl maleimide, a known cysteine reactive probe, would inhibit PurK_{asp} by modifying Cys266.

4.2.2 Probe the cysteine function using N-methyl maleimide

The effect of N-methyl maleimide on PurK was measured by the PK/LDH coupled assay. Various concentrations of N-methyl maleimide were incubated with PurK from different organisms. Different effects of N-methyl maleimide were observed against PurK_{Asp} and

PurK_{E. coli}. For PurK_{Asp}, activity was inhibited, and the progress curves showed a time-dependent curvature. For PurK_{E. coli}, N-methyl maleimide appeared to have no effect (Figure 32). To further confirm that N-methyl maleimide directly inhibits PurK_{Asp} in a time dependent fashion, N-methyl maleimide was pre-incubated with PurK_{Asp}, and after 20 min, 93.5% of the enzymatic activity was lost. The curvature observed from N-methyl maleimide inhibiting PurK_{Asp} could result from several factors including N-methyl maleimide reacting with the enzyme or reagents in the system, or the induction of conformational changes of the enzyme. Using the negative result from PurK_{E. coli}, we can rule out the possibilities that N-methyl maleimide reacts with reagents in the assay.

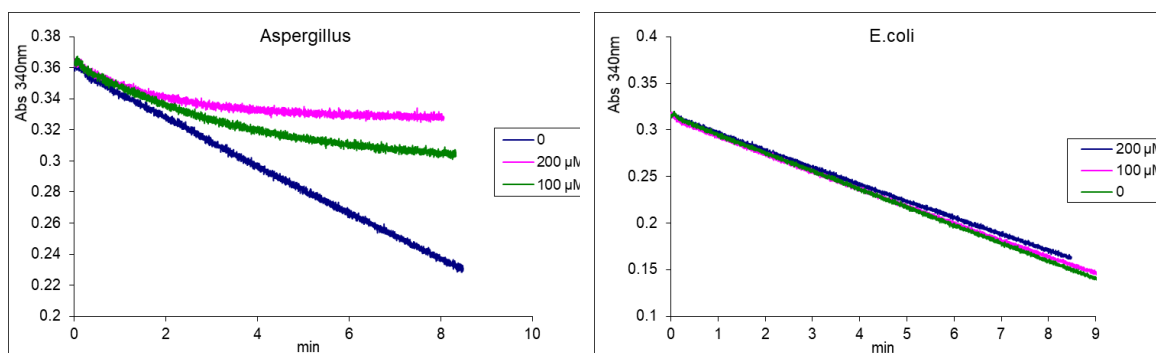


Figure 32. PK/LDH coupled PurK reaction was initiated with PurK at time 0 and the conversion of NADH to NAD⁺ was measured at 340 nm.

4.2.3 N-FITC maleimide binds PurK_{Asp} and PurK_{E. coli} covalently

Based on the reactive nature of maleimide with the thiol of cysteines, it is logical to believe that N-methyl maleimide inhibits PurK by covalent modification. To confirm this, N-FITC maleimide was incubated with PurK_{Asp} and PurK_{E. coli} at room temperature for 30 min. Excess N-FITC maleimide was removed by spin columns with 10K molecular weight cutoff. The enzymes were examined by reducing SDS-PAGE and fluorescent bands of both PurK_{Asp} and PurK_{E. coli} (Figure 33) were observed indicating that N-FITC maleimide modified both enzymes covalently.

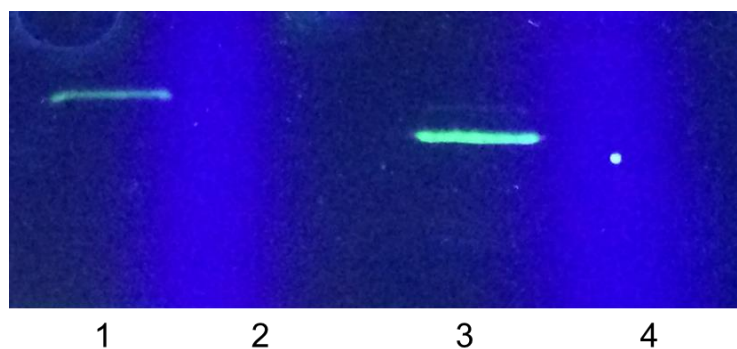


Figure 33. FITC-maleimide covalently labeled both PurK_{Asp} (45 kDa) and PurK_{E. Coli} (40 kDa). 1. PurK_{Asp} + FITC-maleimide; 2. PurK_{Asp} + DMSO; 3. PurK_{E. Coli} + FITC-maleimide; 4. PurK_{E. Coli} + DMSO.

4.2.4 ATP protected PurK_{Asp} from the time-dependent inhibition of N-methyl maleimide

The fact that FITC-maleimide also binds to PurK_{E. coli} indicates that there are multiple cysteines that can be modified by the maleimide reagents. Thus, it is unclear whether the inhibition of PurK_{Asp} is due to inhibition of Cys266. To investigate the cause of the time-dependent inhibition of PurK_{Asp}, kinetic studies were carried out to see if ATP could protect PurK_{Asp} from the inhibition of N-methyl maleimide. If the modification of PurK_{Asp} by N-methyl maleimide could be prevented by the binding of ATP, increasing the ATP concentration should result in a decrease in the observed rate of inactivation (k_{obs}). The PK/LDH assay was used to monitor the progress curve of PurK_{Asp} with a fixed 100 μ M concentration of N-methylmaleimide while various concentrations of ATP were added. The resulting curves were fitted using Equation 1 to determine k_{obs} for each experiment. A decrease k_{obs} versus increase in ATP concentration indicates that ATP protects PurK_{Asp} from N-methyl maleimide inhibition (Figure 34). This suggests that the inactivation of PurK_{Asp} occurs because of a modification of a cysteine near the ATP-binding site.

$$[P] = \frac{v_i}{k_{obs}} [1 - \exp(-k_{obs} * t)]$$

Eq. 1

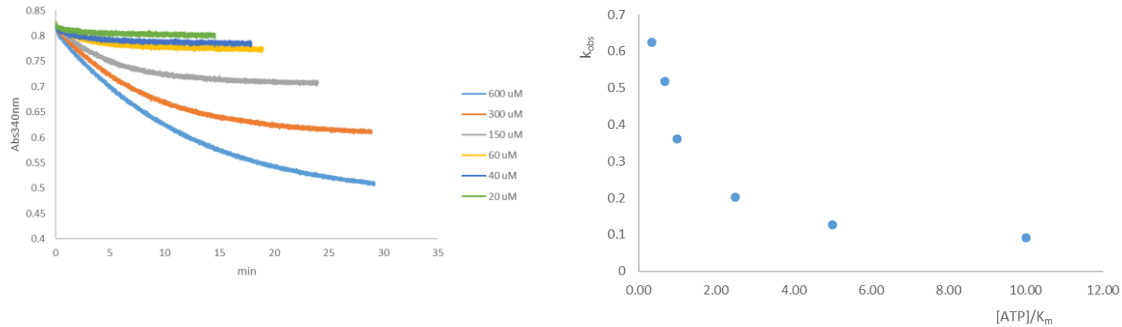


Figure 34. PK/LDH coupled PurK reaction was initiated with PurK at time 0, and the conversion of NADH to NAD⁺ was measured at 340 nm. A fixed concentration of 100 μM N-methylmaleimide was presented in all reactions with increased concentrations of ATP as shown in the left. The progression curves were fitted to equation 1 to generate k_{obs} . The secondary plot of k_{obs} vs. $[ATP]/K_m$ ($K_{m[ATP]} = 60 \mu\text{M}^{142}$) was shown to the right and demonstrates a clear decrease in rate as the ATP concentration increases.

4.2.5 The time-dependent inhibition of N-methyl maleimide against PurK_{Asp} is not due to the modification of Cys266, but Cys216

To further narrow the cause of the time-dependent inhibition, two mutant proteins C266S and C266A were made. We anticipated that both proteins would be active yet would not display inhibition in the presence of N-methyl maleimide. Both proteins indeed retained their catalytic activity. However, to our surprise, treatment with N-methyl maleimide resulted in time-dependent inhibition for both mutant proteins (Figure 35). This interesting, yet unexpected result, generated a few hypotheses. First, N-methyl maleimide does not covalently modify Cys266. Although Cys266 is an exposed residue, there is no direct evidence to indicate that it is modified. A second hypothesis is that N-methyl maleimide

covalently labels Cys266, yet this modification does not influence the enzymatic activity. To explore these hypotheses, we conducted additional experiments aimed at identifying the cysteine residue responsible for the inhibition of PurK_{Asp}.

A close examination of all of the cysteines in PurK_{Asp} revealed that there are five cysteines (Figure 36). The remaining four cysteines are not conserved among ATP-grasp enzymes. Other than Cys266, Cys216 is the closest to the active sites. Therefore we made a mutant protein, C216S, and like the C266 mutants, this mutant also retained catalytic activity. To our great surprise, N-methyl maleimide did not inhibit the activity of the C216S mutant (Figure 35). It is challenging to form a plausible hypothesis as for how modification of Cys216 results in inhibition of the enzyme. The residue does not appear to interact with any substrate, although the sulfur atom is about 7.5 Å away from the free phosphate in the crystal structure (Figure 37). Cys216 is not a conserved residue and the analogous residue in PurK_{E. coli} is Leu189.

These experiments showed that labeling Cys266 by N-methyl maleimide, if it does occur, did not render PurK_{Asp} inactive. Our original idea to add a covalent warhead in pyrido[2,3-d]pyrimidine to target this residue requires modification.

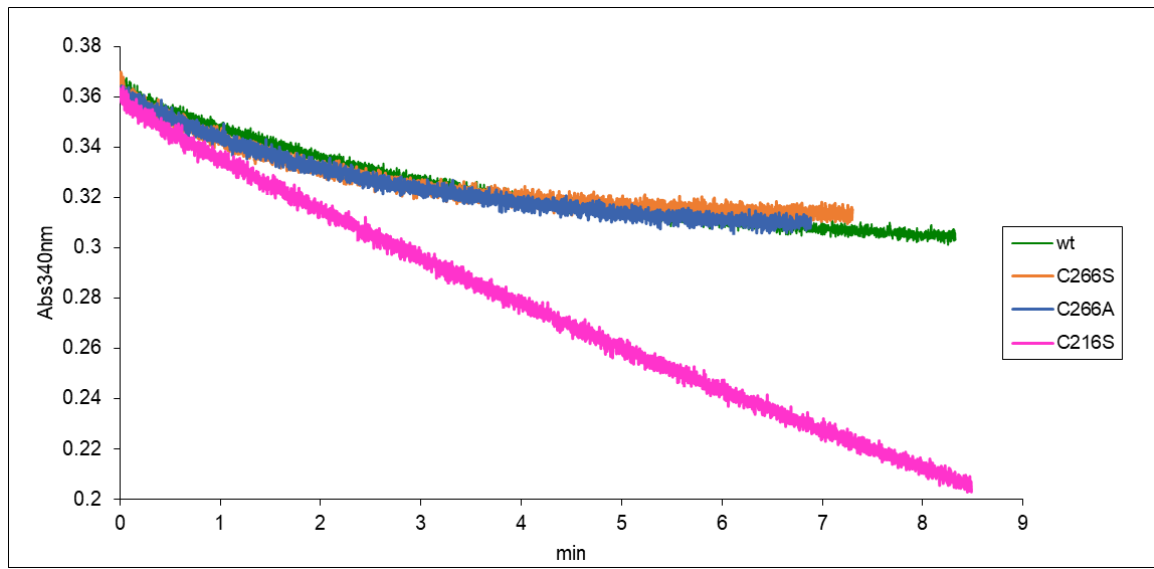


Figure 35. PK/LDH coupled PurK reaction was initiated with PurK (WT or mutants) at time 0 and the conversion of NADH to NAD⁺ was measured at 340 nm. A fixed concentration of 100 μ M N-methylmaleimide was presented in all runs.

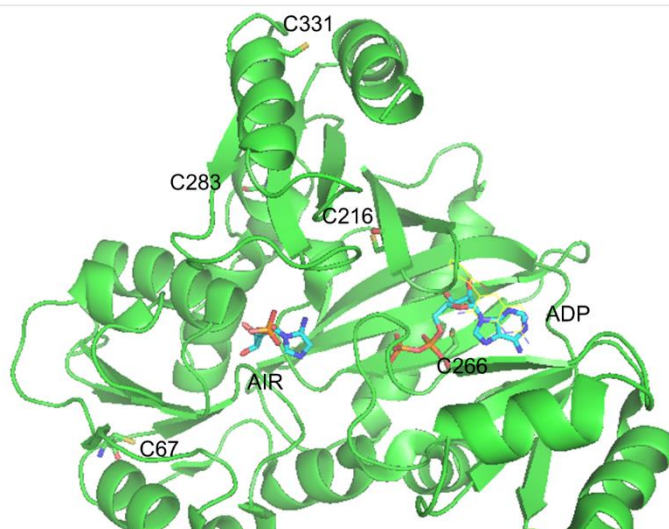


Figure 36. PurK_{Asp} (pdb: 3K5I). 5 cys, ADP, and AIR are shown in sticks.

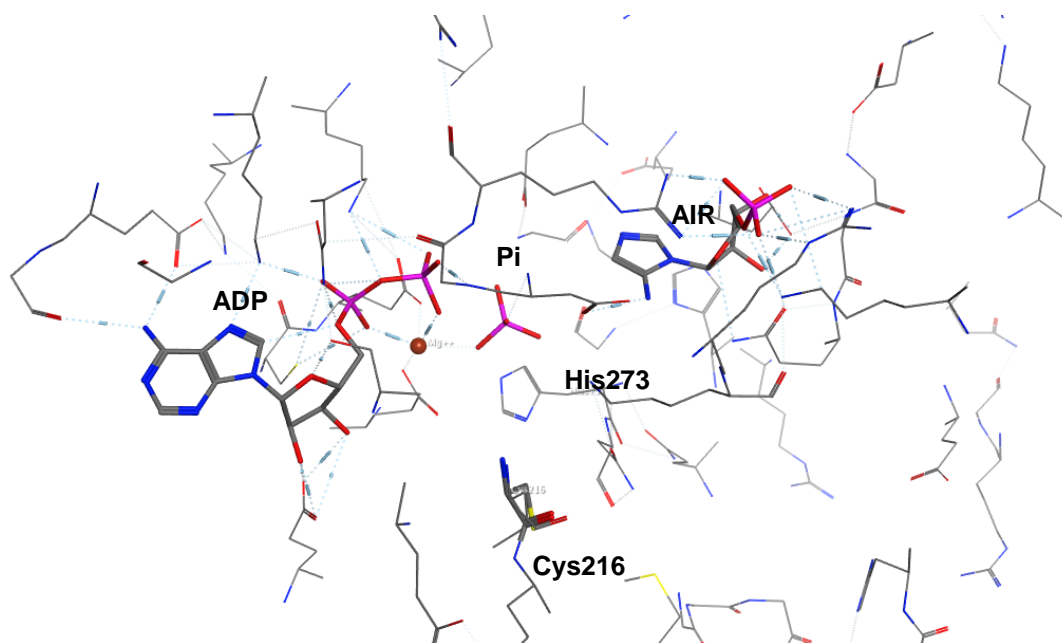


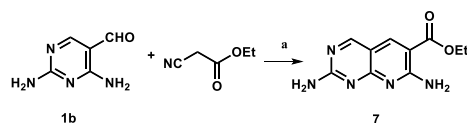
Figure 37. The relative position of Cys216 compared to the enzymatic substrates. (This is a preliminary figure just to show the position).

CHAPTER 5 METHODS AND MATERIALS

5.1 Chemistry

Reactions were run in anhydrous solvents purchased from Acros and used without further purification unless otherwise indicated. Argon was purchased from Airgas. Starting materials were purchased from Acros, Fisher, or Sigma and used without further purification unless otherwise indicated. Solvents used for work-ups and chromatography (methanol, acetone, dichloromethane, chloroform, ethyl acetate and hexanes) were purchased in bulk from Fisher.

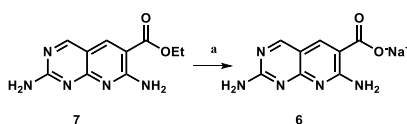
Microwave irradiation reactions were performed using a single-mode Initiator™ Microwave Synthesizer from Biotage using standard Biotage vessels. Column chromatography was carried out on silica gel (Sorbtech). Reactions were monitored by analytical TLC (w/UV 254 nm) and visualized by UV (254 nm and 360 nm). ¹H and ¹³C NMR spectra were recorded on Varian 600 MHz NMR without temperature regulation. Chemical shifts are given in ppm (δ) using tetramethylsilane (TMS) as an internal standard. Mass spectra were recorded by Micromass LCT Premier XE instrument (Waters) with ESI/TOF.



Scheme 10. Synthesis of **7**. Reagents and conditions: (a) NaH, EtOH, reflux, 24 h, 24%.

Ethyl 2,7-diaminopyrido[2,3-*d*]pyrimidine-6-carboxylate (7). To a solution of sodium ethoxide prepared from NaH (4 mmol, 160 mg, 60% slurry in Hexanes) and ethanol (10 mL) was added ethyl cyanoacetate (10 mmol, 1.66 mL). The mixture was stirred under argon at room temperature for 15 min. To this, **1b**¹⁹² (5 mmol, 680 mg) was added and the reaction was heated to reflux for 24 h and then cooled to room temperature. The resulting precipitate was collected by filtration and the solid washed with water, CH₃CN and Et₂O, sequentially.

Column chromatography (99/1 to 97.5/2.5 to 90/10 CH₂Cl₂/MeOH) gave **7** (276 mg, 1.18 mmol, yield 24%) as a white solid. TLC (90/10 CH₂Cl₂/MeOH, *R_f* = 0.38). ¹H NMR (600 MHz, DMSO-*d*₆) δ 8.84 (1H, s, -ArH₄), 8.56 (1H, s, -ArH₅), 7.71 (2H, s, -NH₂), 7.19 (2H, s, -NH₂), 4.31 (2H, q, *J* = 7.1 Hz, -CH₂CH₃), 1.34 (3H, t, *J* = 7.1 Hz, -CH₂CH₃). ¹³C NMR (150 MHz, DMSO-*d*₆) δ 166.3 (COO), 165.2 (C₂), 163.7 (C₇), 162.7 (C₆), 162.1 (C_{7a}), 143.1 (C₄), 108.1 (C_{4a}), 105.2 (C₅), 61.2 (CH₂), 14.6 (CH₃). ES-MS [M+1] found 234.1, calculated for C₁₀H₁₂N₅O₂ 234.2.



Scheme 11. Synthesis of **6**. Reagents and conditions: (a) 2 N NaOH, MeOH, reflux, 3 h, 34%.

2,7-Diaminopyrido[2,3-*d*]pyrimidine-6-carboxylic acid (6). A suspension of **7** (267 mg, 1.1 mmol) in 2 N NaOH (10 mL) was heated at reflux for 3 h. The suspension became clear after heating for 15 min and remained clear. Water was removed *in vacuo* and the solid was recrystallization from water to give **6** as the sodium salt (pale yellow solid, 90 mg, 0.4 mmol, yield 34%). TLC (90/10 CH₂Cl₂/MeOH, *R_f* = 0). ¹H NMR (600 MHz, DMSO-*d*₆) δ 10.14 (1H, d, *J* = 6.1 Hz, -NH₂), 8.57 (1H, s, -ArH₄), 8.23 (1H, s, -ArH₅), 6.94 (1H, d, *J* = 6.1 Hz, -NH₂), 6.53 (2H, s, -NH₂). ¹³C NMR (150 MHz, CD₃OD) δ 172.0 (COOH), 169.7 (C₂), 163.4 (C₇), 163.1 (C_{8a}), 162.0 (C₄), 140.9 (C₅), 112.7 (C₆), 106.6 (C_{4a}). ES-MS [M-1] found 204.1, calculated for C₈H₆N₅O₂ 204.0.

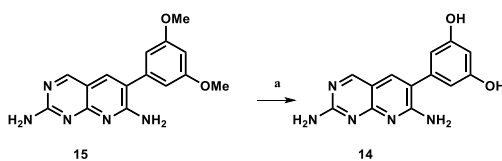
General method for cyclization (1, 8-13, 15-22, 62-66, 71)¹⁹³. The reactions were run in 0.2 – 1 mmol scale. 2-Ethoxyethanol was dried over K₂CO₃, distilled and stored over molecular sieves. To a solution of sodium 2-ethoxyethoxide (4 eq), prepared from NaH and 2-ethoxyethanol, was added various acetonitriles (2 eq). The mixture was stirred under

argon at room temperature for 30 min to 3 h. To the reaction, **1b**¹⁹² (**8c** for 1,6-naphthyridines) (1 eq) was added and the reaction was heated at reflux for 4 h. The reaction was cooled to room temperature, poured into cold water and chilled at 4 °C overnight. The resulting precipitate was collected by filtration and sequentially washed with water, CH₃CN and Et₂O. The solids were dried in vacuo to give **1**, **8-13**, and **15-22**, **71**. Compound **1**, **5**, **9-13**, **15-17** was synthesized following a literature method¹⁶¹. Compound **19**, **21**, and **22** were made based on a patent¹⁹⁴. Compound **20** was made based on a patent¹⁹⁵. Naphthyridines **62-66** were made based on the literature¹⁹⁶⁻¹⁹⁸. NMR analysis of the literature compounds agreed with the published values and thus are not listed below.

2-Ethoxyethyl 2,7-diaminopyrido[2,3-*d*]pyrimidine-6-carboxylate (8). Brown solid (42%). TLC (90/10 CH₂Cl₂/MeOH, *R_f* = 0.42). ¹H NMR δ 8.86 (1H, s, -ArH4), 8.54 (1H, s, -ArH5), 7.69 (2H, s, -NH₂), 7.20 (2H, s, -NH₂), 4.38 (2H, d, *J* = 4.3 Hz, -COOCH₂CH₂), 3.70 (2H, d, *J* = 4.7 Hz, -COOCH₂CH₂), 3.51 (2H, q, *J* = 7.0 Hz, -OCH₂CH₃), 1.13 (3H, t, *J* = 7.0 Hz, -OCH₂CH₃). ¹³C NMR (150 MHz, DMSO-*d*₆) δ 166.2 (COO), 163.2 (C2), 161.7 (C7), 157.1 (C7a), 145.1 (C4), 135.2 (C5), 115.7 (C6), 109.1 (C4a), 68.2 (CH₂CH₂), 67.2 (CH₂CH₃), 63.2 (CH₂CH₂), 14.6 (CH₃). ES-MS [*M*+1] found 278.1, calculated for C₁₂H₁₆N₅O₃ 278.3.

6-(Naphthalen-2-yl)pyrido[2,3-*d*]pyrimidine-2,7-diamine (18). Yellow solid (yield 69%). TLC (89/10/1 CH₂Cl₂/MeOH/NH₄OH, *R_f* = 0.54). ¹H NMR (600 MHz, DMSO-*d*₆) δ 8.70 (1H, s, -ArH4), 8.05 – 7.95 (5H, m, -NapH), 7.77 (1H, s, -ArH5), 7.61 – 7.52 (4H, m, -NapH, -NH₂), 6.74 (2H, s, -NH₂). ¹³C NMR (150 MHz, DMSO-*d*₆) δ 163.9 (C2), 161.5 (C7), 160.9 (C8a), 160.8 (C4), 137.4 (C5), 135.0 (C2'), 133.7 (C4a'), 132.8 (C8a'), 128.9 (C5'), 128.5 (C8'), 128.0 (C3'), 128.0 (C4'), 127.3 (C7'), 126.8 (C6'), 126.7 (C1'), 121.0 (C6), 109.2 (C4a). ES-MS [*M*+1] 288.0, calculated for C₁₇H₁₄N₅ 288.1.

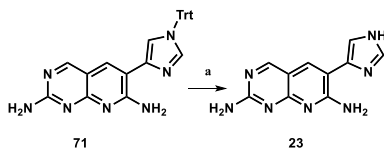
6-(1-Trityl-1H-imidazol-4-yl)pyrido[2,3-d]pyrimidine-2,7-diamine (71). The solid and the CH₃CN fraction were combined and concentrate to dryness in vacuo. Column chromatography (0 to 4% MeOH in DCM to 94.5/5/0.5 to 92/7.5/0.5 CH₂Cl₂/MeOH/NH₄OH) gave **71** (yield 45%) as a dark brown solid. TLC (94.5/5/0.5 CH₂Cl₂/MeOH/NH₄OH, *R_f* = 0.17). ¹H NMR (600 MHz, CDCl₃) δ 8.57 (1H, s, -ArH4), 7.71 (1H, s, -ArH5), 7.52 (1H, d, *J* = 1.3 Hz, -imidH2'), 7.42 – 7.35 (10H, m, -TrtH), 7.22 (1H, d, *J* = 1.4 Hz, -imidH5'), 7.21 – 7.17 (7H, m, -TrtH, -NH₂), 5.12 (2H, s, -NH₂). ¹³C NMR (150 MHz, CDCl₃) δ 162.7 (C2), 161.2 (C7), 160.0 (C8a), 159.7 (C4), 141.9 (Ph), 138.1 (C4'), 138.0 (C2'), 131.8 (C5), 129.7 (Ph), 128.3 (Ph), 128.2 (Ph), 118.5 (C5'), 113.1 (C6), 109.3 (C4a), 75.9 (C). ES-MS [*M*+1] 470.0, calculated for C₂₉H₂₄N₇ 470.2.



Scheme 12. Synthesis of **14**. Reagents and conditions: (a) BBr₃, CH₂Cl₂, 0 °C to r.t., 24 h, 43%.

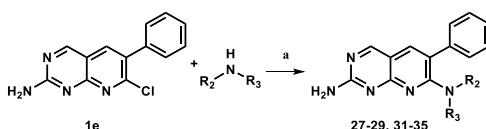
5-(2,7-Diaminopyrido[2,3-d]pyrimidin-6-yl)benzene-1,3-diol (14). A solution of **15**¹⁹² (148 mg, 0.5 mmol) in anhydrous CH₂Cl₂ (3 mL) was cooled to 4 °C in an ice bath. A solution of BBr₃ in CH₂Cl₂ (5 mmol, 1M, 5 mL) was added dropwise to the reaction and the reaction was stirred overnight. Water (2 mL) was added to quench the reaction and the precipitate was collected by filtration and dried *in vacuo*. Column chromatography (78/20/2 CH₂Cl₂/MeOH/NH₄OH) gave **14** (58 mg, 0.21 mmol, yield 43%) as a dark brown solid. TLC (4/1 EtOAc/MeOH, *R_f* = 0.16). ¹H NMR (600 MHz, DMSO-*d*₆) δ 9.43 (2H, s, 2×-OH), 8.64 (1H, s, -ArH4), 7.58 (1H, s, -ArH5), 6.64 (2H, s, -NH₂), 6.26 (2H, d, *J* = 2.1 Hz, -PhH2', 6'), 6.24 (1H, t, *J* = 2.1 Hz, -PhH4'). ¹³C NMR (150 MHz, DMSO-*d*₆) δ 162.4 (C2), 162.1 (C4),

160.0 (C7), 159.4 (C3'), 156.5 (C8a), 137.9 (C1'), 137.2 (C5), 121.9 (C6), 108.0 (C4a), 107.2 (C2'), 103.0 (C4'). ES-MS [M+1] found 270.1, calculated for C₁₃H₁₂N₅O₂ 270.1.



Scheme 13. Synthesis of **23**. Reagents and conditions: (a) TFA, r.t., 1 h, 83%.

6-(1*H*-Imidazol-4-yl)pyrido[2,3-*d*]pyrimidine-2,7-diamine (23). A suspension of **71** (47 mg, 0.1 mmol) in TFA (1 mL) was stirred in a sealed vial at room temperature for 1 h. The reaction was concentrated to dryness in vacuo and the residue purified by column chromatography (94.5/5/0.5 to 78/20/2 CH₂Cl₂/MeOH/NH₄OH) to give **23** (19 mg, 0.08 mmol, yield 83%) as a yellow solid. TLC (89/10/1 CH₂Cl₂/MeOH/NH₄OH, *R_f* = 0.07). ¹H NMR (600 MHz, DMSO-*d*₆) δ 12.46 (1H, s, -imidNH), 8.57 (1H, s, -ArH4), 8.08 (1H, s, -ArH5), 7.82 (1H, d, *J* = 1.2 Hz, -imidH2'), 7.69 (1H, d, *J* = 1.3 Hz, -imidH5'), 6.65 (2H, s, -NH₂). ¹³C NMR (150 MHz, CDCl₃) δ 163.7 (C2), 158.2 (C7), 167.0 (C8a), 150.7 (C4), 139.1 (C4'), 138.8 (C2'), 135.8 (C5), 118.5 (C5'), 118.1 (C6), 109.3 (C4a). ES-MS [M+1] found 228.1, calculated for C₁₃H₁₂N₅O₂ 228.1.



Scheme 14. Synthesis of pyrido[2,3-*d*]pyrimidines with various substitutions at the 7-NH₂ position. Reagents and conditions: (a) neat amine, reflux, 6-12 h, 34-68 %.

General method for *N*⁷-substitution (27-29, 31-35). A suspension of **1e**¹⁹⁴ (51 mg, 0.2 mmol) in various neat amines (1-3 mL, 60-150 eq) was refluxed for 6 to 12 h, and the excess amines were removed in vacuo. Column chromatography of the residue gave **27-29, 31-35**

in moderate yields. Compound **27** was made following a patent method¹⁹⁴. NMR analysis of **27** was consistent with the literature analysis.

***N'*-Cyclopentyl-6-phenylpyrido[2,3-*d*]pyrimidine-2,7-diamine (28).** Column chromatography (1 to 3% MeOH/CH₂Cl₂ to 94/5/1 CH₂Cl₂/MeOH/NH₄OH) gave **28** as a yellow solid (30 mg, yield 50%). TLC (94.5/5/0.5 CH₂Cl₂/MeOH/NH₄OH, *R_f* = 0.57). ¹H NMR (600 MHz, CDCl₃) δ 8.59 (1H, s, -ArH4), 7.53 – 7.47 (2H, m, -Ph), 7.47 – 7.41 (2H, m, -Ph), 7.43 – 7.37 (2H, m, -ArH5, -Ph), 5.53 – 5.41 (2H, m, -NH₂), 5.22 (1H, d, *J* = 7.5 Hz, -NH), 4.78 – 4.69 (1H, m, -CH), 2.18 – 2.09 (2H, m, -CH₂), 1.66 – 1.58 (4H, m, -CH₂CH₂-), 1.39 – 1.29 (2H, m, -CH₂). ¹³C NMR (600 MHz, CDCl₃) δ 163.1 (C2), 161.3 (C7), 159.8 (C4), 159.4 (C8a), 136.5 (C1'), 135.0 (C5), 129.4 (C3'), 128.9 (C2'), 128.4 (C4'), 123.1 (C6), 109.2 (C4a), 52.6 (CH), 33.2 (CH₂), 23.6 (CH₂). ES-MS [*M*+1] 306.2, calculated for C₁₈H₂₀N₅ 306.2.

***N'*-Cyclopropyl-6-phenylpyrido[2,3-*d*]pyrimidine-2,7-diamine (29).** Column chromatography (1 to 3% MeOH/CH₂Cl₂) gave **29** as a yellow solid (22 mg, yield 40%). TLC (94.5/5/0.5 CH₂Cl₂/MeOH/NH₄OH, *R_f* = 0.49). ¹H NMR (600 MHz, CDCl₃) δ 8.64 (1H, s, -ArH4), 7.52 – 7.45 (3H, m, -ArH5, -Ph2'), 7.46 – 7.40 (1H, m, -Ph4'), 7.39 – 7.34 (2H, m, -Ph3'), 5.39 – 5.28 (3H, m, -NH, -NH₂), 3.10 (1H, tq, *J* = 3.7, 7.3 Hz, -CH), 0.94 – 0.85 (2H, m, -CH₂), 0.52 – 0.45 (2H, m, -CH₂). ¹³C NMR (600 MHz, CDCl₃) δ 163.0 (C2), 161.2 (C8a), 160.9 (C7), 160.1 (C4), 136.3 (C1'), 135.1 (C5), 129.4 (C3'), 128.9 (C2'), 128.5 (C4'), 123.0 (C6), 109.6 (C4a), 24.7 (CH), 7.5 (CH₂). ES-MS [*M*+1] 278.0, calculated for C₁₆H₁₆N₅ 278.1.

***N',N'*-Diethyl-6-phenylpyrido[2,3-*d*]pyrimidine-2,7-diamine (31).** Column chromatography (1 to 3% MeOH/CH₂Cl₂ to 94/5/1 CH₂Cl₂/MeOH/NH₄OH) gave **31** as a yellow solid (36 mg, yield 68%). TLC (94.5/5/0.5 CH₂Cl₂/MeOH/NH₄OH, *R_f* = 0.43). ¹H NMR (600 MHz, CDCl₃) δ 8.65 (1H, s, -ArH4), 7.52 (1H, s, -ArH5), 7.45 – 7.39 (4H, m, -Ph2', 3'), 7.38 – 7.30 (1H, m, -Ph4'), 5.55 (2H, s, -NH₂), 3.39 (4H, q, *J* = 7.0 Hz, 2x-CH₂CH₃), 1.04

(6H, t, $J = 7.1$ Hz, $2 \times \text{-CH}_2\text{CH}_3$). ^{13}C NMR (600 MHz, CDCl_3) δ 163.1 (C2), 162.5 (C7), 160.2 (C4), 159.7 (C8a), 140.5 (C1'), 138.8 (C5), 128.8 (C3'), 127.6 (C2'), 127.3 (C4'), 124.7 (C6), 109.7 (C4a), 44.2 (CH_2), 13.0 (CH_3). ES-MS $[\text{M}+1]$ 266.1, calculated for $\text{C}_{17}\text{H}_{20}\text{N}_5$ 266.1.

6-Phenyl-*N*'-(prop-2-yn-1-yl)pyrido[2,3-*d*]pyrimidine-2,7-diamine (32). Column chromatography (1 to 3% MeOH/ CH_2Cl_2) gave **32** as a yellow solid (36 mg, yield 67%). TLC (94.5/5/0.5 CH_2Cl_2 /MeOH/ NH_4OH , $R_f = 0.25$). ^1H NMR (600 MHz, CDCl_3) δ 8.66 (1H, s, -ArH4), 7.55 – 7.48 (3H, m, -ArH5, -Ph), 7.48 – 7.40 (3H, m, -Ph), 5.54 (2H, s, -NH_2), 5.38 (1H, t, $J = 5.1$ Hz, -NH), 4.44 (2H, dd, $J = 2.6, 5.1$ Hz, CH_2), 2.22 (1H, t, $J = 2.5$ Hz, $\text{-C}\equiv\text{CH}$). ^{13}C NMR (600 MHz, CDCl_3) δ 163.1 (C2), 160.8 (C8a), 160.4 (C4), 158.8 (C7), 135.9 (C1'), 135.6 (C5), 129.5 (C3'), 129.0 (C2'), 128.6 (C4'), 122.9 (C6), 109.5 (C4a), 80.1 ($\text{C}\equiv\text{CH}$), 71.6 ($\text{C}\equiv\text{CH}$), 31.4 (CH_2). ES-MS $[\text{M}+1]$ 276.3, calculated for $\text{C}_{16}\text{H}_{14}\text{N}_5$ 276.1.

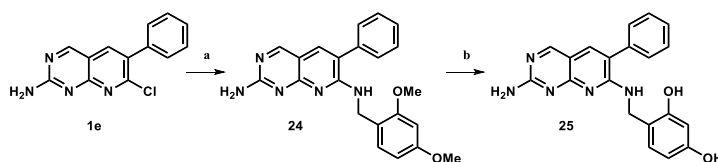
***N*'-Methyl-6-phenyl-*N*'-(prop-2-yn-1-yl)pyrido[2,3-*d*]pyrimidine-2,7-diamine (33).** Column chromatography (1st 1 to 3% MeOH/ CH_2Cl_2 ; 2nd 67 to 100% EtOAc/hexane) gave **33** as a yellow solid (20 mg, yield 34%). TLC (94.5/5/0.5 CH_2Cl_2 /MeOH/ NH_4OH , $R_f = 0.41$). ^1H NMR (600 MHz, CDCl_3) δ 8.74 (1H, s, -ArH4), 7.66 (1H, s, -ArH5), 7.49 – 7.42 (4H, m, -Ph2', 3'), 7.41 – 7.33 (1H, m, -Ph4'), 5.52 (2H, s, -NH_2), 4.21 (2H, d, $J = 2.4$ Hz, CH_2), 2.88 (3H, s, -CH_3), 2.18 (1H, t, $J = 2.5$ Hz, CH). ^{13}C NMR (600 MHz, CDCl_3) δ 163.2 (C2), 162.6 (C7), 160.8 (C4), 159.3 (C8a), 139.6 (C1'), 139.2 (C5), 129.0 (C3'), 127.7 (C2'), 127.5 (C4'), 124.1 (C6), 110.2 (C4a), 79.4 ($\text{-C}\equiv\text{CH}$), 72.2 ($\text{-C}\equiv\text{CH}$), 41.7 (CH_2), 38.9 (CH_3). ES-MS $[\text{M}+1]$ 290.2, calculated for $\text{C}_{17}\text{H}_{16}\text{N}_5$ 290.1.

***N*'-(3-(Dimethylamino)propyl)-6-phenylpyrido[2,3-*d*]pyrimidine-2,7-diamine (34).** Column chromatography (3% MeOH/ CH_2Cl_2 to 94/5/1 to 89/10/1/ CH_2Cl_2 /MeOH/ NH_4OH) gave **34** as a yellow solid (28 mg, yield 43%). TLC (94.5/5/0.5 CH_2Cl_2 /MeOH/ NH_4OH , $R_f = 0.18$). ^1H NMR (600 MHz, CDCl_3) δ 8.55 (1H, s, -ArH4), 7.55 (1H, t, $J = 4.4$ Hz, -NH), 7.49

– 7.43 (2H, m, -Ph), 7.46 – 7.35 (4H, m, -ArH5, -Ph), 5.52 (2H, s, -NH₂), 3.75 – 3.69 (2H, m, -NHCH₂CH₂CH₂), 2.32 (2H, d, *J* = 5.8 Hz, -NHCH₂CH₂CH₂), 1.86 (6H, s, -N(CH₃)₂), 1.68 (2H, p, *J* = 5.9 Hz, -NHCH₂CH₂CH₂). ¹³C NMR (600 MHz, CDCl₃) δ 163.1 (C2), 161.4 (C8a) 160.2 (C7), 159.5 (C4), 136.9 (C1'), 134.7 (C5), 129.2 (C3'), 128.9 (C2'), 127.9 (C4'), 123.8 (C6), 109.0 (C4a), 59.2 (-NHCH₂CH₂CH₂), 44.9 (-N(CH₃)₂), 42.6 (-NHCH₂CH₂CH₂), 24.8 (-NHCH₂CH₂CH₂). ES-MS [M+1] 323.2, calculated for C₁₈H₂₃N₆ 323.2.

***N*⁷-(2-(dimethylamino)ethyl)-6-phenylpyrido[2,3-*d*]pyrimidine-2,7-diamine (35).**

Column chromatography (1st 1 to 3% MeOH/CH₂Cl₂ to 94/5/1 to 89/10/1 CH₂Cl₂/MeOH/NH₄OH; 2nd 94/5/1 CH₂Cl₂/MeOH/NH₄OH) gave **35** as a yellow solid (30 mg, yield 48%). TLC (94.5/5/0.5 CH₂Cl₂/MeOH/NH₄OH, *R_f* = 0.13). ¹H NMR (600 MHz, CDCl₃) δ 8.59 (1H, s, -ArH4), 7.51 – 7.45 (3H, m, -ArH5, -Ph), 7.45 – 7.39 (3H, m, -Ph), 6.08 (1H, t, *J* = 4.8 Hz, -NH), 5.42 (2H, s, -NH₂), 3.67 (2H, td, *J* = 4.8, 6.0 Hz, -NHCH₂CH₂), 2.49 (2H, t, *J* = 6.0 Hz, -NHCH₂CH₂), 2.17 (6H, s, -N(CH₃)₂). ¹³C NMR (600 MHz, CDCl₃) δ 163.1 (C2), 161.3 (C7), 159.8 (C4), 159.7 (C8a), 136.4 (C1'), 135.0 (C5), 129.2 (C3'), 128.9 (C2'), 128.3 (C4'), 123.4 (C6), 109.3 (C4a), 57.4 (-NHCH₂CH₂), 45.0 (-N(CH₃)₂), 38.9 (-NHCH₂CH₂). ES-MS [M+1] 309.1, calculated for C₁₇H₂₁N₆ 309.2.



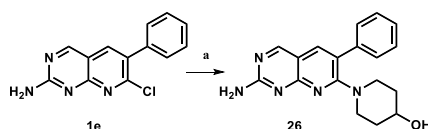
Scheme 15. Synthesis of **24** and **25**. Reagents and conditions: (a) 2,4-dimethoxybenzylamine, Cs₂CO₃, dioxane, reflux, 4 h, 40%; (b) BBr₃, CH₂Cl₂, 0 °C to r.t., 24 h, 20%.

***N*⁷-(2,4-Dimethoxybenzyl)-6-phenylpyrido[2,3-*d*]pyrimidine-2,7-diamine (24).** A suspension of 2,4-dimethoxybenzylamine (33 μL, 0.22 mmol) and Cs₂CO₃ (215 mg, 0.66 mmol) in dioxane (3 mL) was refluxed for 45 min before adding **1e** (51 mg, 0.2 mmol). The

reaction was continued to reflux for 10 h. The reaction solids were removed by filtration and the filtrate was dried *in vacuo*. Column chromatography of the filtrate (0 to 5% MeOH in CH₂Cl₂ to 89/10/1 CH₂Cl₂/MeOH/NH₄OH) gave **24** (31 mg, yield 40%) as a brown solid. TLC (4/1 EtOAc/MeOH, *R_f* = 0.66). ¹H NMR (600 MHz, CDCl₃) δ 8.58 (1H, s, -ArH4), 7.48 – 7.37 (6H, m, -ArH5, -Ph), 7.27 (1H, d, *J* = 8.9 Hz, -Ph), 6.44 – 6.39 (2H, m, -Ph), 6.01 (1H, t, *J* = 5.5 Hz, -NH), 5.47 (2H, s, -NH₂), 4.77 (2H, d, *J* = 5.5 Hz, -CH₂), 3.77 (3H, s, -CH₃), 3.67 (3H, s, -CH₃). ¹³C NMR (150 MHz, CDCl₃) δ 163.0 (C2), 161.2 (C7), 160.4 (C4''), 159.8 (C4), 159.5 (C8a), 158.7 (C2''), 136.5 (C1'), 135.0 (C5), 130.6 (C6''), 129.2 (C3'), 129.0 (C2'), 128.3 (C4'), 123.4 (C1''), 118.7 (C6), 109.3 (C4a), 103.8 (C5''), 98.6 (C3''), 55.4 (CH₃), 55.0 (CH₃), 41.4 (CH₂). ES-MS [M+1] found 388.2, calculated for C₂₂H₂₂N₅O₂ 388.2.

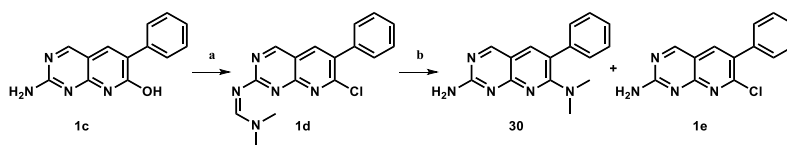
4-(((2-Amino-6-phenylpyrido[2,3-*d*]pyrimidin-7-yl)amino)methyl)benzene-1,3-diol

(25). The synthesis of compound **25** followed the same procedure as for compound **14**. Column chromatography (0 to 3% MeOH in CH₂Cl₂ to 94.5/5/0.5 CH₂Cl₂/MeOH/NH₄OH) gave **25** (yield 20%) as a brown solid. TLC (4/1 EtOAc/MeOH, *R_f* = 0.23). ¹H NMR (600 MHz, DMSO-*d*₆) δ 11.06 (1H, d, *J* = 6.3 Hz, -OH), 9.13 (1H, s, -OH), 8.67 (1H, s, -ArH4), 7.62 (1H, s, -ArH5), 7.54 – 7.39 (5H, m, -Ph), 7.20 (1H, t, *J* = 6.1 Hz, -NH), 6.99 (1H, d, *J* = 8.2 Hz, -Ph5'), 6.86 (2H, s, -NH₂), 6.19 (1H, d, *J* = 2.5 Hz, -Ph4'), 6.15 (1H, dd, *J* = 2.4, 8.1 Hz, -Ph2'), 4.35 (2H, s, -NH₂). ¹³C NMR (150 MHz, DMSO-*d*₆) δ 163.2 (C2), 161.2 (C7), 158.5 (C8a), 158.4 (C4''), 155.4 (C2''), 150.8 (C4), 136.4 (C1'), 135.0 (C5), 130.6 (C6''), 129.2 (C3'), 129.0 (C2'), 128.3 (C4'), 115.4 (C1''), 110.8 (C6), 109.3 (C4a), 108.8 (C5''), 103.4 (C3''), 41.4 (CH₂). ES-MS [M+1] found 359.9, calculated for C₂₀H₁₈N₅O₂ 360.1.



Scheme 16. Synthesis of **26**. Reagents and conditions: (a) piperidin-4-ol, KO_tBu , dioxane, reflux, 4 h, 29%.

1-(2-Amino-6-phenylpyrido[2,3-d]pyrimidin-7-yl)piperidin-4-ol (26). A solution of piperidin-4-ol (21 mg, 0.2 mmol) and KO_tBu (0.22 mmol, 25 mg) in dioxane (5 mL) was stirred under argon at room temperature for 1 h. To the reaction, **1e** (51 mg, 0.2 mmol) was added and the reaction was heated to reflux for 4h. The resulting solids were removed by filtration and the solution was dried *in vacuo*. Column chromatography (1% MeOH in CH_2Cl_2 to 94.5/5/0.5 $\text{CH}_2\text{Cl}_2/\text{MeOH}/\text{NH}_4\text{OH}$) of the residue gave **26** as a yellow solid (19 mg, yield 29%). TLC (94.5/5/0.5 $\text{CH}_2\text{Cl}_2/\text{MeOH}/\text{NH}_4\text{OH}$, $R_f = 0.18$). ^1H NMR (600 MHz, $\text{DMSO}-d_6$) δ 8.80 (1H, s, -ArH4), 7.79 (1H, s, -ArH5), 7.54 (2H, dd, $J = 1.4, 8.1$ Hz, -Ph3'), 7.47 (2H, t, $J = 7.7$ Hz, -Ph2'), 7.36 (1H, t, $J = 7.4$ Hz, -Ph4'), 6.86 (1H, s, -NH₂), 4.65 (1H, d, $J = 4.1$ Hz, -OH), 3.61 – 3.54 (3H, m, -CH, -piperH), 2.88 (2H, td, $J = 2.8, 11.5$ Hz, -piperH), 1.65 – 1.60 (2H, m, -piperH), 1.34 – 1.25 (2H, m, -piperH). ^{13}C NMR (150 MHz, CDCl_3) δ 163.6 (C2), 163.0 (C7), 160.6 (C4), 159.6 (C8a), 139.9 (C1'), 138.8 (C5), 129.1 (C3'), 127.6 (C4'), 127.2 (C2'), 124.9 (C6), 110.4 (C4a), 67.6 (-CHOH), 46.1 (-NCH₂CH₂), 34.0 (-NCH₂CH₂). ES-MS [M+1] found 322.0, calculated for $\text{C}_{18}\text{H}_{20}\text{N}_5\text{O}$ 322.2.



Scheme 17. Synthesis of **30**. Reagents and conditions: (a) SOCl_2 , DMF, CH_2Cl_2 , mw, 70 °C, 1 h, 78%; (b) EtOH, reflux, 12 h, 57%.

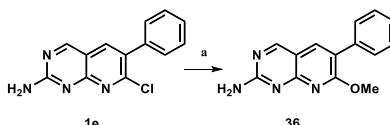
***N'*-(7-chloro-6-phenylpyrido[2,3-d]pyrimidin-2-yl)-*N,N*-dimethylformimidamide**

(**1d**)¹⁹³. In a 20-mL microwave reaction vessel, a solution of **1c**¹⁹³ (952 mg, 4 mmol) in

anhydrous DMF (3 mL) and freshly distilled SOCl_2 (15 mL) was irradiated at 70 °C for 1 h (absorbance: high). The reaction was transferred to a 250-mL round bottom flask and dried in vacuo. The residue was dissolved in ice water and the pH was adjusted to 10 using 6 N NaOH. After chilling at 4 °C overnight, the precipitate was collected by filtration, rinsed with cold water and dried in vacuo to give **1d** (969 mg, yield 78%) as a pale yellow solid. TLC (9/1 EtOAc/MeOH, $R_f = 0.26$). ^1H NMR (600 MHz, $\text{DMSO}-d_6$) δ 9.45 (1H, s, -ArH4), 8.90 (1H, s, -ArH5), 8.45 (1H, s, -N=CH-), 7.59 – 7.45 (5H, m, -Ph), 3.24 (3H, s, -NCH₃), 3.14 (3H, s, -NCH₃). ES-MS [M+1] found 312.1, calculated for $\text{C}_{16}\text{H}_{10}\text{ClN}_5$ 312.1.

7-Chloro-6-phenylpyrido[2,3-*d*]pyrimidin-2-amine (1e)¹⁹³, N⁷,N⁷-dimethyl-6-phenylpyrido[2,3-*d*]pyrimidine-2,7-diamine (30) (Method 1). A mixture of **1d** (2 g, 6.4 mmol) and ethanol (100 mL) was refluxed overnight. The solution was reduced to about 50 mL in vacuo and chilled at 4 °C for 5 h. The precipitate was collected by filtration. Column chromatography (3/2 $\text{CH}_2\text{Cl}_2/\text{EtOAc}$) of the residue gave the major product **1e** as the first fraction and by-product **30** as the second fraction. Compound **1e** was obtained as a bright yellow solid (935 mg, yield 57%). TLC (4/1 hexane/EtOAc, $R_f = 0.45$). ^1H NMR (600 MHz, $\text{DMSO}-d_6$) δ 9.24 (1H, s, -ArH4), 8.29 (1H, s, -ArH5), 7.55 – 7.43 (7H, m, -Ph, -NH₂). ^{13}C NMR (150 MHz, $\text{DMSO}-d_6$) δ 164.5 (C4), 164.2 (C2), 159.0 (C8a), 155.5 (C7), 140.5 (C5), 137.4 (C6), 130.6 (C1'), 130.0 (C3'), 128.8 (C2'), 128.6 (C4'), 113.1 (C4a). ES-MS [M+1] found 257.1, calculated for $\text{C}_{13}\text{H}_{10}\text{ClN}_4$ 257.1. Compound **30** was obtained as a pale yellow solid (326 mg, yield 19%). TLC (4/1 hexane/EtOAc, $R_f = 0.08$). ^1H NMR (600 MHz, $\text{DMSO}-d_6$) δ 8.77 (1H, s, -ArH4), 7.77 (1H, s, -ArH5), 7.49 – 7.40 (4H, m, -Ph), 7.38 – 7.32 (1H, m, -Ph), 6.80 (2H, s, -NH₂). ^{13}C NMR (150 MHz, $\text{DMSO}-d_6$) δ 163.1 (C2), 163.0 (C7), 160.4 (C4), 159.6 (C8a), 140.3 (C1'), 138.8 (C5), 128.8 (C3'), 127.7 (C2'), 127.3 (C4'), 123.9 (C6), 109.8 (C4a), 41.3 (NCH₃). ES-MS [M+1] found 266.1, calculated for $\text{C}_{15}\text{H}_{16}\text{N}_5$ 266.1.

***N*⁷,*N*⁷-Dimethyl-6-phenylpyrido[2,3-*d*]pyrimidine-2,7-diamine (30)** (Method 2). In a 5-mL microwave reaction vessel, **1e** (51 mg, 0.2 mmol) was added to a dimethylamine/THF solution (2 M, 2 mL, 4 mmol). The mixture was irradiated at 70 °C for 2.5 h (absorption: poor) and the solvent was removed in vacuo. Column chromatography (94.5/5/0.5 to 78/20/2 CH₂Cl₂/MeOH/NH₄OH) gave **30** (51 mg, yield 97%) as a yellow solid.



Scheme 18. Synthesis of **36**. Reagents and conditions: (a) MeOH, DIPEA, reflux, 12 h, 80%.

7-Methoxy-6-phenylpyrido[2,3-*d*]pyrimidin-2-amine (36). A suspension of **1e**¹⁹⁴ (51 mg, 0.2 mmol) and DIPEA (70 μ L, 0.4 mmol) in MeOH (3 mL) was refluxed for 12 h, and then concentrated to dryness *in vacuo*. Column chromatography (94.5/5/0.5 to 78/20/2 CH₂Cl₂/MeOH/NH₄OH) gave **36** (40 mg, yield 80%) as a yellow solid. TLC (4/1 hexane/EtOAc, R_f = 0.2). ¹H NMR (600 MHz, CDCl₃) δ 8.89 (1H, s, -ArH₄), 7.86 (1H, s, -ArH₅), 7.60 – 7.53 (2H, m, -Ph₂'), 7.49 – 7.43 (2H, m, -Ph₃'), 7.43 – 7.37 (1H, m, -Ph₁'), 5.49 (2H, s, -NH₂), 4.15 (3H, s, -OCH₃). ¹³C NMR (600 MHz, CDCl₃) δ 163.1 (C₂), 158.0 (C₇), 159.6 (C_{8a}), 148.4 (C₄), 138.8 (C₅), 136.3 (C₁'), 128.8 (C₃'), 127.5 (C₂'), 127.3 (C₄'), 125.9 (C₆), 109.8 (C_{4a}), 54.4 (OCH₃). ES-MS [M+1] found 253.1, calculated for C₁₄H₁₃N₄O 253.1.

General method for urea formation (38-50). To a solution of **1** (48 mg, 0.2 mmol) in DMF (5 mL) was added 60% NaH (10 mg, 0.24 mmol). The reaction mixture was stirred at room temperature for 1 h, followed by the addition of various isocyanates (0.24 mmol, 1.2 eq). The reaction mixture stirred at room temperature overnight and the solvent was removed under high vacuum and the residue was directly purified by column

chromatography (94.5/5/0.5 to 78/20/2 CH₂Cl₂/MeOH/NH₄OH) to give **38-50** in moderate yields. Compound **38, 39, 43-46** was made following a patent method¹⁹⁴. Compound **40-42** was made following the literature¹⁵³. Compound **47-50** was made following the literature¹⁶⁹. NMR analysis of the literature compounds were in agreement with the literature values and are not reported here.

2,6-Difluoro-5-iodonicotinaldehyde (7c)¹⁷². **7c** was made from commercially available 2,6-difluoronicotinaldehyde using a modified procedure¹⁷². A solution of 2,6-difluoronicotinaldehyde (2.86 g, 20 mmol), triethyl orthoformate (5 mL, 30 mmol) and *p*-toluenesulfonic acid (380 mg, 2 mmol) in ethanol (60 mL) was heated at reflux overnight. The solvent was removed and the residue was diluted with EtOAc and washed with sat. NaHCO₃ and brine. The organic layer was dried over MgSO₄ and concentrated in vacuo. Silica column chromatography (0 to 5% EtOAc in pet ether) gave the protected compound **7a** (3.6 g, yield 83%) as a clear, colorless oil. TLC (4/1 EtOAc/Hexanes, *R_f* = 0.68). This material was used in the next step. In a flame-dried 250 mL 3-neck round bottom flask, a solution of freshly distilled diisopropylamine (3.37 mL, 24 mmol) in anhydrous THF (8 mL) was cooled in a dry ice-acetone bath. A thermometer was inserted into the reaction to monitor temperature. After the mixture was cooled to under -60 °C, a solution of *n*-butyllithium (1.5 M in hexanes) (14.4 mL, 21.6 mmol) was added dropwise through a dropping funnel. The speed of addition was controlled so that the temperature was always below -60 °C. The mixture was stirred at -60 °C for 5 min and warmed to room temperature and stirred for 10 min. The mixture was re-cooled to -70 °C in the dry ice-acetone bath and a solution of **7a** (1.736 g, 8 mmol) in 8 mL THF was injected slowly to prevent the temperature rising above -60 °C. The mixture was stirred at -70 °C for 90 min. To this reaction, a solution of iodine (2.64g, 10.4 mmol) in 40 mL THF was added using a syringe

pump (20 mL/h) over a 2 h period. After the addition of iodine, the reaction was removed from the dry ice-acetone bath and the temperature slowly rose to room temperature. The reaction was treated with sat. NaHSO₃ (40 mL) for 60 min before diluting with 250 mL EtOAc and washed with 1 N HCl (2×100 mL) and brine (150 mL). The organic phase was dried over MgSO₄ and concentrated *in vacuo* to give an oil that slowly solidified affording **7b** (2.65 g, 7.7 mmol, yield 96%) as a white solid. TLC (4/1 EtOAc/Hexanes, *R_f* = 0.78). The final product was obtained as follows. A solution of **7b** (1.11 g, 3.2 mmol) and HCl (1 N in water, 12 mL, 12 mmol) in THF (12 mL) was added to a round-bottom flask and the flask was sealed by septum and parafilm. The reaction was incubated at room temperature for 4 days. The reaction was directly poured into a separation funnel and diluted with 50 mL EtOAc. The organic layer was washed with sat. NaHCO₃ followed by brine. The organic layer was dried over MgSO₄ and concentrated *in vacuo*. Silica column chromatography (0 to 5% EtOAc in Hexanes) gave **7c** (0.84 g, yield 96%) as a white solid. TLC (4/1 EtOAc/Hexanes, *R_f* = 0.88). ¹H NMR (600 MHz, CDCl₃) δ 10.18 (1H, s, -CHO), 8.73 (1H, t, *J* = 8.1 Hz, -ArH). ¹³C NMR (150 MHz, CDCl₃) δ 183.4 (CHO), 163.7 (dd, *J* = 14.6, 10.2 Hz, C6), 162.0 (dd, *J* = 14.5, 3.9 Hz, C2), 152.5 (dd, *J* = 5.2, 2.5 Hz, C4), 117.6 (dd, *J* = 20.9, 5.8 Hz, C3), 71.3 (dd, *J* = 41.3, 5.7 Hz, C5). ES-MS [M+1] found 269.7, calculated for C₆H₃F₂INO 269.9.

6-((3-(Dimethylamino)propyl)amino)-2-fluoro-5-iodonicotinaldehyde (7d)¹⁷³. To a reaction under argon, a solution of **7c** (716 mg, 2.67 mmol) in anhydrous DMSO (20 mL) was treated with 3-(dimethylamino)propylamine (352 μL, 2.79 mmol) and K₂CO₃ (735 mg, 5.34 mmol) and stirred at room temperature for 2 h. The reaction mixture was poured into 200 mL of water and chilled at 4 °C overnight. A pale-yellow precipitate was collected by filtration and the solid was washed with cold water. The solid was re-dissolved with 5 mL 1:1 CH₂Cl₂ / MeOH, and the insoluble impurities were discarded. The organic solution was

concentrated and dried *in vacuo* to give **7d** (733 mg, 78% yield) as a pale yellow solid. TLC (94.5/5/0.5 CH₂Cl₂/MeOH/NH₄OH, *R_f* = 0.15). ¹H NMR (600 MHz, CDCl₃) δ 9.88 (1H, s, -CHO), 8.88 (1H, s, -NH), 8.31 (1H, d, *J* = 9.0 Hz, -ArH), 3.61-3.58 (2H, m, -NHCH₂CH₂CH₂N), 2.56 (2H, t, *J* = 5.4 Hz, -NHCH₂CH₂CH₂N), 2.31 (6H, s, -N(CH₃)₂), 1.81-1.77 (2H, m, -NHCH₂CH₂CH₂N). ¹³C NMR (150 MHz, CDCl₃) δ 183.6 (CHO), 165.6 (d, *J* = 240 Hz, C2), 159.3 (d, *J* = 15 Hz, C6), 147.1 (C4), 108.2 (d, *J* = 30 Hz, C3), 73.2 (C5), 59.4 (-NHCH₂CH₂CH₂N), 45.4 (-N(CH₃)₂), 44.1 (-NHCH₂CH₂CH₂N), 24.2 (-NHCH₂CH₂CH₂N). ES-MS [M+1] found 352.0, calculated for C₁₁H₁₆FIN₃O 352.2. Note: The regioselectivity of **7d** was characterized by the coupling constant (*J*) in ¹³C NMR.

N⁷-(3-(Dimethylamino)propyl)-6-iodopyrido[2,3-*d*]pyrimidine-2,7-diamine (7e)¹⁹⁹. In a 5-mL microwave vessel, a solution of **7d** (105 mg, 0.3 mmol) in anhydrous acetonitrile (3 mL) was treated with guanidine nitrate (44mg, 0.36 mmol) and triethyl amine (101 μL, 0.72 mmol). The mixture was irradiated with stirring at 150 °C for 60 min (absorption: normal). The reaction was subsequently transferred into a 100-mL round bottom flask and dried *in vacuo*. Silica column chromatography (94.5/5/0.5 to 89/10/1 CH₂Cl₂/MeOH/NH₄OH) gave **7e** (37 mg, yield 33%) as a brown oil. TLC (develop twice in 89/10/1 CH₂Cl₂/MeOH/NH₄OH, *R_f* = 0.09). ¹H NMR (600 MHz, CDCl₃) δ 8.50 (1H, s, -ArH4), 8.13 (1H, s, -NH), 8.08 (1H, s, -ArH5), 5.29 (2H, s, -NH₂), 3.75 (2H, q, *J* = 5.6 Hz, -NHCH₂CH₂CH₂N), 2.59 (2H, t, *J* = 6.0 Hz, -NHCH₂CH₂CH₂N), 2.35 (6H, s, -N(CH₃)₂), 1.87-1.83 (2H, m, -NHCH₂CH₂CH₂N). ¹³C NMR (150 MHz, CDCl₃) δ 163.1 (C7), 160.9 (C2), 159.4 (C8a), 158.9 (C4), 145.3 (C5), 110.8 (C4a), 77.9 (C6), 58.9 (-NHCH₂CH₂CH₂N), 45.4 (-N(CH₃)₂), 43.1 (-NHCH₂CH₂CH₂N), 24.6 (-NHCH₂CH₂CH₂N). ES-MS [M+1] found 373.0, calculated for C₁₂H₁₈IN₆ 373.0.

General method for Suzuki coupling (51-57)¹⁹⁹⁻²⁰⁰. A mixture of **7e** (1 eq), boronic acid (1.1 eq), Pd(PPh₃)₄ (0.1 eq) and Na₂CO₃ (2 eq) was purged with argon three times. A

mixture of solvents (1/0.5/0.1 CH₃CN/DMF/H₂O) was degassed by bubbling with argon for 10 min and the solvents were added to the solids. The reaction was heated to 90 °C for 5 h. The resulting solids were moved by filtration, and the filtrate was dried *in vacuo*. Column chromatography over silica gel using the methods below gave the desired compounds, **51-55**.

6-(2,6-Dimethoxyphenyl)-N⁷-(3-(dimethylamino)propyl)pyrido[2,3-d]pyrimidine-2,7-diamine (51). Column chromatography (94.5/5/0.5 to 89/10/1 CH₂Cl₂/MeOH/NH₄OH) gave **51** (yield 70%) as a yellow solid. TLC (89/10/1 CH₂Cl₂/MeOH/NH₄OH, *R_f* = 0.45). ¹H NMR (600 MHz, CDCl₃) δ 8.51 (1H, s, -ArH₄), 7.36-7.34 (2H, m, -ArH₅, -Ph₄'), 6.87 (1H, s, -NH), 6.65 (2H, d, *J* = 8.4 Hz, -Ph₃', 5'), 5.36 (2H, s, -NH₂), 3.71-3.68 (8H, m, -NHCH₂CH₂CH₂N, 2x-OCH₃), 2.30 (2H, t, *J* = 6.0 Hz, -NHCH₂CH₂CH₂N), 1.89 (6H, s, -N(CH₃)₂), 1.68-1.64 (2H, m, -NHCH₂CH₂CH₂N). ¹³C NMR (150 MHz, CDCl₃) δ 162.9 (C2), 161.6 (C7), 160.8 (C8a), 159.2 (C2', C6'), 158.6 (C4), 140.0 (C5), 130.0 (C4'), 116.4 (C6), 113.0 (C4a), 109.2 (C1'), 104.1 (C3', C5'), 59.0 (-NHCH₂CH₂CH₂N), 55.8 (-OCH₃), 44.9 (-N(CH₃)₂), 41.9 (-NHCH₂CH₂CH₂N), 25.2 (-NHCH₂CH₂CH₂N). ES-MS [M+1] found 382.3, calculated for C₂₀H₂₇N₆O₂ 382.2.

6-(3,5-Dimethoxyphenyl)-N⁷-(3-(dimethylamino)propyl)pyrido[2,3-d]pyrimidine-2,7-diamine (52). Column chromatography (94.5/5/0.5 to 89/10/1 CH₂Cl₂/MeOH/NH₄OH) gave **52** (yield 66%) as a yellow solid. TLC (develop twice in 89/10/1 CH₂Cl₂/MeOH/NH₄OH, *R_f* = 0.47). ¹H NMR (600 MHz, CDCl₃) δ 8.56 (1H, s, -ArH₄), 7.53 (1H, t, *J* = 4.2 Hz, -NH), 7.41 (1H, s, -ArH₅), 6.51 (3H, s, -Ph₂', 4', 6'), 5.37 (2H, s, -NH₂), 3.82 (6H, s, 2x-OCH₃), 3.73-3.70 (2H, m, -NHCH₂CH₂CH₂N), 2.34 (2H, t, *J* = 5.4 Hz, -NHCH₂CH₂CH₂N), 1.92 (6H, s, -N(CH₃)₂), 1.71-1.67 (2H, p, *J* = 12 Hz, -NHCH₂CH₂CH₂N). ¹³C NMR (150 MHz, CDCl₃) δ 163.1 (C2), 161.4 (C7), 161.1 (C3', C5'), 160.1 (C8a), 159.5 (C4), 138.8 (C1'), 134.3 (C5),

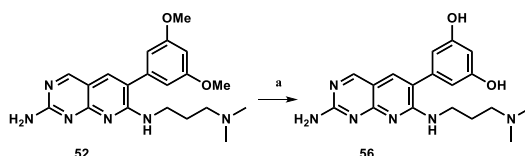
123.7 (C6), 108.8 (C4a), 107.2 (C2', C6'), 100.0 (C4'), 59.2 (-NHCH₂CH₂CH₂N), 55.4 (-OCH₃), 44.9 (-N(CH₃)₂), 42.5 (-NHCH₂CH₂CH₂N), 24.9 (-NHCH₂CH₂CH₂N). ES-MS [M+1] found 382.2, calculated for C₂₀H₂₇N₆O₂ 382.2.

N⁷-(3-(Dimethylamino)propyl)-6-(1*H*-indol-6-yl)pyrido[2,3-*d*]pyrimidine-2,7-diamine (53). Column chromatography (94.5/5/0.5 to 89/10/1 CH₂Cl₂/MeOH/NH₄OH) gave **53** (yield 71%) as a pale yellow solid. TLC (89/10/1 CH₂Cl₂/MeOH/NH₄OH, *R_f* = 0.18). ¹H NMR (600 MHz, CDCl₃) δ 11.23 (1H, s, -lnNH), 8.62 (1H, s, -ArH4), 7.65 (1H, d, *J* = 8.0 Hz, -lnH4'), 7.55 (1H, s, -ArH5), 7.42 (1H, t, *J* = 2.8 Hz, -lnH2'), 7.40 (1H, s, -lnH7'), 7.27 (1H, t, *J* = 5.2 Hz, -lnH3'), 6.99 (1H, dt, *J* = 8.1, 1.1 Hz, -lnH5'), 6.60 (2H, s, -NH₂), 6.49 (1H, t, *J* = 2.5 Hz, -NH), 3.46 (2H, q, *J* = 6.1 Hz, -NHCH₂CH₂CH₂N), 2.24 (2H, s, -NHCH₂CH₂CH₂N), 1.82 (6H, s, -N(CH₃)₂), 1.63 (2H, p, *J* = 6.4 Hz, -NHCH₂CH₂CH₂N). ¹³C NMR (150 MHz, CD₃OD) δ 162.8 (C2), 161.1 (C7), 160.7 (C8a), 159.3 (C4), 136.5 (C6'), 134.7 (C5), 128.8 (C7'a), 128.1 (C3'a), 125.4 (C2'), 125.3 (C6), 120.6 (C4'), 119.7 (C5'), 111.5 (C7'), 108.6 (C4a), 101.0 (C4'), 57.4 (-NHCH₂CH₂CH₂N), 43.6 (-N(CH₃)₂), 40.2 (-NHCH₂CH₂CH₂N), 25.4 (-NHCH₂CH₂CH₂N). ES-MS [M+1] found 362.3, calculated for C₂₀H₂₄N₇ 362.2.

N⁷-(3-(Dimethylamino)propyl)-6-(1*H*-indol-5-yl)pyrido[2,3-*d*]pyrimidine-2,7-diamine (54). Column chromatography (97/3/0 to 94.5/5/0.5 to 89/10/1 CH₂Cl₂/MeOH/NH₄OH) gave **54** (yield 69%) as a yellow solid. TLC (89/10/1 CH₂Cl₂/MeOH/NH₄OH, *R_f* = 0.41). ¹H NMR (600 MHz, CDCl₃) δ 9.17 (1H, s, -lnNH), 8.55 (1H, s, -ArH4), 7.63 (1H, s, -lnH4'), 7.48 (1H, d, *J* = 8.3 Hz, -lnH6'), 7.43 (1H, s, -ArH5), 7.31 (1H, s, -lnH7'), 7.24 (1H, t, *J* = 2.7 Hz, -NH), 7.13 (1H, d, *J* = 8.2 Hz, -lnH2'), 6.57 (1H, t, *J* = 2.4 Hz, -lnH3'), 5.34 (2H, s, -NH₂), 3.7 (2H, q, *J* = 5.7 Hz, -NHCH₂CH₂CH₂N), 2.28 (2H, t, *J* = 6.1 Hz, -NHCH₂CH₂CH₂N), 1.78 (6H, s, -N(CH₃)₂), 1.67 (2H, p, *J* = 6.2 Hz, -NHCH₂CH₂CH₂N). ¹³C NMR (150 MHz, CDCl₃) δ 162.8 (C2), 161.3 (C8a), 161.0 (C7), 159.3 (C4), 135.6 (C5'), 134.5 (C5), 128.3 (C7'a), 127.8

(C3'a), 125.4 (C2'), 125.3 (C6), 123.0 (C4'), 121.3 (C6'), 111.7 (C7'), 109.3 (C4a), 102.6 (C3'), 58.8 (-NHCH₂CH₂CH₂N), 44.8 (-N(CH₃)₂), 42.0 (-NHCH₂CH₂CH₂N), 25.3 (-NHCH₂CH₂CH₂N). ES-MS [M+1] found 362.2, calculated for C₂₀H₂₄N₇ 362.2.

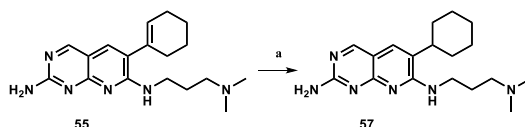
6-(Cyclohex-1-en-1-yl)-N7-(3-(dimethylamino)propyl)pyrido[2,3-d]pyrimidine-2,7-diamine (55). Column chromatography (99/1/0 to 97/3/0 to 94.5/5/0.5 to 89/10/1 CH₂Cl₂/MeOH/NH₄OH) gave **55** (yield 71%) as a brown solid. TLC (89/10/1 CH₂Cl₂/MeOH/NH₄OH, *R_f* = 0.35). ¹H NMR (600 MHz, CDCl₃) δ 8.51 (1H, s, -ArH4), 7.28 (1H, s, -ArH5), 6.89 (1H, t, *J* = 5.1 Hz, -NH), 5.83 (1H, dq, *J* = 3.8, 1.8 Hz, -cyhxH2'), 5.17 (2H, s, -NH₂), 3.73 (2H, q, *J* = 5.7 Hz, -NHCH₂CH₂CH₂N), 2.46 (2H, t, *J* = 6.1 Hz, -NHCH₂CH₂CH₂N), 2.27 (6H, s, -N(CH₃)₂), 2.24-2.16 (4H, m, cyhxH), 1.84-1.73 (4H, m, cyhxH), 1.76-1.67 (2H, m, -NHCH₂CH₂CH₂N). ¹³C NMR (150 MHz, CDCl₃) δ 162.8 (C2), 160.9 (C8a), 160.0 (C7), 159.2 (C4), 134.1 (C1'), 132.7 (C5), 128.9 (C2'), 126.1 (C6), 109.0 (C4a), 59.1 (-NHCH₂CH₂CH₂N), 45.6 (-N(CH₃)₂), 41.7 (-NHCH₂CH₂CH₂N), 29.3 (C6'), 25.6 (-NHCH₂CH₂CH₂N), 25.4 (C3'), 22.9 (C5'), 21.8 (C4'). ES-MS [M+1] found 327.2, calculated for C₁₈H₂₇N₆ 327.2.



Scheme 19. Synthesis of **56**. Reagents and conditions: (a) BBr₃, CH₂Cl₂, 0 °C, 2 h, 9%.

5-(2-Amino-7-((3-(dimethylamino)propyl)amino)pyrido[2,3-d]pyrimidin-6-yl)benzene-1,3-diol (56). The synthesis of compound **56** followed the same procedure as for compound **14**. A cation exchange column was used for purification. The phosphate cellulose resin (Whatman P11 cation exchange) was prepared by soaking the resin in water for 30 min before packing. A solution of 1 mL sat. NH₄Cl in 25 mL water was used to charge the resin followed by flushing with water to remove the excess salt. The material was

dissolved in water to load onto the column. The column was eluted by ammonia gradient (0-0.8%) and monitored by TLC (78/20/2 CH₂Cl₂/MeOH/NH₄OH, *R_f* = 0.42). The fractions containing the desired product was pooled and lyophilized to give **56** as a white solid (yield 9%). ¹H NMR (600 MHz, CD₃OD) 9.42 (1H, s, -ArH4), 8.58 (1H, s, -ArH5), 6.58 (2H, d, *J* = 2.1 Hz, -PhH2', 6'), 6.24 (1H, t, *J* = 2.1 Hz, -PhH4'), 3.49 (2H, q, *J* = 6.1 Hz, -NHCH₂CH₂CH₂N), 2.38 (2H, s, -NHCH₂CH₂CH₂N), 1.98 (6H, s, -N(CH₃)₂), 1.63 (2H, p, *J* = 6.4 Hz, -NHCH₂CH₂CH₂N). ¹³C NMR (150 MHz, CD₃OD) δ 162.4 (C2), 160.0 (C7), 159.4 (C3'), 156.5 (C8a), 148.1 (C4), 139.9 (C1'), 137.2 (C5), 118.7 (C6), 110.8 (C4a), 107.2 (C2'), 103.5 (C4'), 47.2 (-N(CH₃)₂), 43.0 (-NHCH₂CH₂CH₂N), 42.0 (-NHCH₂CH₂CH₂N), 26.3 (-NHCH₂CH₂CH₂N). ES-MS [M+1] found 355.2, calculated for C₁₈H₂₃N₆O₂ 355.2.



Scheme 20. Synthesis of **57**. Reagents and conditions: (a) 10% Pd/C, H₂, 40 psi, r.t., 2 h, 46%.

6-Cyclohexyl-*N*'-(3-(dimethylamino)propyl)pyrido[2,3-*d*]pyrimidine-2,7-diamine (57**)²⁰⁰.** A solution of **55** (26 mg, 0.08 mmol) in MeOH (10 mL) was degassed and purged with argon three times. To the solution, 10% Pd on activated carbon (6 mg) was added. The argon was evacuated and exchanged with H₂ gas three times and the reaction was shaken under H₂ at 40 psi for 2 h. The mixture was filtered through Celite and the filtrate was dried *in vacuo*. Column chromatography (99/1/0 to 97/3/0 to 94.5/5/0.5 CH₂Cl₂/MeOH/NH₄OH) gave **57** (12 mg, yield 46%) as a brown solid. TLC (89/10/1 CH₂Cl₂/MeOH/NH₄OH, *R_f* = 0.35). ¹H NMR (600 MHz, CDCl₃) δ 8.53 (1H, s, -ArH4), 7.84 (1H, s, -NH), 7.38 (1H, s, -ArH5), 5.10 (2H, s, -NH₂), 3.78 (2H, q, *J* = 5.4 Hz, -NHCH₂CH₂CH₂N), 2.55 (2H, t, *J* = 5.4 Hz, -NHCH₂CH₂CH₂N), 2.37-2.29 (7H, m, -N(CH₃)₂, cyhxH1'), 1.97-1.87 (4H, m, cyhxH),

1.87-1.77 (3H, m, cyhxH), 1.44-1.25 (5H, m, -NHCH₂CH₂CH₂N, cyhxH). ¹³C NMR (150 MHz, CDCl₃) δ 162.6 (C2), 160.4 (C6), 160.4 (C7a), 159.0 (C3), 130.2 (C4), 127.4 (C5), 109.2 (C3a), 60.1 (-NHCH₂CH₂CH₂N), 45.6 (-N(CH₃)₂), 43.3 (-NHCH₂CH₂CH₂N), 37.6 (C1'), 32.8 (C2'), 27.1 (C3'), 26.2 (-NHCH₂CH₂CH₂N), 24.5 (C4'). ES-MS [M+1] found 329.2, calculated for C₁₈H₂₉N₆ 329.2.

General method for the synthesis of 1,8-naphthyridines (67-70). 2-Ethoxyethanol was dried over K₂CO₃, distilled and stored over molecular sieves. To a solution of sodium 2-ethoxyethoxide (2 eq), prepared from NaH and 2-ethoxyethanol, was added various acetonitriles (2 eq). The mixture was stirred under argon at room temperature for 30 min to 3 h. To the reaction, **9a** (1 eq) was added and the reaction was heated at reflux for 3 to 7 h. The reaction was cooled to room temperature, poured into cold water and chilled at 4 °C overnight. The emulsion was transferred into a separation funnel and extracted by EtOAc 3 times. The organic layer was combined and washed with brine and then dried over MgSO₄. After concentration to dryness *in vacuo* the residue was purified by column chromatography using the conditions listed below.

3-Phenyl-1,8-naphthyridine-2,7-diamine (67). Column chromatography (97/3/0 to 89/10/1 CH₂Cl₂/MeOH/NH₄OH) gave **67** (yield 74%) as a yellow solid. TLC (94/5/1 CH₂Cl₂/MeOH/NH₄OH, R_f = 0.22). ¹H NMR (600 MHz, DMSO-*d*₆) δ 7.68 (2H, d, *J* = 8.4 Hz, -ArH4), 7.58 (1H, s, -ArH5), 7.48-7.47 (4H, m, -Ph2', 3'), 7.40-7.37 (1H, m, -Ph4'), 6.45-6.43 (3H, m, -ArH3, -NH₂), 5.97 (2H, s, -NH₂). ¹³C NMR (150 MHz, DMSO-*d*₆) δ 161.0 (C2), 157.8 (C7), 146.6 (C8a), 138.4 (C1'), 137.6 (C5), 137.6 (C4), 129.4 (C3', C5'), 129.1 (C2', C6'), 127.8 (C4'), 119.3 (C6), 114.9 (C4a), 107.8 (C3). ES-MS [M+1] found 237.1, calculated for C₁₄H₁₃N₄ 237.1.

3-(2,6-Dichlorophenyl)-1,8-naphthyridine-2,7-diamine (68). Column chromatography (97/3/0 to 89/10/1 CH₂Cl₂/MeOH/NH₄OH) gave **68** (yield 19%) as a yellow solid. TLC (89/10/1 CH₂Cl₂/MeOH/NH₄OH, *R_f* = 0.45). ¹H NMR (600 MHz, DMSO-*d*₆) δ 7.65 (1H, d, *J* = 9.0 Hz, -ArH4), 7.56 (2H, d, *J* = 8.4 Hz, -Ph3', 5'), 7.47 (1H, s, -ArH5), 7.43 (1H, t, *J* = 8.4 Hz), 6.51 (2H, s, -NH₂), 6.42 (1H, d, *J* = 8.4 Hz, -ArH3), 5.92 (2H, s, -NH₂). ¹³C NMR (150 MHz, DMSO-*d*₆) δ 161.0 (C2), 157.5 (C5), 157.0 (C8a), 138.2 (C4), 137.8 (C7), 135.8 (C2', C6'), 135.3 (C1'), 131.0 (C4'), 129.0 (C3', C5'), 114.7 (C6), 110.0 (C4a), 107.6 (C3). ES-MS [M+1] found 305.0, calculated for C₁₄H₁₃N₄ 305.0.

3-(3,5-Dimethylphenyl)-1,8-naphthyridine-2,7-diamine (69). Column chromatography (97/3/0 to 89/10/1 CH₂Cl₂/MeOH/NH₄OH) gave **69** (yield 79%) as a yellow solid. TLC (89/10/1 CH₂Cl₂/MeOH/NH₄OH, *R_f* = 0.5 2). ¹H NMR (600 MHz, DMSO-*d*₆) δ 7.64 (2H, d, *J* = 8.4 Hz, -ArH4), 7.51 (1H, s, -ArH5), 7.04 (2H, s, -Ph2', 6'), 6.98 (1H, s, -Ph4'), 6.40 (1H, d, *J* = 8.4 Hz, -ArH3), 6.35 (2H, s, -NH₂), 5.87 (2H, s, -NH₂), 2.30 (6H, s, -CH₃). ¹³C NMR (150 MHz, DMSO-*d*₆) δ 161.0 (C2), 157.8 (C7), 156.2 (C8a), 138.3 (C3', C5'), 138.2 (C1'), 137.5 (C5), 137.2 (C4), 129.2 (C4'), 126.8 (C2', C6'), 119.4 (C6), 110.9 (C4a), 107.7 (C3). ES-MS [M+1] found 265.1, calculated for C₁₆H₁₆N₄ 265.1.

3-(3,5-Dimethoxyphenyl)-1,8-naphthyridine-2,7-diamine (70). Column chromatography (97/3/0 to 89/10/1 CH₂Cl₂/MeOH/NH₄OH) gave **70** (yield 97%) as a yellow solid. TLC (89/10/1 CH₂Cl₂/MeOH/NH₄OH, *R_f* = 0.25). ¹H NMR (600 MHz, DMSO-*d*₆) δ 7.67 (2H, d, *J* = 8.4 Hz, -ArH4), 7.61 (1H, s, -ArH5), 6.60 (2H, d, *J* = 1.8 Hz, -Ph2', 6'), 6.51 (1H, t, *J* = 2.1 Hz, -Ph4'), 6.44-6.43 (3H, m, -ArH3, -NH₂), 6.05 (2H, s, -NH₂), 3.79 (6H, s, -OCH₃). ¹³C NMR (150 MHz, DMSO-*d*₆) δ 162.1 (C3', C5'), 161.0 (C2), 157.7 (C7), 156.6 (C8a), 140.3 (C1'), 137.6 (C5), 137.4 (C4), 119.2 (C6), 110.7 (C4a), 107.8 (C3), 107.0 (C2', C6'), 100.0 (C4'), 55.7 (OCH₃). ES-MS [M+1] found 297.1, calculated for C₁₄H₁₃N₄ 297.1.

5.2 Biology

B-PER (Pierce Biotechnologies) were purchased from Fisher. Ampicillin sodium salt, Isopropyl β -D-1 thiogalactopyranoside (IPTG) and HisPur Cobalt resin were purchased from Gold Biotechnology. ATP was purchased from Sigma-Aldrich. PEP, NADH were purchased from Acros. AIR and CAIR were synthesized using literature methods^{73-74, 104}. PurK from *A. clavatus* was purified and stored according to the published methods¹³⁹⁻¹⁴⁰. PurK from *E. coli* was purified by Jordan Rantucci and stored at -80 °C. All proteins were determined to be >95% pure based on SDS-PAGE analysis. Buffers were stored at 4 °C and stock solutions were stored at -20 °C. Recombinant cells were purchased from Fisher and stored at -80 °C. During assays, reagents and enzyme were stored on crushed ice.

UV assays were carried in 1 mL quartz cuvettes on a 1-Bio Cary-3 UV-vis spectrophotometer equipped with a temperature controller (Varian) or in flat-bottom 96 well plates using a Synergy2 plate reader (BioTek). Thermal shift assays were conducted on a Mx3005P qPCR System. Curve fitting was conducted using GraphPad Prism.

5.2.1 Phosphate Assay (Malachite green assay)

Reactions were conducted in a flat-bottom 96-well plate (USA Scientific 655101). Buffer (190 μ L) was added to each well of the plate (100 mM HEPES, pH 7.8 buffer containing 20 mM KCl and 6.0 mM MgCl₂) followed by the addition of 100 μ M AIR, 100 μ M ATP, 1 mM NaHCO₃ and 0.01% (v/v) triton. Compound stocks in DMSO (10 μ L, 5% v/v) were added to the sample wells. For single concentration testing, the compound concentration was 200 μ M unless restricted by solubility. Each compound was dispensed into six wells using a single channel pipette. To three wells, PurK (A_{sam}) was added (see below for details) and to the remaining three wells, the same volume of buffer was added with these wells serving as UV background for that particular compound (C_{sam}). For dose-response testing, a series

of concentrations selected around the estimated IC_{50} were used, and each concentration was tested in triplicate. For kinetic assays, additional variables included ATP concentrations. Each plate contained three wells of positive controls (5% DMSO + PurK) (A_{DMSO}) and three wells of negative controls (5% DMSO) (C_{DMSO}). Compound **1** served as internal quality controls for plates tested on different days. In the reaction wells, 168 ng PurK in 4 μ L of buffer was added. The UV background and negative control wells were supplemented with 4 μ L of buffer. The reactions were incubated at room temperature for 15 minutes and were quenched by the addition of 50 μ L of the malachite green reagent (Bioassay Systems) to each well. The plates were incubated at room temperature for an additional 30 minutes and the absorbance (620 nm) of each well was measured using a Synergy2 plate reader by BioTek. The quality of the plate was verified by the percent residual activity (RA%) of compound **1** ($43 \pm 5\%$). The plates that passed the quality check were used to calculate the RA% of other compounds based on Equation 2. For plates in which the RA% of compound **1** met the quality cut but was not 43%, RA% of all the compounds were further normalized so that RA% of compound **1** was 43%.

$$RA\% = \frac{A_{sam} - C_{sam}}{A_{DMSO} - C_{DMSO}} \times 100\% \quad \text{Eq. 2}$$

5.2.2 PK/LDH coupled PurK assay

Reactions were conducted in a 1 mL quartz cuvette at 37 °C. A master mix containing the following components (100 mM HEPES, pH 7.5, 20 mM KCl, 6 mM $MgCl_2$, AIR 25 μ M, 100 μ M ATP, NADH 200 μ M, PEP 2 mM, triton 0.01% (v/v), 1 mM $NaHCO_3$, 5 units of pyruvate kinase/lactate dehydrogenase) was made to ensure consistency. The assay was run as follows. Master mix (950 μ L) was added to the cuvette followed by the addition of compound stock in DMSO; the final DMSO concentration is 5% (v/v). For single concentration testing, the compound concentration was 200 μ M unless restricted by

solubility or high UV absorbance. For dose-response testing, a series of concentrations selected around the estimated IC_{50} were used, and each concentration was tested in triplet. For kinetic assays, additional variables included ATP concentrations. The reaction was initiated by the addition of 70 ng PurK. NADH oxidation was monitored at 340 nm and the initial velocity of each assay was determined from the slope of the change in absorbance during the first three minutes.

5.2.3 Thermal shift assay

Reactions were conducted in a 200 μ M PCR tubes with clear lids. The total volume of each reaction is 20 μ L. MES buffer (20 mM, pH 6.0) was added followed by the addition of 0.01 % (v/v) triton, 5x SYPRO Orange and 2 μ M PurK_{Asp} (mw 45 kDa calculated as a monomer). A series of concentrations of the compound to be tested (stocks in DMSO) were added and the final DMSO concentration was kept at 5% (v/v). Thermal melting curve was collected using a RT-PCR instrument (Mx3005P qPCR System) from 25-95 °C (ramp rate: 1 °C/minute) while monitoring the fluorescence of SYPRO Orange (ex = 492 nm, em = 610 nm). The melting temperature (T_m) was calculated from the maximum of the first derivate curve. The dissociation constant K_d was calculated in GraphPad Prism based on a single binding model following Equation 3.

$$Y = Tm_{min} + (Tm_{max} - Tm_{min}) \times \left(1 - \left(P - K_d - X + \sqrt{\frac{(P + X + K_d)^2 - (4 \times P \times X)}{2 \times P}} \right) \right) \quad \text{Eq. 2}$$

Tm_{max} : Melting temperature at infinite inhibitor concentration. Tm_{min} : Melting temperature at no inhibitor concentration. P : Protein concentration (2 μ M). X : Inhibitor concentration in log unit.

5.2.4 Construction, expression and purification of PurK mutant proteins.

The PurK_{Asp}-pET28 plasmid with an N-terminal His tag of the following sequence (MGSSHHHHHSENLYFQGH) was used to generate the desired mutant proteins. The plasmids for the mutant proteins were generated following the protocol of the Quikchange II site-directed mutagenesis kit (Agilent Technologies) using the primers listed in Table 11. The nucleotide sequence of each mutant protein was verified by Sanger sequencing at the Applied Genomics Technology Center, Wayne State University. The plasmids obtained from the mutagenesis was transformed into *E. coli* BL21(DE3) pLysS recombinant cells for protein expression and purification. The expression and purification of the proteins were following established methods for PurK_{Asp}^{139, 142}. The purified N-His proteins were used directly without cleavage of the His tag.

Table 11. Primers used for the creation of mutant PurK_{Asp}.

Mutant	Primers
C266A	5' cagcatca tgctggccga gatcgccagc 3' 5' gctggcgatc tcggccagca tgatgctg 3'
C266S	5' cagcatca tgctgagcga gatcgccagc 3' 5' gctggcgatc tcctcagca tgatgctg 3'
C216S	5' ggaggact cgatatccaa gctcgtgtacgcg 3' 5' cgctacacgagc ttggatatcg agtcctcc 3'

5.2.5 PK/LDH coupled PurK assay used in the study of cysteines functions

The reactions were run similar as described in section 5.2.2 with N-methyl maleimide used as the inhibitor. For continuous assay, the reactions were initiated with the protein addition. For reactions where PurK was pre-incubated with N-methyl maleimide, the PurK/N-methyl maleimide mixture was used to initiate the reaction.

REFERENCES

1. Rosing, M. T., ¹³C-Depleted carbon microparticles in >3700-Ma sea-floor sedimentary rocks from west greenland. *Science* **1999**, 283 (5402), 674-6.
2. Arndt, N. T.; Nisbet, E. G., Processes on the Young Earth and the Habitats of Early Life. *Annu Rev Earth Pl Sc* **2012**, 40, 521-549.
3. Catling, D. C.; Glein, C. R.; Zahnle, K. J.; McKay, C. P., Why O₂ is required by complex life on habitable planets and the concept of planetary "oxygenation time". *Astrobiology* **2005**, 5 (3), 415-38.
4. Holland, H. D., The oxygenation of the atmosphere and oceans. *Philos Trans R Soc Lond B Biol Sci* **2006**, 361 (1470), 903-15.
5. Microbiology by numbers. *Nat Rev Microbiol* **2011**, 9 (9), 628.
6. Luckey, T. D., Introduction to the ecology of the intestinal flora. *Am J Clin Nutr* **1970**, 23 (11), 1430-2.
7. Savage, D. C., Microbial ecology of the gastrointestinal tract. *Annu Rev Microbiol* **1977**, 31, 107-33.
8. Sender, R.; Fuchs, S.; Milo, R., Revised Estimates for the Number of Human and Bacteria Cells in the Body. *PLoS Biol* **2016**, 14 (8), e1002533.
9. Yong, E., *I contain multitudes : the microbes within us and a grander view of life*. First U.S. edition. ed.; Ecco, an imprint of HarperCollinsPublishers: New York, NY, 2016; p 357 pages, 8 unnumbered pages of plates.
10. Rieder, R.; Wisniewski, P. J.; Alderman, B. L.; Campbell, S. C., Microbes and mental health: A review. *Brain Behav Immun* **2017**, 66, 9-17.
11. Bruce-Keller, A. J.; Salbaum, J. M.; Berthoud, H. R., Harnessing Gut Microbes for Mental Health: Getting From Here to There. *Biol Psychiatry* **2018**, 83 (3), 214-223.

12. Mayer, A. J.; Marks, R. V., Differentials in infant mortality by race, economic level and cause of death, for Detroit: 1940 and 1950. *Hum Biol* **1954**, *26* (2), 143-55.
13. Centers for Disease, C.; Prevention, Ten great public health achievements--worldwide, 2001-2010. *MMWR Morb Mortal Wkly Rep* **2011**, *60* (24), 814-8.
14. Centers for Disease, C.; Prevention, Ten great public health achievements--United States, 2001-2010. *MMWR Morb Mortal Wkly Rep* **2011**, *60* (19), 619-23.
15. Centers for Disease, C.; Prevention, Control of infectious diseases. *MMWR Morb Mortal Wkly Rep* **1999**, *48* (29), 621-9.
16. Centers for Disease, C.; Prevention, Status report on the Childhood Immunization Initiative: national, state, and urban area vaccination coverage levels among children aged 19-35 months--United States, 1996. *MMWR Morb Mortal Wkly Rep* **1997**, *46* (29), 657-64.
17. Verdine, G. L., The combinatorial chemistry of nature. *Nature* **1996**, *384* (6604 Suppl), 11-3.
18. Treffers, H. P., Studies on resistance to antibiotics; the action of penicillin on some gram-positive and gram-negative organisms and its potentiation by various inhibitors. *Yale J Biol Med* **1946**, *18*, 609-23.
19. Klimek, J. W.; Cavallito, C. J.; Bailey, J. H., Induced resistance of *Staphylococcus aureus* to antibiotics. *J Bacteriol* **1946**, *51*, 580.
20. Ortiz-Martinez, Y.; Galindo-Regino, C.; Valdes-Villegas, F.; Mendoza-Borja, K.; Gonzalez-Hurtado, M. R.; Chavez-Verbel, V., World Antibiotic Awareness Week 2017 and its influence on digital information seeking on antibiotic resistance: A Google Trends study. *J Hosp Infect* **2018**.
21. Hampton, T., Report reveals scope of US antibiotic resistance threat. *JAMA* **2013**, *310* (16), 1661-3.

22. Miller, C. P.; Bohnhoff, M., Studies on the action of penicillin; development of penicilli resistance by gonococcus. *Proc Soc Exp Biol Med* **1945**, *60*, 354-6.
23. Eriksen, K. R., Studies on induced resistance to penicillin in a pneumococcus type I. *Acta Pathol Microbiol Scand* **1945**, *22* (4), 398-405.
24. Plough, H. H., Penicillin resistance of *Staphylococcus aureus* and its clinical implications. *Am J Clin Pathol* **1945**, *15*, 446-51.
25. Fleming, A., Antiseptics - the Lister Memorial Lecture. *Chem Ind-London* **1945**, (3), 18-23.
26. Clatworthy, A. E.; Pierson, E.; Hung, D. T., Targeting virulence: a new paradigm for antimicrobial therapy. *Nat Chem Biol* **2007**, *3* (9), 541-8.
27. Palumbi, S. R., Humans as the world's greatest evolutionary force. *Science* **2001**, *293* (5536), 1786-90.
28. Barlow, M.; Hall, B. G., Phylogenetic analysis shows that the OXA beta-lactamase genes have been on plasmids for millions of years. *J Mol Evol* **2002**, *55* (3), 314-21.
29. Hall, B. G.; Barlow, M., Evolution of the serine beta-lactamases: past, present and future. *Drug Resist Updat* **2004**, *7* (2), 111-23.
30. Baltz, R. H., Renaissance in antibacterial discovery from actinomycetes. *Curr Opin Pharmacol* **2008**, *8* (5), 557-63.
31. Bhullar, K.; Waglechner, N.; Pawlowski, A.; Koteva, K.; Banks, E. D.; Johnston, M. D.; Barton, H. A.; Wright, G. D., Antibiotic resistance is prevalent in an isolated cave microbiome. *PLoS One* **2012**, *7* (4), e34953.
32. D'Costa, V. M.; King, C. E.; Kalan, L.; Morar, M.; Sung, W. W.; Schwarz, C.; Froese, D.; Zazula, G.; Calmels, F.; Debruyne, R.; Golding, G. B.; Poinar, H. N.; Wright, G. D., Antibiotic resistance is ancient. *Nature* **2011**, *477* (7365), 457-61.

33. Toth, M.; Smith, C.; Frase, H.; Mobashery, S.; Vakulenko, S., An antibiotic-resistance enzyme from a deep-sea bacterium. *J Am Chem Soc* **2010**, *132* (2), 816-23.
34. Brown, M. G.; Balkwill, D. L., Antibiotic resistance in bacteria isolated from the deep terrestrial subsurface. *Microb Ecol* **2009**, *57* (3), 484-93.
35. D'Costa, V. M.; McGrann, K. M.; Hughes, D. W.; Wright, G. D., Sampling the antibiotic resistome. *Science* **2006**, *311* (5759), 374-7.
36. Pawlowski, A. C.; Wang, W.; Koteva, K.; Barton, H. A.; McArthur, A. G.; Wright, G. D., A diverse intrinsic antibiotic resistome from a cave bacterium. *Nat Commun* **2016**, *7*, 13803.
37. Perry, J. A.; Westman, E. L.; Wright, G. D., The antibiotic resistome: what's new? *Curr Opin Microbiol* **2014**, *21*, 45-50.
38. Martinez, J. L., The antibiotic resistome: challenge and opportunity for therapeutic intervention. *Future Med Chem* **2012**, *4* (3), 347-59.
39. Wright, G. D., The antibiotic resistome. *Expert Opin Drug Discov* **2010**, *5* (8), 779-88.
40. Wright, G. D., The antibiotic resistome: the nexus of chemical and genetic diversity. *Nat Rev Microbiol* **2007**, *5* (3), 175-86.
41. Skold, O., [A new antibacterial agent can stop resistance development. Expectations are connected to linezolid, an oxazolidinone with a new pharmacological action]. *Lakartidningen* **1999**, *96* (37), 3866-7.
42. Budanov, S. V.; Smirnova, L. B., [Linezolid--new antibacterial agent of the oxazolidinone group: its importance in the control of spreading and treatment of the multidrug resistance gram-positive infections]. *Antibiot Khimioter* **2002**, *47* (7), 38-42.

43. Shah, P. M.; Stille, W., Bactericidal activity of LY 146032. *J Antimicrob Chemother* **1987**, *20* (1), 140-1.
44. Watanakunakorn, C., In-vitro activity of LY 146032, a novel cyclic lipopeptide, alone and in combination with gentamicin or tobramycin against enterococci. *J Antimicrob Chemother* **1987**, *19* (4), 445-8.
45. Eliopoulos, G. M.; Willey, S.; Reiszner, E.; Spitzer, P. G.; Caputo, G.; Moellering, R. C., Jr., In vitro and in vivo activity of LY 146032, a new cyclic lipopeptide antibiotic. *Antimicrob Agents Chemother* **1986**, *30* (4), 532-5.
46. Prystowsky, J.; Siddiqui, F.; Chosay, J.; Shinabarger, D. L.; Millichap, J.; Peterson, L. R.; Noskin, G. A., Resistance to linezolid: characterization of mutations in rRNA and comparison of their occurrences in vancomycin-resistant enterococci. *Antimicrob Agents Chemother* **2001**, *45* (7), 2154-6.
47. Fang, C. T.; Chang, S. C.; Chen, Y. C.; Hsieh, S. M.; Hsieh, W. C., In vitro activity of linezolid against clinical Gram-positive bacterial isolates from Taiwan: an area with a high prevalence of antibiotic resistance. *Int J Antimicrob Agents* **2001**, *18* (3), 267-70.
48. Kloss, P.; Xiong, L.; Shinabarger, D. L.; Mankin, A. S., Resistance mutations in 23 S rRNA identify the site of action of the protein synthesis inhibitor linezolid in the ribosomal peptidyl transferase center. *J Mol Biol* **1999**, *294* (1), 93-101.
49. Gomez Casanova, N.; Siller Ruiz, M.; Munoz Bellido, J. L., Mechanisms of resistance to daptomycin in *Staphylococcus aureus*. *Rev Esp Quimioter* **2017**, *30* (6), 391-396.
50. Lewis, J. S., 2nd; Owens, A.; Cadena, J.; Sabol, K.; Patterson, J. E.; Jorgensen, J. H., Emergence of daptomycin resistance in *Enterococcus faecium* during daptomycin therapy. *Antimicrob Agents Chemother* **2005**, *49* (4), 1664-5.

51. Silverman, J. A.; Oliver, N.; Andrew, T.; Li, T., Resistance studies with daptomycin. *Antimicrob Agents Chemother* **2001**, *45* (6), 1799-802.
52. Blanchard, S. C., A Much-Needed Boost for the Dwindling Antibiotic Pipeline. *Mol Cell* **2018**, *70* (1), 3-5.
53. Burki, T., Antibiotic development pipeline slows to a trickle. *Lancet Infect Dis* **2017**, *17* (11), 1128-1129.
54. Luepke, K. H.; Suda, K. J.; Boucher, H.; Russo, R. L.; Bonney, M. W.; Hunt, T. D.; Mohr, J. F., 3rd, Past, Present, and Future of Antibacterial Economics: Increasing Bacterial Resistance, Limited Antibiotic Pipeline, and Societal Implications. *Pharmacotherapy* **2017**, *37* (1), 71-84.
55. Falagas, M. E.; Mavroudis, A. D.; Vardakas, K. Z., The antibiotic pipeline for multi-drug resistant gram negative bacteria: what can we expect? *Expert Rev Anti Infect Ther* **2016**, *14* (8), 747-63.
56. Lutgring, J. D.; Machado, M. J.; Benahmed, F. H.; Conville, P.; Shawar, R. M.; Patel, J.; Brown, A. C., FDA-CDC Antimicrobial Resistance Isolate Bank: a Publicly Available Resource To Support Research, Development, and Regulatory Requirements. *J Clin Microbiol* **2018**, *56* (2).
57. Kahn, L. H., Antimicrobial resistance: a One Health perspective. *Trans R Soc Trop Med Hyg* **2017**, *111* (6), 255-260.
58. Ferri, M.; Ranucci, E.; Romagnoli, P.; Giaccone, V., Antimicrobial resistance: A global emerging threat to public health systems. *Crit Rev Food Sci Nutr* **2017**, *57* (13), 2857-2876.
59. Sciarretta, K.; Rottingen, J. A.; Opalska, A.; Van Hengel, A. J.; Larsen, J., Economic Incentives for Antibacterial Drug Development: Literature Review and Considerations From

- the Transatlantic Task Force on Antimicrobial Resistance. *Clinical Infectious Diseases* **2016**, 63 (11), 1470-1474.
60. Tinker, S. C.; Crider, K. S.; Ailes, E. C., Antibiotics and risk for birth defects. *Br J Clin Pharmacol* **2018**, 84 (7), 1626-1627.
61. Weiner, M., Opportunities and Threats in the Post-Antibiotic Era. *Health Probl Civiliz* **2018**, 12 (2), 88-93.
62. Folsch, C.; Rickert, M., Bone Replacement Materials and Antibiotics in Revision Surgery. *Orthopade* **2018**, 47 (1), 1-2.
63. O'Neill, J., *Tackling drug-resistant infections globally: final report and recommendations*. The Review on Antimicrobial resistance: <https://amr-review.org/Publications.html>, 2016.
64. Brogan, D. M.; Mossialos, E., A critical analysis of the review on antimicrobial resistance report and the infectious disease financing facility. *Global Health* **2016**, 12, 8.
65. *Antibiotic resistance threats in the United States*. Centers for Disease Control and Prevention: <https://www.cdc.gov/drugresistance/threat-report-2013/index.html>, 2013.
66. MacFadden, D. R.; Lipsitch, M.; Olesen, S. W.; Grad, Y., Multidrug-resistant *Neisseria gonorrhoeae*: implications for future treatment strategies. *Lancet Infect Dis* **2018**, 18 (6), 599.
67. Poncin, T.; Fouere, S.; Braille, A.; Camelena, F.; Agsous, M.; Bebear, C.; Kumanski, S.; Lot, F.; Mercier-Delarue, S.; Ngangro, N. N.; Salmona, M.; Schnepf, N.; Timsit, J.; Unemo, M.; Bercot, B., Multidrug-resistant *Neisseria gonorrhoeae* failing treatment with ceftriaxone and doxycycline in France, November 2017. *Euro Surveill* **2018**, 23 (21).

68. UK man has world-first case of super-strength gonorrhoea. The Guardian: <https://www.theguardian.com/society/2018/mar/28/uk-man-super-strength-gonorrhoea>, 2018.
69. Stephens, J. W.; Gable, D. R.; Hurel, S. J.; Miller, G. J.; Cooper, J. A.; Humphries, S. E., Increased plasma markers of oxidative stress are associated with coronary heart disease in males with diabetes mellitus and with 10-year risk in a prospective sample of males. *Clin Chem* **2006**, 52 (3), 446-52.
70. Strollo, S.; Lionakis, M. S.; Adjemian, J.; Steiner, C. A.; Prevots, D. R., Epidemiology of Hospitalizations Associated with Invasive Candidiasis, United States, 2002-2012(1). *Emerg Infect Dis* **2016**, 23 (1), 7-13.
71. Nelson, D. L.; Cox, M. M., *Lehninger Principles of Biochemistry Fourth Edition*. Sara Tenney: 2005.
72. Zhang, Y.; Morar, M.; Ealick, S. E., Structural biology of the purine biosynthetic pathway. *Cell Mol Life Sci* **2008**, 65 (23), 3699-724.
73. Firestine, S. M.; Poon, S. W.; Mueller, E. J.; Stubbe, J.; Davisson, V. J., Reactions catalyzed by 5-aminoimidazole ribonucleotide carboxylases from *Escherichia coli* and *Gallus gallus*: a case for divergent catalytic mechanisms. *Biochemistry* **1994**, 33 (39), 11927-34.
74. Firestine, S. M.; Davisson, V. J., Carboxylases in de novo purine biosynthesis. Characterization of the *Gallus gallus* bifunctional enzyme. *Biochemistry* **1994**, 33 (39), 11917-26.
75. Mueller, E. J.; Meyer, E.; Rudolph, J.; Davisson, V. J.; Stubbe, J., N5-carboxyaminoimidazole ribonucleotide: evidence for a new intermediate and two new

enzymatic activities in the de novo purine biosynthetic pathway of *Escherichia coli*. *Biochemistry* **1994**, *33* (8), 2269-78.

76. Schendel, F. J.; Cheng, Y. S.; Otvos, J. D.; Wehrli, S.; Stubbe, J., Characterization and chemical properties of phosphoribosylamine, an unstable intermediate in the de novo purine biosynthetic pathway. *Biochemistry* **1988**, *27* (7), 2614-23.

77. Zhou, G.; Charbonneau, H.; Colman, R. F.; Zalkin, H., Identification of sites for feedback regulation of glutamine 5-phosphoribosylpyrophosphate amidotransferase by nucleotides and relationship to residues important for catalysis. *J Biol Chem* **1993**, *268* (14), 10471-81.

78. Kim, J. H.; Krahn, J. M.; Tomchick, D. R.; Smith, J. L.; Zalkin, H., Structure and function of the glutamine phosphoribosylpyrophosphate amidotransferase glutamine site and communication with the phosphoribosylpyrophosphate site. *J Biol Chem* **1996**, *271* (26), 15549-57.

79. Krahn, J. M.; Kim, J. H.; Burns, M. R.; Parry, R. J.; Zalkin, H.; Smith, J. L., Coupled formation of an amidotransferase interdomain ammonia channel and a phosphoribosyltransferase active site. *Biochemistry* **1997**, *36* (37), 11061-8.

80. Smith, J. L.; Zaluzec, E. J.; Wery, J. P.; Niu, L.; Switzer, R. L.; Zalkin, H.; Satow, Y., Structure of the allosteric regulatory enzyme of purine biosynthesis. *Science* **1994**, *264* (5164), 1427-33.

81. Grandoni, J. A.; Switzer, R. L.; Makaroff, C. A.; Zalkin, H., Evidence that the iron-sulfur cluster of *Bacillus subtilis* glutamine phosphoribosylpyrophosphate amidotransferase determines stability of the enzyme to degradation in vivo. *J Biol Chem* **1989**, *264* (11), 6058-64.

82. Chen, S.; Tomchick, D. R.; Wolle, D.; Hu, P.; Smith, J. L.; Switzer, R. L.; Zalkin, H., Mechanism of the synergistic end-product regulation of *Bacillus subtilis* glutamine phosphoribosylpyrophosphate amidotransferase by nucleotides. *Biochemistry* **1997**, *36* (35), 10718-26.
83. Wong, J. Y.; Bernlohr, D. A.; Turnbough, C. L.; Switzer, R. L., Purification and properties of glutamine phosphoribosylpyrophosphate amidotransferase from *Bacillus subtilis*. *Biochemistry* **1981**, *20* (20), 5669-74.
84. Muchmore, C. R.; Krahn, J. M.; Kim, J. H.; Zalkin, H.; Smith, J. L., Crystal structure of glutamine phosphoribosylpyrophosphate amidotransferase from *Escherichia coli*. *Protein Sci* **1998**, *7* (1), 39-51.
85. Messenger, L. J.; Zalkin, H., Glutamine phosphoribosylpyrophosphate amidotransferase from *Escherichia coli*. Purification and properties. *J Biol Chem* **1979**, *254* (9), 3382-92.
86. Dahms, T. E.; Sainz, G.; Giroux, E. L.; Caperelli, C. A.; Smith, J. L., The apo and ternary complex structures of a chemotherapeutic target: human glycinamide ribonucleotide transformylase. *Biochemistry* **2005**, *44* (29), 9841-50.
87. Cheng, H.; Hwang, I.; Chong, Y.; Tavassoli, A.; Webb, M. E.; Zhang, Y.; Wilson, I. A.; Benkovic, S. J.; Boger, D. L., Synthesis and biological evaluation of N-[4-[5-(2,4-diamino-6-oxo-1,6-dihydropyrimidin-5-yl)-2-(2,2,2-trifluoroacetyl)pe ntyl]benzoyl]-L-glutamic acid as a potential inhibitor of GAR Tfase and the de novo purine biosynthetic pathway. *Bioorg Med Chem* **2005**, *13* (10), 3593-9.
88. Marsilje, T. H.; Hedrick, M. P.; Desharnais, J.; Capps, K.; Tavassoli, A.; Zhang, Y.; Wilson, I. A.; Benkovic, S. J.; Boger, D. L., 10-(2-benzoxazolcarbonyl)-5,10-dideaza-

acyclic-5,6,7,8-tetrahydrofolic acid: a potential inhibitor of GAR transformylase and AICAR transformylase. *Bioorg Med Chem* **2003**, *11* (20), 4503-9.

89. Zhang, Y.; Desharnais, J.; Marsilje, T. H.; Li, C.; Hedrick, M. P.; Gooljarsingh, L. T.; Tavassoli, A.; Benkovic, S. J.; Olson, A. J.; Boger, D. L.; Wilson, I. A., Rational design, synthesis, evaluation, and crystal structure of a potent inhibitor of human GAR Tfase: 10-(trifluoroacetyl)-5,10-dideazaacyclic-5,6,7,8-tetrahydrofolic acid. *Biochemistry* **2003**, *42* (20), 6043-56.

90. Greasley, S. E.; Marsilje, T. H.; Cai, H.; Baker, S.; Benkovic, S. J.; Boger, D. L.; Wilson, I. A., Unexpected formation of an epoxide-derived multisubstrate adduct inhibitor on the active site of GAR transformylase. *Biochemistry* **2001**, *40* (45), 13538-47.

91. Greasley, S. E.; Yamashita, M. M.; Cai, H.; Benkovic, S. J.; Boger, D. L.; Wilson, I. A., New insights into inhibitor design from the crystal structure and NMR studies of *Escherichia coli* GAR transformylase in complex with beta-GAR and 10-formyl-5,8,10-trideazafolic acid. *Biochemistry* **1999**, *38* (51), 16783-93.

92. Boger, D. L.; Haynes, N. E.; Warren, M. S.; Ramcharan, J.; Kitos, P. A.; Benkovic, S. J., Functionalized analogues of 5,8,10-trideazafolate: development of an enzyme-assembled tight binding inhibitor of GAR Tfase and a potential irreversible inhibitor of AICAR Tfase. *Bioorg Med Chem* **1997**, *5* (9), 1839-46.

93. Thoden, J. B.; Firestine, S. M.; Benkovic, S. J.; Holden, H. M., PurT-encoded glycinamide ribonucleotide transformylase. Accommodation of adenosine nucleotide analogs within the active site. *J Biol Chem* **2002**, *277* (26), 23898-908.

94. Thoden, J. B.; Firestine, S.; Nixon, A.; Benkovic, S. J.; Holden, H. M., Molecular structure of *Escherichia coli* PurT-encoded glycinamide ribonucleotide transformylase. *Biochemistry* **2000**, *39* (30), 8791-802.

95. Marolewski, A. E.; Mattia, K. M.; Warren, M. S.; Benkovic, S. J., Formyl phosphate: a proposed intermediate in the reaction catalyzed by *Escherichia coli* PurT GAR transformylase. *Biochemistry* **1997**, *36* (22), 6709-16.
96. Nagy, P. L.; McCorkle, G. M.; Zalkin, H., purU, a source of formate for purT-dependent phosphoribosyl-N-formylglycinamide synthesis. *J Bacteriol* **1993**, *175* (21), 7066-73.
97. Jelsbak, L.; Mortensen, M. I. B.; Kilstrup, M.; Olsen, J. E., The In Vitro Redundant Enzymes PurN and PurT Are Both Essential for Systemic Infection of Mice in *Salmonella enterica* Serovar Typhimurium. *Infect Immun* **2016**, *84* (7), 2076-2085.
98. Anand, R.; Hoskins, A. A.; Stubbe, J.; Ealick, S. E., Domain organization of *Salmonella typhimurium* formylglycinamide ribonucleotide amidotransferase revealed by X-ray crystallography. *Biochemistry* **2004**, *43* (32), 10328-42.
99. Hoskins, A. A.; Anand, R.; Ealick, S. E.; Stubbe, J., The formylglycinamide ribonucleotide amidotransferase complex from *Bacillus subtilis*: metabolite-mediated complex formation. *Biochemistry* **2004**, *43* (32), 10314-27.
100. Tanwar, A. S.; Sindhikara, D. J.; Hirata, F.; Anand, R., Determination of the formylglycinamide ribonucleotide amidotransferase ammonia pathway by combining 3D-RISM theory with experiment. *ACS Chem Biol* **2015**, *10* (3), 698-704.
101. Anand, R.; Hoskins, A. A.; Bennett, E. M.; Sintchak, M. D.; Stubbe, J.; Ealick, S. E., A model for the *Bacillus subtilis* formylglycinamide ribonucleotide amidotransferase multiprotein complex. *Biochemistry* **2004**, *43* (32), 10343-52.
102. Suzuki, S.; Yanai, H.; Kanagawa, M.; Tamura, S.; Watanabe, Y.; Fuse, K.; Baba, S.; Sampei, G.; Kawai, G., Structure of N-formylglycinamide ribonucleotide amidotransferase

II (PurL) from *Thermus thermophilus* HB8. *Acta Crystallogr Sect F Struct Biol Cryst Commun* **2012**, *68* (Pt 1), 14-9.

103. Watanabe, Y.; Yanai, H.; Kanagawa, M.; Suzuki, S.; Tamura, S.; Okada, K.; Baba, S.; Kumasaka, T.; Agari, Y.; Chen, L.; Fu, Z. Q.; Chrzas, J.; Wang, B. C.; Nakagawa, N.; Ebihara, A.; Masui, R.; Kuramitsu, S.; Yokoyama, S.; Sampei, G. I.; Kawai, G., Crystal structures of a subunit of the formylglycinamide ribonucleotide amidotransferase, PurS, from *Thermus thermophilus*, *Sulfolobus tokodaii* and *Methanocaldococcus jannaschii*. *Acta Crystallogr F Struct Biol Commun* **2016**, *72* (Pt 8), 627-35.

104. Meyer, E.; Leonard, N. J.; Bhat, B.; Stubbe, J.; Smith, J. M., Purification and characterization of the purE, purK, and purC gene products: identification of a previously unrecognized energy requirement in the purine biosynthetic pathway. *Biochemistry* **1992**, *31* (21), 5022-32.

105. Firestine, S. M.; Misialek, S.; Toffaletti, D. L.; Klem, T. J.; Perfect, J. R.; Davisson, V. J., Biochemical role of the *Cryptococcus neoformans* ADE2 protein in fungal de novo purine biosynthesis. *Arch Biochem Biophys* **1998**, *351* (1), 123-34.

106. Taschner, M.; Basquin, J.; Benda, C.; Lorentzen, E., Crystal structure of the invertebrate bifunctional purine biosynthesis enzyme PAICS at 2.8 Å resolution. *Proteins* **2013**, *81* (8), 1473-8.

107. Li, S. X.; Tong, Y. P.; Xie, X. C.; Wang, Q. H.; Zhou, H. N.; Han, Y.; Zhang, Z. Y.; Gao, W.; Li, S. G.; Zhang, X. C.; Bi, R. C., Octameric structure of the human bifunctional enzyme PAICS in purine biosynthesis. *J Mol Biol* **2007**, *366* (5), 1603-14.

108. Firestine, S. M.; Wu, W.; Youn, H.; Davisson, V. J., Interrogating the mechanism of a tight binding inhibitor of AIR carboxylase. *Bioorg Med Chem* **2009**, *17* (2), 794-803.

109. Meyer, E.; Kappock, T. J.; Osuji, C.; Stubbe, J., Evidence for the direct transfer of the carboxylate of N5-carboxyaminoimidazole ribonucleotide (N5-CAIR) to generate 4-carboxy-5-aminoimidazole ribonucleotide catalyzed by *Escherichia coli* PurE, an N5-CAIR mutase. *Biochemistry* **1999**, *38* (10), 3012-8.
110. Constantine, C. Z.; Starks, C. M.; Mill, C. P.; Ransome, A. E.; Karpowicz, S. J.; Francois, J. A.; Goodman, R. A.; Kappock, T. J., Biochemical and structural studies of N5-carboxyaminoimidazole ribonucleotide mutase from the acidophilic bacterium *Acetobacter acetii*. *Biochemistry* **2006**, *45* (27), 8193-208.
111. Tranchimand, S.; Starks, C. M.; Mathews, II; Hockings, S. C.; Kappock, T. J., *Treponema denticola* PurE Is a bacterial AIR carboxylase. *Biochemistry* **2011**, *50* (21), 4623-37.
112. Brugarolas, P.; Duguid, E. M.; Zhang, W.; Poor, C. B.; He, C., Structural and biochemical characterization of N5-carboxyaminoimidazole ribonucleotide synthetase and N5-carboxyaminoimidazole ribonucleotide mutase from *Staphylococcus aureus*. *Acta Crystallogr D Biol Crystallogr* **2011**, *67* (Pt 8), 707-15.
113. Schwarzenbacher, R.; Jaroszewski, L.; von Delft, F.; Abdubek, P.; Ambing, E.; Biorac, T.; Brinen, L. S.; Canaves, J. M.; Cambell, J.; Chiu, H. J.; Dai, X.; Deacon, A. M.; DiDonato, M.; Elsliger, M. A.; Eshagi, S.; Floyd, R.; Godzik, A.; Grittini, C.; Grzechnik, S. K.; Hampton, E.; Karlak, C.; Klock, H. E.; Koesema, E.; Kovarik, J. S.; Kreusch, A.; Kuhn, P.; Lesley, S. A.; Levin, I.; McMullan, D.; McPhillips, T. M.; Miller, M. D.; Morse, A.; Moy, K.; Ouyang, J.; Page, R.; Quijano, K.; Robb, A.; Spraggon, G.; Stevens, R. C.; van den Bedem, H.; Velasquez, J.; Vincent, J.; Wang, X.; West, B.; Wolf, G.; Xu, Q.; Hodgson, K. O.; Wooley, J.; Wilson, I. A., Crystal structure of a phosphoribosylaminoimidazole mutase PurE (TM0446) from *Thermotoga maritima* at 1.77-Å resolution. *Proteins* **2004**, *55* (2), 474-8.

114. Brown, A. M.; Hoopes, S. L.; White, R. H.; Sarisky, C. A., Purine biosynthesis in archaea: variations on a theme. *Biology direct* **2011**, *6*, 63.
115. Mathews, II; Kappock, T. J.; Stubbe, J.; Ealick, S. E., Crystal structure of Escherichia coli PurE, an unusual mutase in the purine biosynthetic pathway. *Structure* **1999**, *7* (11), 1395-406.
116. Shi, Z. Site-Directed Mutagenesis of Conserved Amino Acids Residues in N5-Carboxyaminoimidazole Ribonucleotide Mutase: converting N5-CAIR mutase into Aminoimidazole Ribonucleotide carboxylase & Developing a High-Throughput Screening Assay for the Discovery of N5-Carboxyaminoimidazole Ribonucleotide Mutase Inhibitors. Wayne State University, 2014.
117. Hamilton, P. T.; Reeve, J. N., Structure of genes and an insertion element in the methane producing archaeobacterium Methanobrevibacter smithii. *Molecular & general genetics : MGG* **1985**, *200* (1), 47-59.
118. Hamilton, P. T.; Reeve, J. N., Sequence divergence of an archaeobacterial gene cloned from a mesophilic and a thermophilic methanogen. *Journal of molecular evolution* **1985**, *22* (4), 351-60.
119. Fawaz, M. V.; Topper, M. E.; Firestine, S. M., The ATP-grasp enzymes. *Bioorg Chem* **2011**, *39* (5-6), 185-91.
120. Galperin, M. Y.; Koonin, E. V., A diverse superfamily of enzymes with ATP-dependent carboxylate-amine/thiol ligase activity. *Protein Sci* **1997**, *6* (12), 2639-43.
121. Thoden, J. B.; Kappock, T. J.; Stubbe, J.; Holden, H. M., Three-dimensional structure of N5-carboxyaminoimidazole ribonucleotide synthetase: a member of the ATP grasp protein superfamily. *Biochemistry* **1999**, *38* (47), 15480-92.

122. Rayl, E. A.; Moroson, B. A.; Beardsley, G. P., The human purH gene product, 5-aminoimidazole-4-carboxamide ribonucleotide formyltransferase/IMP cyclohydrolase. Cloning, sequencing, expression, purification, kinetic analysis, and domain mapping. *J Biol Chem* **1996**, 271 (4), 2225-33.
123. Zhang, Y.; White, R. H.; Ealick, S. E., Crystal structure and function of 5-formaminoimidazole-4-carboxamide ribonucleotide synthetase from *Methanocaldococcus jannaschii*. *Biochemistry* **2008**, 47 (1), 205-17.
124. Beardsley, G. P.; Rayl, E. A.; Gunn, K.; Moroson, B. A.; Seow, H.; Anderson, K. S.; Vergis, J.; Fleming, K.; Worland, S.; Condon, B.; Davies, J., Structure and functional relationships in human pur H. *Adv Exp Med Biol* **1998**, 431, 221-6.
125. Greasley, S. E.; Horton, P.; Ramcharan, J.; Beardsley, G. P.; Benkovic, S. J.; Wilson, I. A., Crystal structure of a bifunctional transformylase and cyclohydrolase enzyme in purine biosynthesis. *Nat Struct Biol* **2001**, 8 (5), 402-6.
126. Cheong, C. G.; Wolan, D. W.; Greasley, S. E.; Horton, P. A.; Beardsley, G. P.; Wilson, I. A., Crystal structures of human bifunctional enzyme aminoimidazole-4-carboxamide ribonucleotide transformylase/IMP cyclohydrolase in complex with potent sulfonyl-containing antifolates. *J Biol Chem* **2004**, 279 (17), 18034-45.
127. Xu, L.; Chong, Y.; Hwang, I.; D'Onofrio, A.; Amore, K.; Beardsley, G. P.; Li, C.; Olson, A. J.; Boger, D. L.; Wilson, I. A., Structure-based design, synthesis, evaluation, and crystal structures of transition state analogue inhibitors of inosine monophosphate cyclohydrolase. *J Biol Chem* **2007**, 282 (17), 13033-46.
128. Kim, A.; Wolf, N. M.; Zhu, T.; Johnson, M. E.; Deng, J.; Cook, J. L.; Fung, L. W., Identification of *Bacillus anthracis* PurE inhibitors with antimicrobial activity. *Bioorg Med Chem* **2015**, 23 (7), 1492-9.

129. Firestine, S. M.; Davisson, V. J., A tight binding inhibitor of 5-aminoimidazole ribonucleotide carboxylase. *J Med Chem* **1993**, *36* (22), 3484-6.
130. Firestine, S. M.; Paritala, H.; McDonnell, J. E.; Thoden, J. B.; Holden, H. M., Identification of inhibitors of N5-carboxyaminoimidazole ribonucleotide synthetase by high-throughput screening. *Bioorg Med Chem* **2009**, *17* (9), 3317-23.
131. Bacon, G. A.; Burrows, T. W.; Yates, M., The effects of biochemical mutation on the virulence of *Bacterium typhosum*; the loss of virulence of certain mutants. *Br J Exp Pathol* **1951**, *32* (2), 85-96.
132. Bacon, G. A.; Burrows, T. W.; Yates, M., The effects of biochemical mutation on the virulence of *Bacterium typhosum*: the virulence of mutants. *Br J Exp Pathol* **1950**, *31* (6), 714-24.
133. Bacon, G. A.; Burrows, T. W.; Yates, M., The effects of biochemical mutation on the virulence on *Bacterium typhosum*: the induction and isolation of mutants. *Br J Exp Pathol* **1950**, *31* (6), 703-13.
134. Lan, L.; Cheng, A.; Dunman, P. M.; Missiakas, D.; He, C., Golden pigment production and virulence gene expression are affected by metabolisms in *Staphylococcus aureus*. *Journal of bacteriology* **2010**, *192* (12), 3068-77.
135. Ivanovics, G.; Marjai, E.; Dobozy, A., The growth of purine mutants of *Bacillus anthracis* in the body of the mouse. *Journal of general microbiology* **1968**, *53* (2), 147-62.
136. Perfect, J. R.; Toffaletti, D. L.; Rude, T. H., The gene encoding phosphoribosylaminoimidazole carboxylase (ADE2) is essential for growth of *Cryptococcus neoformans* in cerebrospinal fluid. *Infection and immunity* **1993**, *61* (10), 4446-51.

137. McFarland, W. C.; Stocker, B. A., Effect of different purine auxotrophic mutations on mouse-virulence of a Vi-positive strain of *Salmonella dublin* and of two strains of *Salmonella typhimurium*. *Microbial pathogenesis* **1987**, 3 (2), 129-41.
138. Streeter, C. C. Investigation of the inhibitory mechanism of isatin towards the microbial enzyme N5-CAIR synthetase. Wayne State University, 2017.
139. Thoden, J. B.; Holden, H. M.; Paritala, H.; Firestine, S. M., Structural and functional studies of *Aspergillus clavatus* N(5)-carboxyaminoimidazole ribonucleotide synthetase. *Biochemistry* **2010**, 49 (4), 752-60.
140. Thoden, J. B.; Holden, H. M.; Firestine, S. M., Structural analysis of the active site geometry of N5-carboxyaminoimidazole ribonucleotide synthetase from *Escherichia coli*. *Biochemistry* **2008**, 47 (50), 13346-53.
141. Mueller, E. J.; Oh, S.; Kavalarchik, E.; Kappock, T. J.; Meyer, E.; Li, C.; Ealick, S. E.; Stubbe, J., Investigation of the ATP binding site of *Escherichia coli* aminoimidazole ribonucleotide synthetase using affinity labeling and site-directed mutagenesis. *Biochemistry* **1999**, 38 (31), 9831-9.
142. Dewal, M. B.; Firestine, S. M., Site-directed mutagenesis of catalytic residues in N(5)-carboxyaminoimidazole ribonucleotide synthetase. *Biochemistry* **2013**, 52 (37), 6559-67.
143. Kochanek, S. E.; Clymer, T. M.; Pakkala, V. S.; Hebert, S. P.; Reeping, K.; Firestine, S. M.; Evanseck, J. D., Intramolecular charge-assisted hydrogen bond strength in pseudochair carboxyphosphate. *J Phys Chem B* **2015**, 119 (3), 1184-91.
144. Miller, G. J.; Wilson, M. P.; Majerus, P. W.; Hurley, J. H., Specificity determinants in inositol polyphosphate synthesis: crystal structure of inositol 1,3,4-trisphosphate 5/6-kinase. *Mol Cell* **2005**, 18 (2), 201-12.

145. Esser, L.; Wang, C. R.; Hosaka, M.; Smagula, C. S.; Sudhof, T. C.; Deisenhofer, J., Synapsin I is structurally similar to ATP-utilizing enzymes. *EMBO J* **1998**, *17* (4), 977-84.
146. Lasso, G.; Yu, L. P.; Gil, D.; Xiang, S.; Tong, L.; Valle, M., Cryo-EM analysis reveals new insights into the mechanism of action of pyruvate carboxylase. *Structure* **2010**, *18* (10), 1300-10.
147. Erck, C.; Peris, L.; Andrieux, A.; Meissirel, C.; Gruber, A. D.; Vernet, M.; Schweitzer, A.; Saoudi, Y.; Pointu, H.; Bosc, C.; Salin, P. A.; Job, D.; Wehland, J., A vital role of tubulin-tyrosine-ligase for neuronal organization. *Proc Natl Acad Sci U S A* **2005**, *102* (22), 7853-8.
148. Chou, C. Y.; Yu, L. P.; Tong, L., Crystal structure of biotin carboxylase in complex with substrates and implications for its catalytic mechanism. *J Biol Chem* **2009**, *284* (17), 11690-7.
149. Kappock, T. J.; Ealick, S. E.; Stubbe, J., Modular evolution of the purine biosynthetic pathway. *Curr Opin Chem Biol* **2000**, *4* (5), 567-72.
150. Waite, M.; Wakil, S. J., Studies on the mechanism of action of acetyl coenzyme A carboxylase. II. On the mechanism of action of enzyme-bound biotin. *J Biol Chem* **1963**, *238*, 81-90.
151. Ito, Y.; Kondo, H.; Shiota, Y.; Yoshizawa, K., Theoretical Analysis of the Reaction Mechanism of Biotin Carboxylase. *J Chem Theory Comput* **2008**, *4* (2), 366-74.
152. Tipton, P. A.; Cleland, W. W., Catalytic mechanism of biotin carboxylase: steady-state kinetic investigations. *Biochemistry* **1988**, *27* (12), 4317-25.
153. Tuntland, M. L.; Johnson, M. E.; Fung, L. W.; Santarsiero, B. D., Structure of N5-carboxyaminoimidazole ribonucleotide synthase (PurK) from *Bacillus anthracis*. *Acta Crystallogr D Biol Crystallogr* **2011**, *67* (Pt 10), 870-4.

154. Kondo, S.; Nakajima, Y.; Sugio, S.; Sueda, S.; Islam, M. N.; Kondo, H., Structure of the biotin carboxylase domain of pyruvate carboxylase from *Bacillus thermodenitrificans*. *Acta Crystallogr D Biol Crystallogr* **2007**, 63 (Pt 8), 885-90.
155. Beis, I.; Newsholme, E. A., The contents of adenine nucleotides, phosphagens and some glycolytic intermediates in resting muscles from vertebrates and invertebrates. *Biochem J* **1975**, 152 (1), 23-32.
156. Ventura, J. J.; Nebreda, A. R., Protein kinases and phosphatases as therapeutic targets in cancer. *Clin Transl Oncol* **2006**, 8 (3), 153-60.
157. Fang, G.; Kim, C. N.; Perkins, C. L.; Ramadevi, N.; Winton, E.; Wittmann, S.; Bhalla, K. N., CGP57148B (STI-571) induces differentiation and apoptosis and sensitizes Bcr-Abl-positive human leukemia cells to apoptosis due to antileukemic drugs. *Blood* **2000**, 96 (6), 2246-53.
158. Deininger, M. W.; Goldman, J. M.; Lydon, N.; Melo, J. V., The tyrosine kinase inhibitor CGP57148B selectively inhibits the growth of BCR-ABL-positive cells. *Blood* **1997**, 90 (9), 3691-8.
159. Mochalkin, I.; Miller, J. R.; Narasimhan, L.; Thanabal, V.; Erdman, P.; Cox, P. B.; Prasad, J. V.; Lightle, S.; Huband, M. D.; Stover, C. K., Discovery of antibacterial biotin carboxylase inhibitors by virtual screening and fragment-based approaches. *ACS Chem Biol* **2009**, 4 (6), 473-83.
160. Miller, J. R.; Dunham, S.; Mochalkin, I.; Banotai, C.; Bowman, M.; Buist, S.; Dunkle, B.; Hanna, D.; Harwood, H. J.; Huband, M. D.; Karnovsky, A.; Kuhn, M.; Limberakis, C.; Liu, J. Y.; Mehrens, S.; Mueller, W. T.; Narasimhan, L.; Ogden, A.; Ohren, J.; Prasad, J. V.; Shelly, J. A.; Skerlos, L.; Sulavik, M.; Thomas, V. H.; VanderRoest, S.; Wang, L.; Wang, Z.;

Whitton, A.; Zhu, T.; Stover, C. K., A class of selective antibacterials derived from a protein kinase inhibitor pharmacophore. *Proc Natl Acad Sci U S A* **2009**, *106* (6), 1737-42.

161. Skedelj, V.; Arsovska, E.; Tomasic, T.; Kroflic, A.; Hodnik, V.; Hrast, M.; Bester-Rogac, M.; Anderluh, G.; Gobec, S.; Bostock, J.; Chopra, I.; O'Neill, A. J.; Randall, C.; Zega, A., 6-Arylpyrido[2,3-d]pyrimidines as novel ATP-competitive inhibitors of bacterial D-alanine:D-alanine ligase. *PLoS One* **2012**, *7* (8), e39922.

162. Cheng, C. C.; Shipps, G. W., Jr.; Yang, Z.; Sun, B.; Kawahata, N.; Soucy, K. A.; Soriano, A.; Orth, P.; Xiao, L.; Mann, P.; Black, T., Discovery and optimization of antibacterial AccC inhibitors. *Bioorg Med Chem Lett* **2009**, *19* (23), 6507-14.

163. Annis, D. A.; Shipps, G. W., Jr.; Deng, Y.; Popovici-Muller, J.; Siddiqui, M. A.; Curran, P. J.; Gowen, M.; Windsor, W. T., Method for quantitative protein-ligand affinity measurements in compound mixtures. *Anal Chem* **2007**, *79* (12), 4538-42.

164. Soriano, A.; Radice, A. D.; Herbitter, A. H.; Langsdorf, E. F.; Stafford, J. M.; Chan, S.; Wang, S.; Liu, Y. H.; Black, T. A., Escherichia coli acetyl-coenzyme A carboxylase: characterization and development of a high-throughput assay. *Anal Biochem* **2006**, *349* (2), 268-76.

165. Hamby, J. M.; Connolly, C. J.; Schroeder, M. C.; Winters, R. T.; Showalter, H. D.; Panek, R. L.; Major, T. C.; Olsewski, B.; Ryan, M. J.; Dahrting, T.; Lu, G. H.; Keiser, J.; Amar, A.; Shen, C.; Kraker, A. J.; Slintak, V.; Nelson, J. M.; Fry, D. W.; Bradford, L.; Hallak, H.; Doherty, A. M., Structure-activity relationships for a novel series of pyrido[2,3-d]pyrimidine tyrosine kinase inhibitors. *J Med Chem* **1997**, *40* (15), 2296-303.

166. Trumpp-Kallmeyer, S.; Rubin, J. R.; Humblet, C.; Hamby, J. M.; Showalter, H. D., Development of a binding model to protein tyrosine kinases for substituted pyrido[2,3-d]pyrimidine inhibitors. *J Med Chem* **1998**, *41* (11), 1752-63.

167. Dorsey, J. F.; Jove, R.; Kraker, A. J.; Wu, J., The pyrido[2,3-d]pyrimidine derivative PD180970 inhibits p210Bcr-Abl tyrosine kinase and induces apoptosis of K562 leukemic cells. *Cancer Res* **2000**, *60* (12), 3127-31.
168. Kraker, A. J.; Hartl, B. G.; Amar, A. M.; Barvian, M. R.; Showalter, H. D.; Moore, C. W., Biochemical and cellular effects of c-Src kinase-selective pyrido[2, 3-d]pyrimidine tyrosine kinase inhibitors. *Biochem Pharmacol* **2000**, *60* (7), 885-98.
169. Lee, C. H.; Jiang, M.; Cowart, M.; Gfesser, G.; Perner, R.; Kim, K. H.; Gu, Y. G.; Williams, M.; Jarvis, M. F.; Kowaluk, E. A.; Stewart, A. O.; Bhagwat, S. S., Discovery of 4-amino-5-(3-bromophenyl)-7-(6-morpholino-pyridin-3-yl)pyrido[2,3-d]pyrimidine, an orally active, non-nucleoside adenosine kinase inhibitor. *J Med Chem* **2001**, *44* (13), 2133-8.
170. Tu, S.; Zhang, J.; Zhu, X.; Xu, J.; Zhang, Y.; Wang, Q.; Jia, R.; Jiang, B.; Zhang, J., New potential inhibitors of cyclin-dependent kinase 4: design and synthesis of pyrido[2,3-d]pyrimidine derivatives under microwave irradiation. *Bioorg Med Chem Lett* **2006**, *16* (13), 3578-81.
171. Kammasud, N.; Boonyarat, C.; Sanphanya, K.; Utsintong, M.; Tsunoda, S.; Sakurai, H.; Saiki, I.; Andre, I.; Grierson, D. S.; Vajragupta, O., 5-Substituted pyrido[2,3-d]pyrimidine, an inhibitor against three receptor tyrosine kinases. *Bioorg Med Chem Lett* **2009**, *19* (3), 745-50.
172. Basarab, G. S. Spiro condensed barbituric acid derivatives for use as antibacterial. 2007. WO 2009/010801 A1.
173. Katoh, T.; Tomata, Y.; Tsukamoto, T.; Nakada, Y., Facile preparation of 3-substituted-2,6-difluoropyridines: application to the synthesis of 2,3,6-trisubstituted pyridines. *Tetrahedron Lett* **2015**, *56* (44), 6043-6046.

174. Matulis, D., Selective Precipitation of Proteins. *Curr Protoc Protein Sci* **2016**, 83, 4 5 1-4 5 37.
175. Madeira, A.; Vikeved, E.; Nilsson, A.; Sjogren, B.; Andren, P. E.; Svenningsson, P., Identification of protein-protein interactions by surface plasmon resonance followed by mass spectrometry. *Curr Protoc Protein Sci* **2011**, Chapter 19, Unit19 21.
176. Durmus, A.; Gunbas, G.; Farmer, S. C.; Ohnstead, M. M.; Mascall, M.; Legese, B.; Cho, J. Y.; Beingessner, R. L.; Yamazaki, T.; Fenniri, H., Synthesis of N-substituted Pyrido[4,3-d]pyrimidines for the Large-Scale Production of Self-Assembled Rosettes and Nanotubes. *J Org Chem* **2013**, 78 (22), 11421-11426.
177. Ramanathan, A.; Jimenez, L. S., Reductive Dehalogenation of Aryl Bromides and Chlorides and Their Use as Aryl Blocking Groups. *Synthesis-Stuttgart* **2010**, (2), 217-220.
178. Thompson, A. M.; Rewcastle, G. W.; Boushelle, S. L.; Hartl, B. G.; Kraker, A. J.; Lu, G. H.; Batley, B. L.; Panek, R. L.; Showalter, H. D. H.; Denny, W. A., Synthesis and structure-activity relationships of 7-substituted 3-(2,6-dichlorophenyl)-1,6-naphthyridin-2 (1H)-ones as selective inhibitors of pp60(c-src). *Journal of Medicinal Chemistry* **2000**, 43 (16), 3134-3147.
179. Fenlon, E. E.; Murray, T. J.; Baloga, M. H.; Zimmerman, S. C., Convenient Synthesis of 2-Amino-1,8-Naphthyridines, Building-Blocks for Host-Guest and Self-Assembling Systems. *Journal of Organic Chemistry* **1993**, 58 (24), 6625-6628.
180. *Molecular Operating Environment (MOE)*, 2013.08, Chemical Computing Group ULC, 1010 Sherbooke St. West, Suite #910, Montreal, QC, Canada, H3A 2R7, 2018.
181. Reddy, M. V.; Akula, B.; Cosenza, S. C.; Athuluridivakar, S.; Mallireddigari, M. R.; Pallela, V. R.; Billa, V. K.; Subbaiah, D. R.; Bharathi, E. V.; Vasquez-Del Carpio, R.; Padgaonkar, A.; Baker, S. J.; Reddy, E. P., Discovery of 8-cyclopentyl-2-[4-(4-methyl-

piperazin-1-yl)-phenylamino]-7-oxo-7,8-dihydro-pyrid o[2,3-d]pyrimidine-6-carbonitrile (7x) as a potent inhibitor of cyclin-dependent kinase 4 (CDK4) and AMPK-related kinase 5 (ARK5). *J Med Chem* **2014**, *57* (3), 578-99.

182. Watanabe, W.; Sampei, G.; Aiba, A.; Mizobuchi, K., Identification and sequence analysis of Escherichia coli purE and purK genes encoding 5'-phosphoribosyl-5-amino-4-imidazole carboxylase for de novo purine biosynthesis. *J Bacteriol* **1989**, *171* (1), 198-204.

183. Singh, J.; Petter, R. C.; Baillie, T. A.; Whitty, A., The resurgence of covalent drugs. *Nat Rev Drug Discov* **2011**, *10* (4), 307-17.

184. Powers, J. C.; Asgjan, J. L.; Ekici, O. D.; James, K. E., Irreversible inhibitors of serine, cysteine, and threonine proteases. *Chem Rev* **2002**, *102* (12), 4639-4750.

185. Liu, Q. S.; Sabnis, Y.; Zhao, Z.; Zhang, T. H.; Buhrlage, S. J.; Jones, L. H.; Gray, N. S., Developing Irreversible Inhibitors of the Protein Kinase Cysteine. *Chemistry & Biology* **2013**, *20* (2), 146-159.

186. Potashman, M. H.; Duggan, M. E., Covalent modifiers: an orthogonal approach to drug design. *J Med Chem* **2009**, *52* (5), 1231-46.

187. Mah, R.; Thomas, J. R.; Shafer, C. M., Drug discovery considerations in the development of covalent inhibitors. *Bioorganic & Medicinal Chemistry Letters* **2014**, *24* (1), 33-39.

188. Copeland, R. A., *Evaluation of Enzyme inhibitors in Drug Discovery*. John Wiley & Sons, Inc, 2013.

189. Patick, A. K.; Binford, S. L.; Brothers, M. A.; Jackson, R. L.; Ford, C. E.; Diem, M. D.; Maldonado, F.; Dragovich, P. S.; Zhou, R.; Prins, T. J.; Fuhrman, S. A.; Meador, J. W.; Zalman, L. S.; Matthews, D. A.; Worland, S. T., In vitro antiviral activity of AG7088, a potent

inhibitor of human rhinovirus 3C protease. *Antimicrob Agents Chemother* **1999**, *43* (10), 2444-50.

190. Matthews, D. A.; Dragovich, P. S.; Webber, S. E.; Fuhrman, S. A.; Patick, A. K.; Zalman, L. S.; Hendrickson, T. F.; Love, R. A.; Prins, T. J.; Marakovits, J. T.; Zhou, R.; Tikhe, J.; Ford, C. E.; Meador, J. W.; Ferre, R. A.; Brown, E. L.; Binford, S. L.; Brothers, M. A.; DeLisle, D. M.; Worland, S. T., Structure-assisted design of mechanism-based irreversible inhibitors of human rhinovirus 3C protease with potent antiviral activity against multiple rhinovirus serotypes. *Proc Natl Acad Sci U S A* **1999**, *96* (20), 11000-7.

191. Wissner, A.; Overbeek, E.; Reich, M. F.; Floyd, M. B.; Johnson, B. D.; Mamuya, N.; Rosfjord, E. C.; Discafani, C.; Davis, R.; Shi, X.; Rabindran, S. K.; Gruber, B. C.; Ye, F.; Hallett, W. A.; Nilakantan, R.; Shen, R.; Wang, Y. F.; Greenberger, L. M.; Tsou, H. R., Synthesis and structure-activity relationships of 6,7-disubstituted 4-anilinoquinoline-3-carbonitriles. The design of an orally active, irreversible inhibitor of the tyrosine kinase activity of the epidermal growth factor receptor (EGFR) and the human epidermal growth factor receptor-2 (HER-2). *J Med Chem* **2003**, *46* (1), 49-63.

192. Škedelj, V.; Arsovska, E.; Tomašić, T.; Kroflič, A.; Hodnik, V.; Hrast, M.; Bešter-Rogač, M.; Anderluh, G.; Gobec, S.; Bostock, J.; Chopra, I.; O'Neill, A. J.; Randall, C.; Zega, A., 6-Arylprido[2,3-d]pyrimidines as Novel ATP-Competitive Inhibitors of Bacterial D-Alanine:D-Alanine Ligase. *PLOS ONE* **2012**, *7* (8), e39922.

193. Blankley, C. J.; Doherty, A. M.; Hamby, J. M.; Panek, R. L.; Schroeder, M. C.; Showalter, H. D. H.; Connolly, C. 6-Aryl pyrido[2,3-d]pyrimidines and naphthyridines for inhibiting protein tyrosine kinase mediated cellular proliferation. WO/1996/015128, 1996.

194. Blankley, C. J.; Doherty, A. M.; Hamby, J. M.; Panek, R. L.; Schroeder, M. C.; Showalter, H. D. H.; Connolly, C. Preparation of 6-aryl pyrido[2,3-d]pyrimidines and

naphthyridines for inhibiting protein tyrosine kinase-mediated cellular proliferation. 1996. WO 9615128 A2.

195. Davoll, J. Diuretic 2,7-diamino-6-arylpyrido[2,3-d]pyrimidines. 1969. GB-1967-51042.

196. Thompson, A. M.; Delaney, A. M.; Hamby, J. M.; Schroeder, M. C.; Spoon, T. A.; Crean, S. M.; Showalter, H. D.; Denny, W. A., Synthesis and structure-activity relationships of soluble 7-substituted 3-(3,5-dimethoxyphenyl)-1,6-naphthyridin-2-amines and related ureas as dual inhibitors of the fibroblast growth factor receptor-1 and vascular endothelial growth factor receptor-2 tyrosine kinases. *J Med Chem* **2005**, *48* (14), 4628-53.

197. Thompson, A. M.; Connolly, C. J.; Hamby, J. M.; Boushelle, S.; Hartl, B. G.; Amar, A. M.; Kraker, A. J.; Driscoll, D. L.; Steinkampf, R. W.; Patmore, S. J.; Vincent, P. W.; Roberts, B. J.; Elliott, W. L.; Klohs, W.; Leopold, W. R.; Showalter, H. D.; Denny, W. A., 3-(3,5-Dimethoxyphenyl)-1,6-naphthyridine-2,7-diamines and related 2-urea derivatives are potent and selective inhibitors of the FGF receptor-1 tyrosine kinase. *J Med Chem* **2000**, *43* (22), 4200-11.

198. Thompson, A. M.; Rewcastle, G. W.; Boushelle, S. L.; Hartl, B. G.; Kraker, A. J.; Lu, G. H.; Batley, B. L.; Panek, R. L.; Showalter, H. D.; Denny, W. A., Synthesis and structure-activity relationships of 7-substituted 3-(2, 6-dichlorophenyl)-1,6-naphthyridin-2(1H)-ones as selective inhibitors of pp60(c-src). *J Med Chem* **2000**, *43* (16), 3134-47.

199. Henry, J. R.; Kaufman, M. D.; Peng, S. B.; Ahn, Y. M.; Caldwell, T. M.; Vogeti, L.; Telikepalli, H.; Lu, W. P.; Hood, M. M.; Rutkoski, T. J.; Smith, B. D.; Vogeti, S.; Miller, D.; Wise, S. C.; Chun, L.; Zhang, X.; Zhang, Y.; Kays, L.; Hipskind, P. A.; Wroblewski, A. D.; Lobb, K. L.; Clay, J. M.; Cohen, J. D.; Walgren, J. L.; McCann, D.; Patel, P.; Clawson, D. K.; Guo, S.; Manglicmot, D.; Groshong, C.; Logan, C.; Starling, J. J.; Flynn, D. L., Discovery

of 1-(3,3-dimethylbutyl)-3-(2-fluoro-4-methyl-5-(7-methyl-2-(methylamino)pyrido[2,3-d]pyrimidin-6-yl)phenyl)urea (LY3009120) as a pan-RAF inhibitor with minimal paradoxical activation and activity against BRAF or RAS mutant tumor cells. *J Med Chem* **2015**, *58* (10), 4165-79.

200. Wisniewski, J. A.; Yin, J.; Teuscher, K. B.; Zhang, M.; Ji, H., Structure-Based Design of 1,4-Dibenzoylpiperazines as beta-Catenin/B-Cell Lymphoma 9 Protein-Protein Interaction Inhibitors. *ACS Med Chem Lett* **2016**, *7* (5), 508-13.

ABSTRACT

by

QIAN LIN**August 2018****Advisor:** Dr. Steven M. Firestine**Major:** Pharmaceutical Sciences**Degree:** Doctor of Philosophy

The spread of drug-resistant bacterial infections has increased the need for novel antimicrobial agents. One potential but unexplored target is the *de novo* purine biosynthetic pathway. PurK, found only in bacteria, yeast, and fungi, catalyzes the sixth step in purine biosynthesis and has no human homolog. Herein we disclose the discovery of the first PurK inhibitor with submicromolar potency.

PurK is a member of the ATP-grasp superfamily of enzymes and recently, nanomolar inhibitors of biotin carboxylase, a related enzyme, were published. We hypothesized that those inhibitors, which target the ATP-binding site, could also inhibit PurK. To explore this hypothesis, four compounds were synthesized and tested against PurK from *A. clavatus*. Only one compound, **1** containing a pyridopyrimidine core, weakly inhibits PurK_{Asp} with an IC₅₀ of 167 μM. Kinetic assays have confirmed that **1** is an ATP-competitive inhibitor. With the guidance of computational modeling, further optimizations have been focused on the ribose and phosphate positions within the ATP-binding site. Both positions gave compounds with improved activities. A double-modified compound, **56**, merging the best compound from each position, inhibits PurK_{Asp} with an IC₅₀ of 1.7 μM, a 100-fold improvement in potency. The binding affinity was validated by thermal shift assays. **56** is the most potent ATP-binding site inhibitor against PurK_{Asp} described to date.

AUTOBIOGRAPHICAL STATEMENT

I was born in 1988 in Shiyan, Hubei province, China. In 2006, I came to Beijing for college study. I was majored in Pharmaceutical Sciences in Peking University. After bachelor and a Master in Pharmaceutical Analysis, I came to the United States for doctoral study. Here I majored in Medicinal Chemistry and was under the guidance of Dr. Steven Firestine. I have been happily married since 2015.